Controlling the efficiency of surface fluxes in inductively coupled oxygen-argon plasmas with pulsed power deposition

Theo William Carpenter

Msc by Research

University of York

School of Physics, Engineering and Technology

December 2025

Abstract

The density of transistors continues to increase, which requires the manufacturing of microchips to have a high degree of accuracy. To achieve this, the industry uses plasma based atomic layer etching and deposition processes for the modification of the microchip. However, they use a large amount of energy that releases greenhouse gases that harm the environment. As such, this thesis investigates the effect of varying several input parameters on the input energy per particle fluxed to the surface. This is achieved by utilising a zero-dimensional plasma chemical-kinetics numerical global model with an extensive chemical-radiative reaction scheme to model a cylindrical pulsed powered inductively coupled Ar/O_2 plasma reactor.

The energy per Ar^+ fluxed, in a 100% argon plasma, increases minimally with frequency, decreases with duty cycle and reaches a minimum with pressure at 1 *Pa* and is constant with average power. Additionally, in a 90% argon 10% oxygen plasma, the energy per atomic oxygen fluxed decreases with pressure and increases with average power. Furthermore, the energy per ground and excited states of atomic oxygen fluxed are generally similar to each other. The energy per O^+ fluxed decreases with average power and reaches a minimum in pressure, which shifts to higher pressures as the average power increases. The energy per O_2^+ fluxed reaches a minimum at 5 *Pa* and increases with average power.

In conclusion, for Ar^+ the energy can be decreased using a high duty cycle and a low pressure of 1 *Pa*. For atomic oxygen, the energy can be decreased using high pressure and low average power. For O^+ the energy can be decreased by increasing the average power and selecting the pressure with optimal surface flux. Finally, for O_2^+ the energy can be decreased using a pressure of 5 *Pa* and increasing the average power.

Contents

Acknowledgements

Firstly, I would like to thank my fantastic supervisors Andrew Gibson and James Dedrick for their support, guidance and brilliant attention to detail throughout my MSC. In particular, I wish to thank Andrew Gibson for his constant help in getting me back on track when I get stuck through gentle nudges in the right direction in our weekly meetings. And for timely and useful calm responses to my panicky emails when I think something has gone wrong. In addition, I would like to thank Andrew Gibson again for allowing me to have access to the simulation code used throughout this thesis and for talking me through the theory behind it and how to run my own simulations using it. I would also like to thank Peter Hill for the open, friendly and relaxed technical support.

I would like to acknowledge Derwent college hockey club for always being welcoming and letting me come along and play and blow off some steam. I would also like to thank my friends and my housemates who I spent a lot of time with, who are always happy for a lengthy chat about anything and are always happy to help me if i needed anything. Finally, a big thank you to my mum, dad and brother who supported me throughout my further education journey both, financially and personally especially during my length working for home writing period. Without all of you I would not be where I am today, so thank you.

Declaration

I Theo Carpenter declare that this thesis is a presentation of original work and I am the sole author. This work has not previously been presented for a degree or other qualification at this University or elsewhere. All sources are acknowledged as references. Part of the contents of chapter four have been presented at the 51st Annual Plasma Physics Conference London, UK, April 2025.

The presented numerical simulations have been modified and utilised by the author with the exception of the code base which was provided by Dr Andrew R. Gibson of the University of York. The simulations presented here using the code have been set-up, run and analysed by the author only.

Chapter 1

Introduction

This chapter outlines the history and importance of semiconductors, introduces semiconductor manufacturing techniques, and discusses the theory behind nonequilibrium plasmas, and argon-oxygen plasma chemistry.

1.1 Importance of Semiconductor Manufacturing

Semiconductor microprocessors are vital for the daily running of the modern world. They are used in everything from laptops to cars to life-saving medical equipment. They are so important to the running of the modern world that Furber in 2017 described them as "The engines of the digital age" [1]. This instils recognition of how essential semiconductor manufacturing processes are to the functionality of the digital world. The basic building blocks of semiconductor microprocessors are transistors, which are electronic switches that allow for binary logic, which is essential for digital computation. Since the first transistor was made in 1947, more than 1.3×10^{22} transistors have been manufactured, making them the most produced item ever made by humanity [2]. Such large numbers emphasise the importance of grasping and improving the manufacturing techniques used to create microprocessors.

1.1.1 Evolution of Semiconductor Microchips and Moore's Law

In the early years of microchip manufacturing, Intel Co founder Gordon E. Moore noticed that the number of transistors on a single microchip doubled every 2 years, which has become known as Moore's law [3]. This trend has persisted for over 50 years since 1965 as can be seen in figure 1.1. This has led to incredible increases in the density of transistors in microchips, increasing from 190 to 136 million transistors per square millimetre, with the physical space between each transistor approaching a few atoms thick [4, 5]. The small distance between each

transistor allows quantum tunnelling to become a problem, Where the electrons can ignore the binary state of the transistor and flow anyway, breaking the binary logic calculations inside the microchip. This requires atomic level accuracy for manufacturing processes, as even an additional atom thick layer being removed could lead to quantum tunnelling [6].

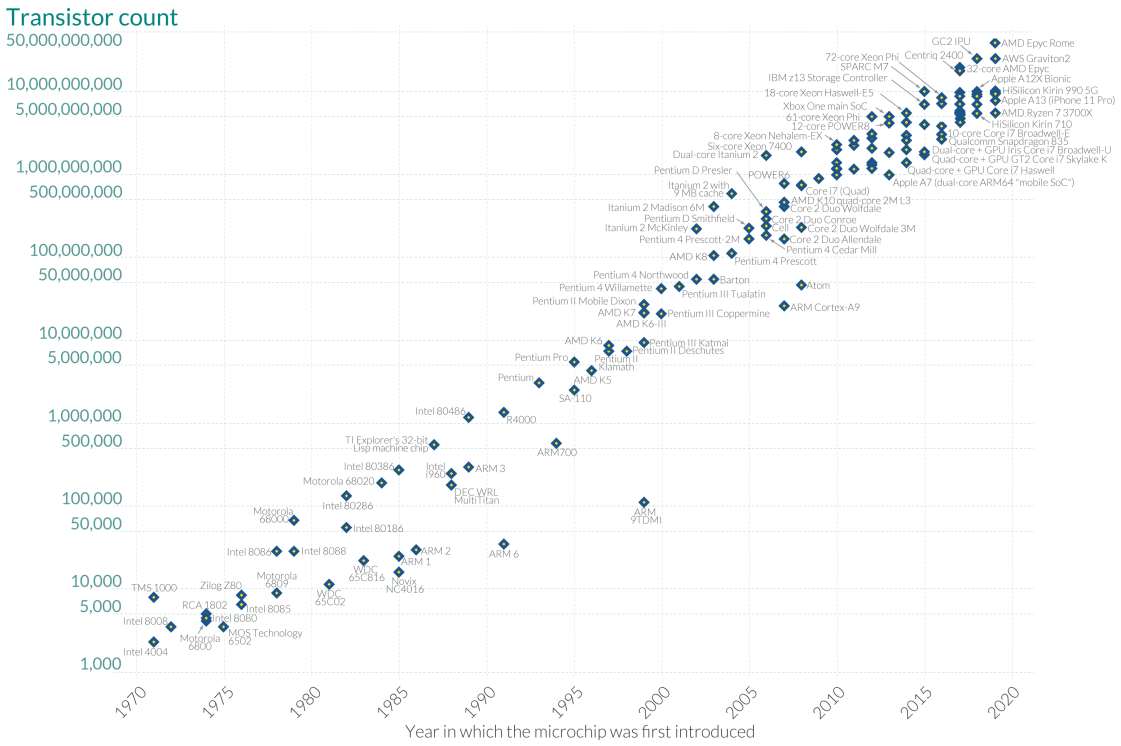

Figure 1.1: Number of transistors on a single chip from 1970 to 2020. Reproduced from Roser et al. (2023) [7], Our World In Data, licensed under CC by 4.0, https://ourworldindata.org/moores-law

1.1.2 Environmental Impact

As the number of devices produced each year skyrockets, the amount of energy used in production increases. Couple that with the energy-intensive nature of the atomic-scale processes required for the latest high-density microchips, the energy used by advanced microchip manufacturers is increasing drastically. The increased energy consumption of these manufacturing plants comes with a growing environmental impact in the form of increased greenhouse gas emissions. This can be seen in figure 1.2 where the greenhouse gas emissions and energy consumption of Taiwan are chosen as Taiwan manufactures 92% of logic semiconductors smaller than 10 nanometres [8].

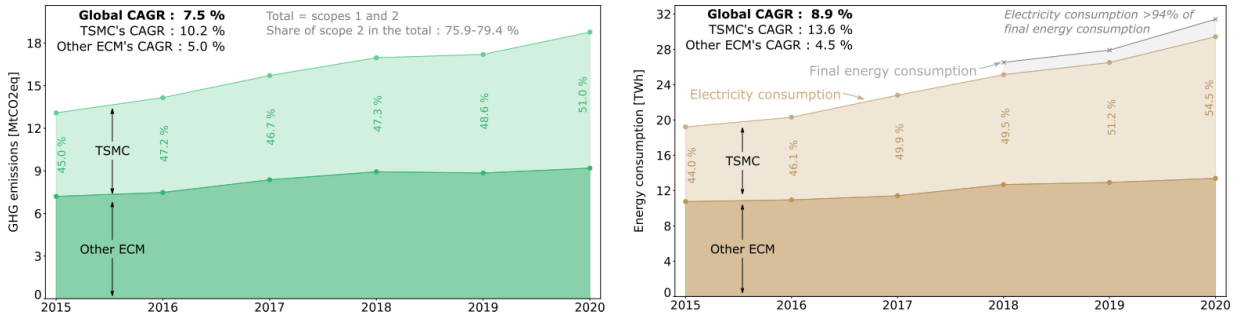

Figure 1.2: Greenhouse gas emissions each year (Left) and Energy consumption each year (Right) of TSMC and fifteen other Taiwanese electronic component manufacturers between 2015 and 2020. Reproduced under fair dealing for academic purposes from Roussilhe et al. (2024) Journal of Industrial Ecology [9] © International Society for Industrial Ecology / John Wiley & Sons

In today's world, keeping rising energy consumption and greenhouse gas emissions under control is not only important for the cost of production but also vital to maintaining the environment to help combat climate change [10, 11]. As such, this thesis will focus on investigating the efficiency of power used for atomic-scale plasma processes used in the production of microchips to gain an understanding of how to most effectively drive these processes.

1.2 Atomic Layer Material Processing

Modifying the surface of semiconductors is critical for the production of microchips. The removal of material, otherwise known as etching, is used to create complex structures required for transistors and channels for wires. The deposition of material is required to build transistors and wires within the circuit and to insulate the components. Therefore, performing these processes as accurately and efficiently as possible is key to producing fast microchips while keeping energy consumption to a minimum [12].

1.2.1 Etching

Etching uses masks, chemicals and ions to selectively remove layers of material creating channels in the semiconductor material. The manufacturing industry has implemented many methods of etching, with three main methods to note. One uses liquid chemicals to react with the surface and remove material, another uses plasma to produce ions and reactive neutrals to continuously etch the surface, known as reactive ion etching (RIE). Finally, atomic layer etching (ALE) utilises a two stage cycle to first modify the surface using a reactive chemical and then the second step uses a plasma to etch the surface in a self-limiting manner. [13, 14].

Chemical and Reactive Ion Etching

Chemical etching works by first creating a mask that outlines the area of the desired structures and covers the rest of the area so that the desired semiconductor material is not removed. Afterward, etching is achieved by covering the material in a liquid chemical that will selectively dissolve the semiconductor but not the mask, leaving behind channels in the desired structure shape [13]. The advantages of chemical etching are high etch-rate, simplicity and low cost. However, there are some serious drawbacks to this method as microchips continue to shrink and increase in complexity [13]. The main problem with chemical etching is the impreciseness of the etch. Chemicals dissolve the semiconductor isotropically, which leads to the etch forming a semicircular shape as seen in figure 1.3b instead of the desired rectangular shape [14]. This makes the etches width at its widest point more than twice the depth of the etch significantly decreasing the density of structures on the semiconductor and, therefore, transistors inside the microchip. Other problems with chemical etching are the lack of selectivity in what the chemical dissolves, potentially affecting different layers and materials already on the microchip, and the lack of control in the number of layers etched due to the continuous nature of the etching method.

Reactive ion etching (RIE) works by still using a mask; however, instead of using reactive chemicals, it uses a partially ionised plasma glow discharge [15]. This glow discharge provides energetic ions and reactive neutral chemical species, which react simultaneously and continuously on the surface. Reactive neutrals modify the surface to form a reactive surface with a lower energy barrier to remove [15]. The energetic ions then react with the surface with enough energy to physically sputter the reactive surface layer away. The ions inside the plasma source are accelerated through an electric field that provides the energy to physically sputter atoms, and the directionality of the electric field accelerates ions normal to the semiconductor, therefore providing the desired anisotropic etching [13, 15]. This provides sharper and more vertical etches, allowing structures to be placed closer together, as shown in figure 1.3c. However, while reactive ion etching provides high etch rates and directional etching, the continuous and simultaneous nature of the process comes with some limitations. The continuous and simultaneous nature of the process produces a thick mixed layer made up of reactant and substrate atoms and voids that have been shown to penetrate more than 20 nm into the surface, whilst making it difficult to precisely control the number of layers etched across the surface. [15–17].

Plasma ALE

To overcome the drawbacks of chemical etching and RIE, plasma-based ALE has been developed. Plasma ALE still uses a mask to outline the desired structure and a plasma based ion source, but instead of applying reactive neutrals and energetic ions simultaneously, they are applied separately to produce a self-limiting reaction [15]. The surface is first modified by the reactive neutrals, which creates a thin reactive layer with a consistent thickness that is easier to remove than the unmodified material. Secondly, in a separate independent reaction the modified layer is removed by the energetic ions, whilst the unmodified material underneath is left intact in a near perfect state as shown in figure 1.4 [15].

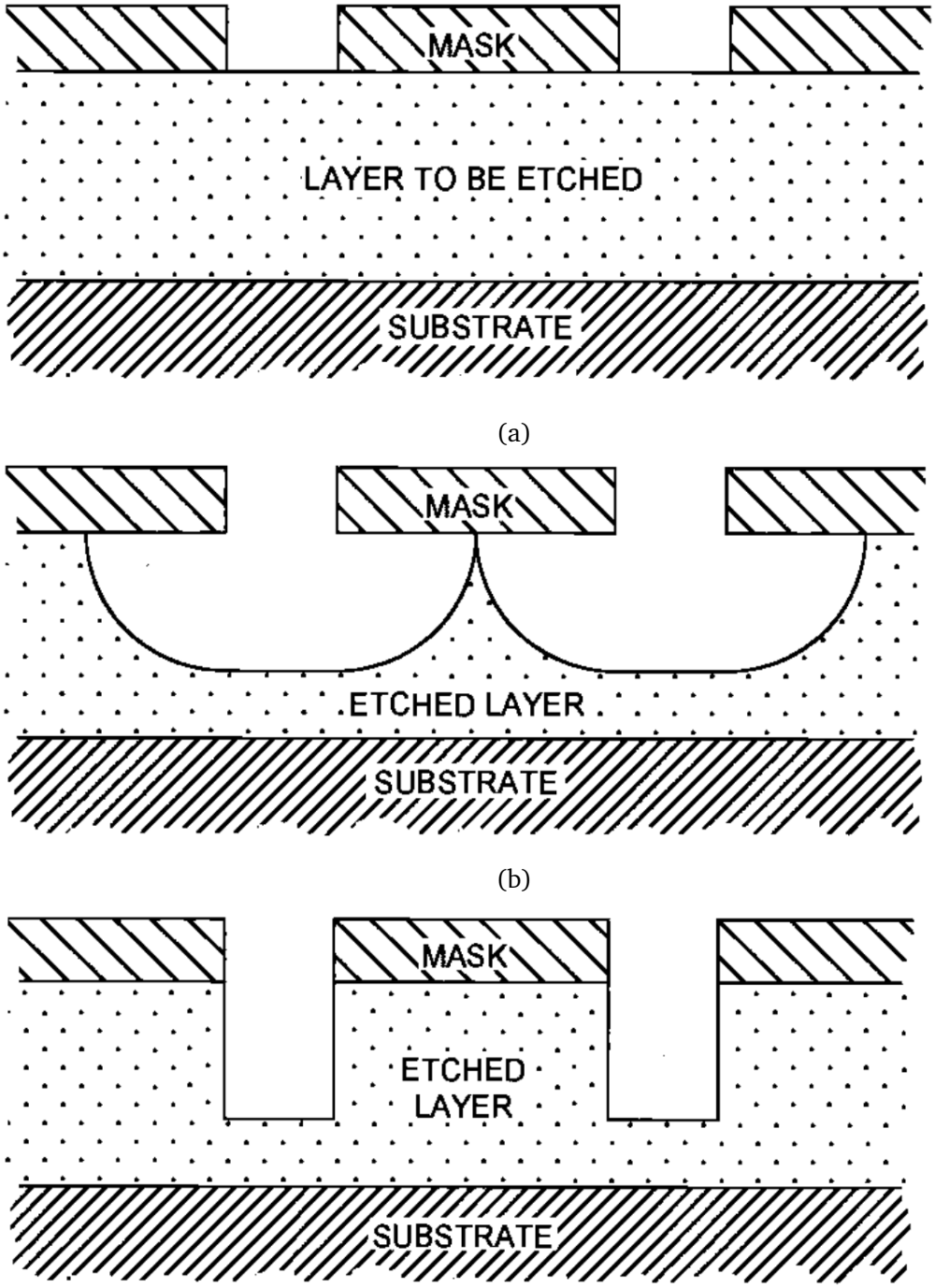

Figure 1.3: Depicts A semiconductor before etching (a), A semiconductor after an isotropic chemical etch (b) and A semiconductor after an anisotropic plasma etch (c). Reproduced under fair dealing for academic purposes from Roth Et Al. (2001) Industrial Plasma Engineering Vol 2 [14] © IOP Publishing Ltd

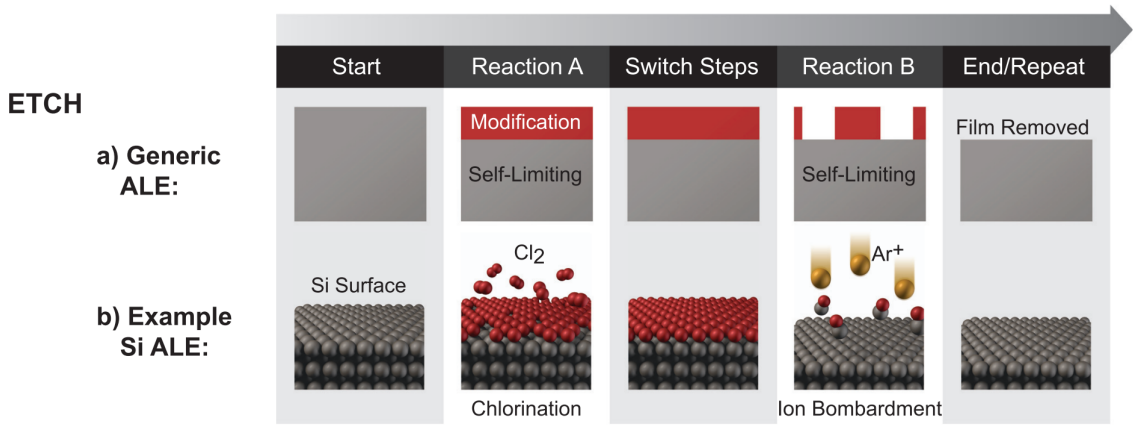

Figure 1.4: Depicts the steps of ALE, with reaction A being the first step involving reactive neutrals and reaction B being the second step involving energetic ions. Here, (a) is a generic concept and (b) is silicon example. Adapted from Kanarik Et Al. (2015) [15], Journal of Vacuum Science & Technology A, licensed under CC by 3.0

The two steps can be repeated with each cycle, removing a thickness of modified material which is precise to the atomic layer and, therefore, allowing the depth of the etch to be set by the number of repeated cycles. The directionality of the ions still provides the desired anisotropic etch as shown in figure 1.3c. Additionally, the separation of reactions in ALE has been shown to avoid the formation of the thick mixed layer present in RIE, allowing greater precision in the etch [15]. Due to the energy required to etch the modified and unmodified material, ions inside the plasma are required to have an energy that is inside the ALE window [15]. This can be illustrated by figure 1.5. Here, in regime I, the ion energy is lower than the energy required to etch the modified material, leading to incomplete removal of the material. In regime III the ions energy is higher than the energy required to etch the unmodified material; as such, this leads to extra sputtering of the material, reducing the surface quality. Finally, in regime II the ions are in the energy window, which means that they have enough energy to etch the modified material but not enough to etch the unmodified material, creating a perfect uniform surface [15]. Therefore, the energy of the ions produced by the plasma needs to be considered when analysing the fluxes of ions for use in ALE to ensure that the ion energy is such that they will remove the modified material whilst leaving the unmodified material intact.

1.2.2 Deposition

Deposition uses reactants to modify the surface of the semiconductor to deposit the desired materials onto the surface. The manufacturing industry has implemented three particular methods that are notable. Chemical vapour deposition (CVD) uses a contentious flow of reactants and a high temperature of the surface to deposit materials. Plasma enhanced chemical vapour deposition (PECVD), which uses a plasma to create more reactive radical neutral particles, which can then more easily react with the surface. Atomic layer deposition (ALD) uses a repeatable

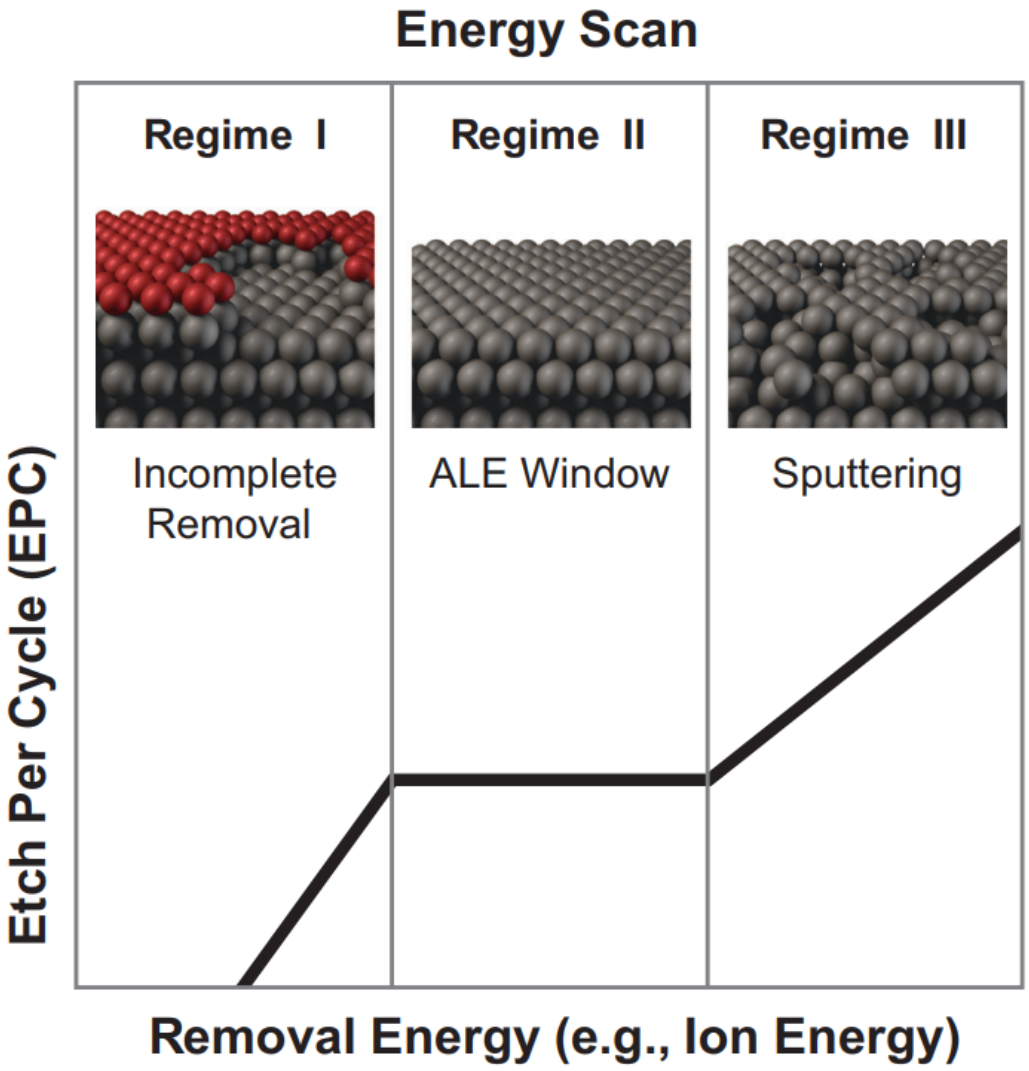

Figure 1.5: Depicts an energy scan of the ALE removal step. Reproduced from Kanarik Et Al. (2015) [15], Journal of Vacuum Science & Technology A, licensed under CC by 3.0

two stage cycle to deposit materials in a self-limiting manner [18–20]

Chemical Vapour Deposition (CVD)

CVD works by using a continuous flow of reactants onto the surface that use their thermal energy and the temperature of the surface to overcome the activation energy of the reaction to produce the desired surface material. This method works well for simple structures and materials; however, there are drawbacks to employing this method to modern microchip manufacturing. The main drawback is the high temperature required for the thermal energy of the reactants and surface, which limits the compatibility with different materials. These materials, such as doped layers, low melting point metals and low-k dielectrics, which are essential to the construction of modern microprocessors, are thermally sensitive and degrade, shrink, melt, or

diffuse at high temperatures [18, 20]. Therefore, the use of advanced materials needed for the production of advanced microprocessors would be impossible or would have degraded properties with the use of CVD. Some of the disadvantages of CVD have been overcome by using PECVD, where a plasma is used to produce more reactive ions and neutral radicals. This allows deposition to be performed at a lower temperature than normal CVD due to the increased reactivity of the energetic species produced by the plasma, allowing the advanced materials required to be used [18]. However, because of the continuous nature of the process, it is difficult to control the exact number of atomic layers deposited onto a material, and in modern dense microchips where accuracy down to the atomic layer is key, this can be a problem.

Atomic Layer Deposition (ALD)

To provide the increased accuracy required in modern microchip manufacturing, ALD has been developed. ALD is a two-step self-limiting process in which a first reactant is adsorbed by the surface, before a second reactant is applied that reacts with the absorbed layer to create the desired material on the surface [19, 20]. This separation of the reaction means that each individual cycle provides a self-limited thickness of material that is precise to the atomic layer to be deposited. This can be repeated in a cycle, where the desired thickness can be easily deposited by repeating the ALD steps until the desired number of atomic layers has been deposited; therefore, the deposition of materials can be achieved with the accuracy of an atomic layer.

1.3 Plasma Theory

Plasma is the fourth state of matter consisting of a gaseous state in which at least some fraction of the atoms has been ionised to form plasma. A plasma possesses a more collective nature than other state's due to long-range electromagnetic interactions [12]. However, even with particles inside the plasma being charged, the overall charge of the plasma is zero, otherwise known as quasineutrality. This state of matter is rarely encountered on earth; however, it is estimated to make up around 99.9% of visible matter in the universe. [21]. Plasma is found in many forms, from stars and solar wind to experimental fusion reactors, plasma cutters and reactors used in semiconductor manufacturing [12, 22–24]. As such understanding the intricacies of the theory behind plasma is important to understanding not only the universe but also for using the state of matter in new technology on earth.

1.3.1 Low Temperature Plasmas

For plasmas being created on Earth the most common type is known as low temperature or non-equilibrium plasmas. These plasmas are not in thermodynamic equilibrium; as such, the temperatures of electrons are significantly higher than those of heavier particles such as ions

and neutrals, which are often at room temperature. This disequilibrium is maintained by coupling power into the plasma, primarily to electrons, and because of the relatively low inertia of electrons compared to heavy particles, there is insignificant heating of heavy particles through collisions [25].

1.3.2 Fundamentals of Low Temperature Plasmas

Understanding the fundamentals behind low temperature plasmas used in ALE and ALD is important for understanding their roles in the processes. As such, this section will explore the formation of plasmas and how the particles inside the plasma interact with each other and other forms of matter.

Plasma Formation

To form a plasma artificially on earth, a chamber that can apply an electric field to the gas and keep it contained is required. This induced electric field in the gas accelerates free electrons, which are generated naturally in the gas from cosmic rays and background radiation. These accelerated free electrons cause collisions with neutral atoms, creating ionisation events that release more electrons. These additional electrons are subsequently accelerated and lead to more ionisation events creating a cascade effect, leading to an avalanche growth of ionised particles where eventually the growth will outweigh the losses and at this point self-sufficient plasma will form known as a breakdown point. This point is determined differently depending on the method of coupling power to the gas inside the reactor with two main methods being employed; capacitively and inductively coupled devices. Capacitively coupled plasma reactors consist of two plates where one has a voltage applied, and the other is grounded to induce a current through the gas. Capacitively coupled reactors have different voltages required to reach the breakdown point depending on the product of distance between the plates and gas pressure, which forms a Paschen curve for the gas used in the reactor [26]. However, in inductively coupled plasmas, like the ones used for the rest of this thesis, there is no easy description of the breakdown point. However, the same principles of capacitively coupled formation still apply, with the only difference being that the electric field used to sustain the plasma after the breakdown is induced through a coil and Faraday's law, as shown in equation 1.3.1.

$$\mathbf{E}_{\mathbf{induced}} = -\frac{d\mathbf{B}}{dt} \tag{1.3.1}$$

Here, $\mathbf{E}_{\mathbf{induced}}$ is the induced electric field and $\frac{d\mathbf{B}}{dt}$ is the rate of change of the applied magnetic field.

Debye Length

A plasma as a whole is considered to be in quasineutrality; however, this assumption only holds on larger length scales. For example if you consider a positively charged sphere inside

the plasma you might expect the force from the charge to propagate infinitely like inside a vacuum. However, inside a plasma the sphere attracts electrons that surround the sphere, forming a cloud of electrons. This effectively obscures the sphere from additional electrons in the bulk as all they 'see' is a negatively charged cloud of electrons, therefore shielding the electromagnetic effect of the sphere from the rest of plasma bulk. The length scale required for a charge inside the plasma to be considered quasi-neutral to the plasma bulk is called the Debye length (λ_D), which is calculated as seen in equation 1.3.2, which depends on parameters inside the plasma [12].

$$\lambda_D = \sqrt{\frac{\epsilon_0 k_b T_e}{n_e e^2}} \tag{1.3.2}$$

Here, T_e and n_e are the temperature and density of the elections, respectively, ϵ_0 is the permittivity of free space, k_b is the Boltzmann constant, and e is the elementary charge.

Sheath Mechanics

Plasma, as a charged state of matter, interacts uniquely with other states of matter. An important process is the formation of sheaths when a plasma interacts with the surface of the reactor. A sheath is a region of positive charge on the plasma boundary, a few Debye lengths wide, formed to maintain net quasineutrality inside the plasma bulk. This forms because when a plasma has become ionised, the lighter electrons which have lower inertia get accelerated in a shorter timescale and therefore arrive at the surface of the reactor sooner. This initial flux of electrons forms a negatively charged wall that repels additional electrons from the surface. This generates a region called a sheath, where the ion density is higher than the negative charged ions and the electron density. This forms a negative electric field towards the surface that accelerates the ions towards the surface, to equalise the flux of negative ions and electron species and positive ion species to maintain bulk quasineutrality [12, 25]. The density of positive and negative species and the potential inside a sheath can be seen in figure 1.6 that illustrates the formation of the negative charge region and the difference in electron and ion densities.

Here, the presheath is a region where the negative and positive species densities are still equal, but a potential drop occurs to accelerate the ions up to the Bohm velocity, which is greater than or equal to the ion sound speed. This is necessary to enter the sheath with enough velocity to maintain flux equilibrium inside the plasma and satisfy sheath formation, known as the Bohm sheath criterion, as shown in equation 1.3.3 [12, 28].

$$u_s \geq u_B = \sqrt{\frac{k_B T_e}{M_i}} \tag{1.3.3}$$

Here, u_s is the ion sound speed, u_B is the Bohm velocity, and M_i is the mass of the ion. The flux into the sheath is simply the product of the density of ions at the edge of the sheath, n_{sh} and the Bohm velocity u_B. In a steady-state collisionless system, since all ions are accelerated to the

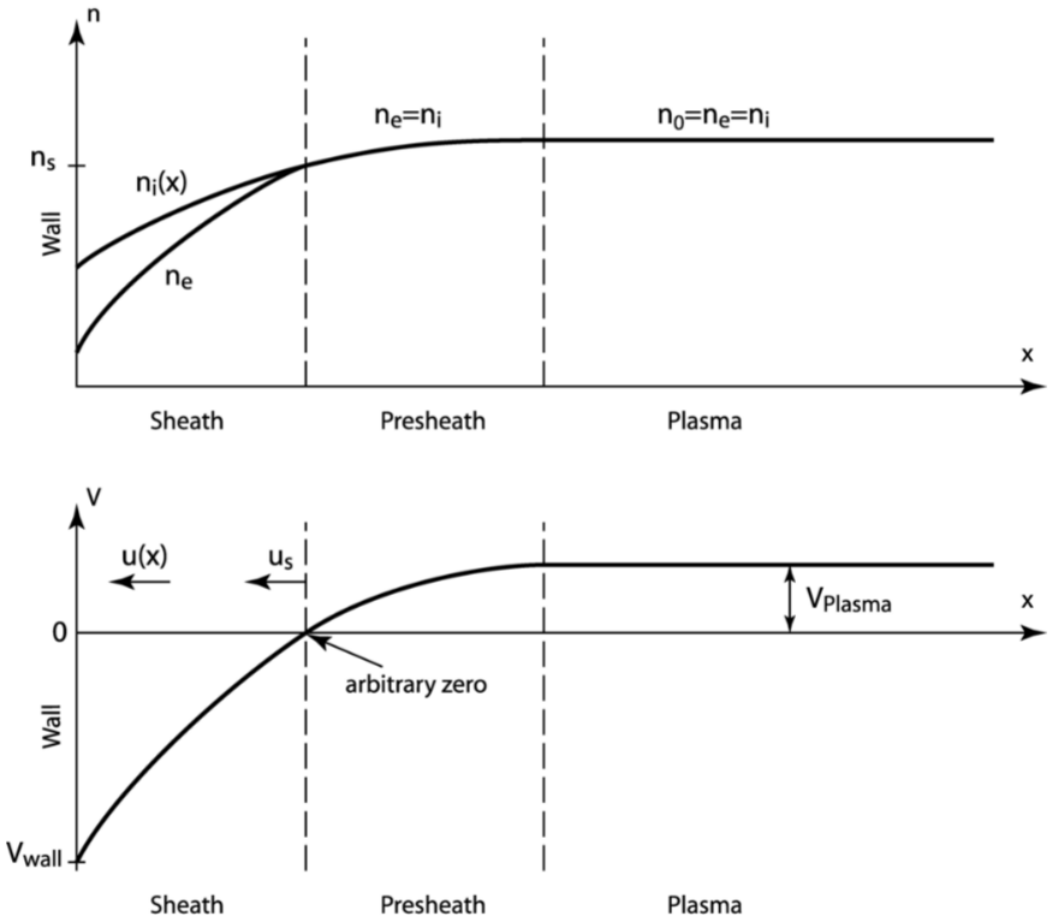

Figure 1.6: Depicts the plasma potential and positive and negative species density as a plasma interacts with a surface wall of the reactor. Reproduced from Scott Doyle (2019) [25], which itself is adapted from Chabert and Braithwaite (2011) Physics of Radio-Frequency Plasmas [27] © Cambridge University Press. Used here under fair dealing for academic purposes

surface of the reactor to maintain the conservation of mass, the flux of ions into the sheath is equal to the flux into the surface as shown in equation 1.3.4.

$$\Gamma_w = \Gamma_{sh} = n_{sh} u_B \tag{1.3.4}$$

Here, Γ_w and Γ_{sh} are the wall and sheath flux, respectively. The negative potential that forms between the plasma bulk and the surface wall of the reactor can be found by equating the flux of negative and positive charge carriers as shown in equation 1.3.5, assuming that there are no heavy negative charge carriers, and modelling electrons using kinetic theory and a Maxwell-Boltzmann velocity distribution [12].

$$n_s \left(\frac{eT_e}{m_i}\right)^{\frac{1}{2}} = \frac{1}{4} n_s \left(\frac{8eT_e}{\pi m_e}\right)^{\frac{1}{2}} \cdot exp\left(\frac{\phi_w}{T_e}\right) \tag{1.3.5}$$

Solving for the sheath potential ϕ_w yields equation 1.3.6 [12].

$$\phi_w = -T_e ln\left(\frac{m_i}{2\pi m_e}\right)^{\frac{1}{2}} \tag{1.3.6}$$

Here, n_s are the density of ions at the sheath edge, T_e is the electron temperature, and m_i and m_e are the mass of ions and electrons, respectively. Because the majority of energy gained by each ion impacting the surface is provided by acceleration caused by this potential, it can be seen that controlling the electron temperature can control the energy of ions impacting the surface.

1.3.3 Collision Processes Inside Plasmas

Inside plasmas, collisions between all types of particles are constantly occurring. These collisions cause various phenomena inside the plasma, depending on the interacting particle species and their energies, and can lead to ionisation, excitation, dissociation, or recombination. In all types of collision, three things are always conserved between the before and after states; momentum, energy and charge. The conserved total energy is made up of the sum of the kinetic and potential energy of the particles colliding. If the potential energy of all particles involved does not change, then the collision is said to be elastic, whereby all energy is exchanged as a change in the particles' velocities. However, if the potential energy of any of the particles changes, this is known as an inelastic collision, with kinetic energy being lost to processes that raise the energy level of an electron or remove the electron from the particle, exciting or ionising the atom. Conversely, if a collision causes an electron to decrease in the energy level, potential energy is converted into kinetic energy. This is known as a super-elastic collision [12]. Since many of the collisions necessary to produce particle species required for atomic layer processes require inelastic collisions and therefore reduce kinetic energy, not wasting energy producing excess particle species that are not necessary for the atomic processes is key to reducing energy consumption in atomic layer processes.

Cross Sections and Rate constants

Reaction cross sections and rate constants are used to quantify the likelihood of particles colliding and the rate at which interactions occur inside the plasma. A useful model is to imagine a stream of particles moving towards an area of stationary target particles. We can define the flux of the particles as $\Gamma = nv$ where n and v are the density and velocity of the particles, repetitively. If the target region has a density of n_g and thickness dx, the interaction rate is dependent on the overlap between these two populations [12]. The rate of change in the flux of the incident beam is therefore proportional to the cross section of the interaction, the density of the target, and the flux of the incident beam, as shown in 1.3.7 [12, 29].

$$d\Gamma = -\sigma \Gamma n_g dx \tag{1.3.7}$$

Here, σ is the cross sectional area of the collision which depends on the type of collision, for example, the electron impact ionisation cross section from Smirinov (1981, p. 253) can be seen in equation 1.3.8 [30].

$$\sigma_{iz} = \frac{\pi}{4}\left(\frac{e}{4\pi\epsilon_0}\right)^2 \frac{1}{\mathscr{E}}\left(\frac{5}{3\mathscr{E}_{iz}} - \frac{1}{\mathscr{E}} - \frac{2\mathscr{E}_{iz}}{3\mathscr{E}^2}\right), \quad \mathscr{E} > \mathscr{E}_{iz} \tag{1.3.8}$$

Here σ_{iz} is the ionisation cross section, $\mathscr{E}$ is the energy of the electron and $\mathscr{E}_{iz}$ is the ionisation energy. Equation 1.3.7, can be integrated to obtain the flux that had undergone collisions as shown in equation 1.3.9 [12, 29].

$$\Gamma(x) = \Gamma_0(1 - e^{-x/\lambda}) \tag{1.3.9}$$

Here, Γ_0 is the initial flux and λ is the mean free path of the beam, which is the distance over which the uncollided flux decreases to $1/e$ of the initial value where the mean free path can be defined in equation 1.3.10 [12].

$$\lambda = \frac{1}{n_g \sigma} \tag{1.3.10}$$

If the beam velocity is v we can define the mean time between interactions as τ, the collision frequency as ν and the collision frequency per unit density is known as the rate constant K. These collision parameters are defined in equations 1.3.11, 1.3.12 and 1.3.13 [12, 29].

$$\tau = \frac{\lambda}{v} \tag{1.3.11}$$

$$\nu \equiv \tau^{-1} = n_g \sigma v \tag{1.3.12}$$

$$K = \sigma v \tag{1.3.13}$$

However, in a realistic plasma the velocity of particles will not be constant and instead will follow a distribution of velocities for each particle. Therefore, to gain accurate rate constants, we integrate over the velocity distribution of the particles. If we consider the velocity distribution to be Maxwellian and the velocity of the target particles to be negligible, as is often assumed for low temperature plasmas, we can form an integral as shown in equation 1.3.14 [12].

$$K(T) = \left(\frac{m}{2\pi k_b T}\right)^{3/2} \int_0^\infty \sigma(v) v \cdot exp\left(-\frac{mv^2}{2k_b T}\right) 4\pi v^2 dv \tag{1.3.14}$$

Here, v is the velocity of the fast particles, and m and T are the mass and temperature of the incident particles, respectively. When integrated and simplified using $\mathscr{E} = \frac{1}{2}mv^2$ as shown in Lieberman and Lichtenberg (2005), these rate constants can be fitted to an Arrhenius form as shown in equation 1.3.15 [12].

$$K = AT_e^B \cdot exp\left(-\frac{\mathscr{E}_{th}}{T_e}\right) \tag{1.3.15}$$

Here, A and B are constants for each specific collision used to fit the equation to the experimental data and $\mathscr{E}_{th}$ is the threshold energy. The reaction rate R can be simply found by multiplying the rate constant by the number densities of the reactants $R = Kn_An_B$.

Atomic energy levels

An atom is made up of a positively charged heavy nucleus and light negatively charged electrons which orbit around the nucleus. For a single-electron hydrogen atom, this creates a force balance where the attractive Coulomb force holds the electron in a circular motion orbit. In a quantum description, the only valid orbits are such that the angular momentum is an integer value n of $\hbar$ where $n \geq 1$ and is called the principal quantum number. We can get a quantised radii as shown in equation 1.3.16 where for $n = 1$, a_o is the Bohr radius [12].

$$a_n = n^2 a_0 \tag{1.3.16}$$

The corresponding energies of each allowed orbit are shown in equation 1.3.17.

$$\mathscr{E}_n = -\frac{\mathscr{E}_{at}}{n^2} \tag{1.3.17}$$

Here, $\mathscr{E}_{at}$ is the ionisation potential of a hydrogen atom at $n = 1$ roughly equal to 13.6 eV [12]. Furthermore, for atoms with many electrons, the valence electrons, which are the electrons in the outermost often unfilled shell, are affected by both the attractive force of the nucleus and the repulsive force of all other electrons orbiting the nucleus. This leads to an altered radius as shown in equation 1.3.18 [12].

$$a_{eff} = a_0\left(\frac{\mathscr{E}_{at}}{\mathscr{E}_{iz}}\right)^{1/2} \tag{1.3.18}$$

Here, a_{eff} is the radius of the first Bohr orbit, $\mathscr{E}_{iz} = Z_{eff}^2\mathscr{E}_{at}$ is the ionisation potential and Z_{eff} is the effective nuclear charge felt by the valence electron reduced from the actual nuclear charge by electron shielding. However, this does not take into account the full quantum mechanical description, with additional quantum numbers of electrons being l, m_l, m_s [12]. Where l is the

orbital angular momentum with restrictions of $l+1 \leq n$, m_l is the component of the angular momentum in a particular direction with restrictions of $|m_l| \leq l$ and m_s is the direction of spin of the electrons where $m_s = \pm\frac{1}{2}$ [12].

For a more accurate model we use the centre-field model, where the atoms move under a symmetric potential field, which is inclusive of the other electrons average potential; the energy level of each orbit is dependent on n and l but each energy level has a degeneracy of $2n^2$ due to the Pauli exclusion principle [12]. The base electronic configurations inside this model are built by filling the lowest energy levels completely before moving onto the next. Where in the notation of AB^C, A is the principle quantum number n, B is the orbital angular momentum l where $l = 0, 1, 2, 3$ are s, p, d and f, respectively, and C is the number of electrons at that energy level, where each energy level can hold a maximum of $2(2l+1)$ electrons, the energy levels for 3s and above are shown in figure 1.7 [12]. For example, the electronic configuration of ground-state oxygen and argon is $1s^2 2s^2 2p^4$ and $1s^2 2s^2 2p^6 3s^2 3p^6$, respectively, where the last term is the energy level that contains the valence electrons. The valence electrons determine the behaviour in collisions of atoms because they are in the outermost electron shell and, therefore, have a lower ionisation energy than all other electrons as they are effected by the repulsive electromagnetic force of the other electrons in-between them are the nucleus. As such, due to their lower ionisation energy, valence electrons are the electrons affected by electron collisions such as ionisation and excitation; therefore, they are the electrons that change their energy level in a collision, and their energy level determines the ionisation energy and the energy required to excite the atom [12]. As such, atomic energy levels are important for understanding the collisions that occur within a plasma and the energy required for the reaction to occur.

1.3.4 Electron Collisions Inside Plasmas

Electron Collisions inside low-temperature plasmas allow for processes that require higher energies than those available from heavier species. This is because electrons involved in the collision can reach significantly higher temperatures than heavier species because of their low mass. Therefore, the average energy available is higher, allowing them to overcome higher threshold energies. The eight main types of electron Collisions inside plasmas are ionisation, excitation, de-excitation, dissociation, dissociative electron attachment, elastic collisions, electron impact detachment and electron ion recombination [12].

Ionisation

Inside a plasma, one of the most important reactions is electron impact ionisation, as it is the process that produces the charged species required to maintain the plasma. This occurs when a high-energy electron interacts with a neutral particle inside the plasma and knocks an electron out of orbit, as shown in equation 1.3.19. This requires a significant threshold energy because of the electrostatic potential well of a particle, and therefore, ionisation is highly dependent on the temperature of electrons. The threshold energy is determined by the size of the potential well for the most readily ionised electron in the particular particle species.

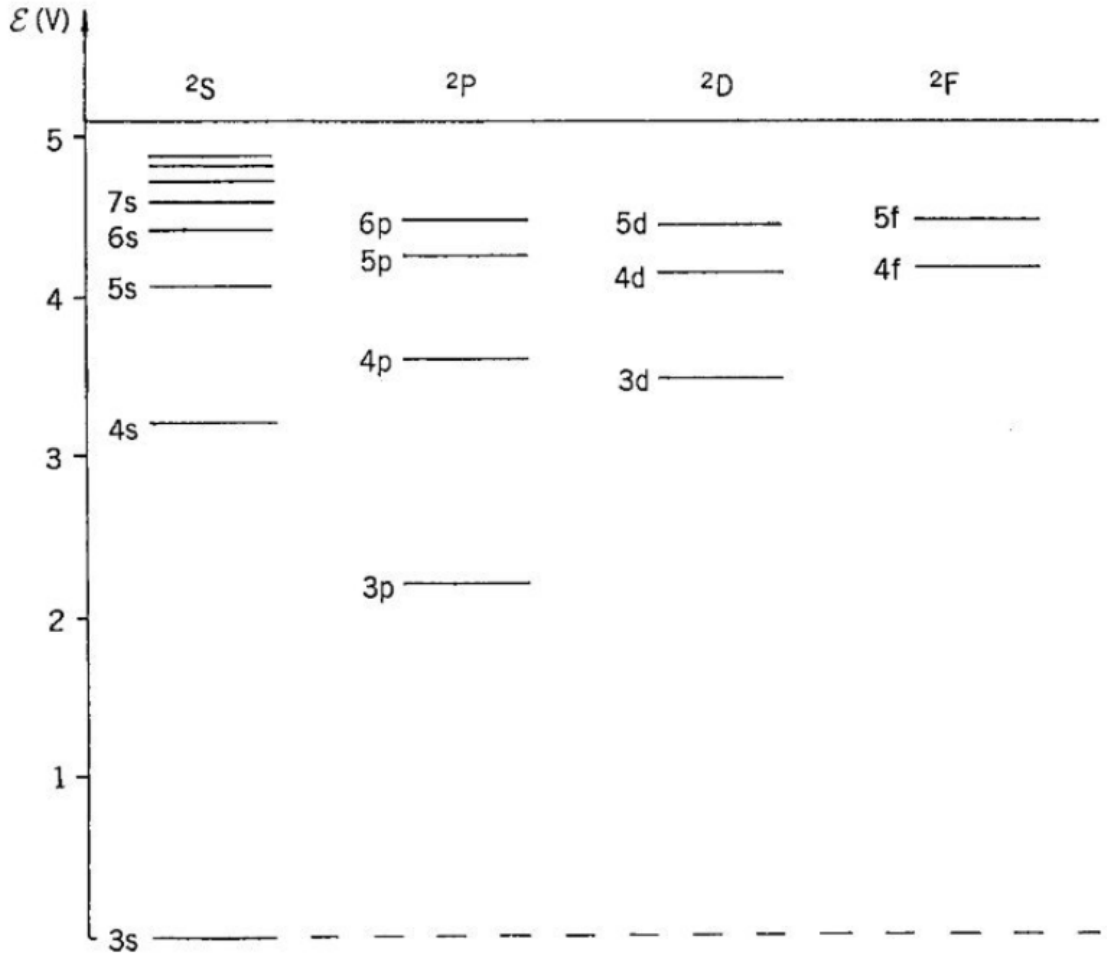

Figure 1.7: Energy level diagram for sodium without fine structure. Reproduced under fair dealing for academic purposes from Lieberman and Lichtenberg (2005) Principles of Plasma Discharges and Materials Processing [12], © John Wiley & Sons Inc.

$$e + A \rightarrow 2e + A^{+} \tag{1.3.19}$$

Here, A is a neutral particle and A^{+} is an ionised particle.

Excitation

Another process that can occur when an electron interacts with a neutral particle is the excitation of an electron to a higher energy level, as shown in equation 1.3.20. This decreases the size of the potential well that must be overcome in the ionisation process, therefore decreasing the threshold energy to produce ions. It also enables a higher probability that surface processes occur in ALD [31].

$$e + A \rightarrow e + A^{*} \tag{1.3.20}$$

Here, A is a neutral particle and A^{*} is an excited neutral particle. For an argon atom that undergoes the lowest energy level transition, it corresponds to the state change shown in equation 1.3.21.

$$3p^{6} \rightarrow 3p^{5}4s^{1} \tag{1.3.21}$$

De-excitation

Similarly to excitation, de-excitation occurs when an electron changes energy level in a neutral particle by dropping to a lower energy level. De-excitation can occur in two main ways, spontaneous or photon driven de-excitation, or collisional de-excitation. In spontaneous or photon driven de-excitation the excited electron drops down in energy levels emitting electromagnetic radiation at specific wavelengths, often in the ultraviolet range of the spectrum as shown in equation 1.3.22. The realised ultraviolet light has various effects on surface processes in various industries, some requiring ultraviolet light and some where ultraviolet light is unwanted [32–35]. In electron-driven de-excitation, an electron interacting with the neutral particle causes the energy level of the excited electron to drop. In this case, instead of emitting ultraviolet light, excess potential energy is converted into kinetic energy, increasing the velocities of the electron and the neutral particle as shown in equation 1.3.23. This requires significantly lower threshold energy than excitation; therefore, most electron collisions with excited particles have the energy required to de-excite the particle even at low electron temperatures.

$$A^{*} \rightarrow A \tag{1.3.22}$$

$$e + A^{*} \rightarrow e + A \tag{1.3.23}$$

Here, A^* is the excited neutral particle and A is the less excited neutral particle where A can be in an excited or ground state.

Dissociation

If the gas inside the plasma consists of molecules, e.g. oxygen, then an additional set of reactions can take place, called dissociation. This process involves breaking the bonds of a molecule so that individual atoms are separated inside the plasma, as shown in equation 1.3.24. The energy required to break the covalent bonds is typically lower than that of the ionisation energy. For example, O_2 has a dissociation energy of 498.4 $KJmol^{-1}$ which is equivalent to 5.17 eV compared to the ionisation energy of O_2 of 12.07 eV [36, 37].

$$e + A_2 \rightarrow e + 2A \tag{1.3.24}$$

Dissociative Electron Attachment

Dissociation can also occur where the electron becomes attached to one of the separated atoms. This creates a neutral atom and a negative ion, as shown in equation 1.3.25. This usually requires a lower threshold energy to occur than pure dissociation such as seen in equation 1.3.24 and therefore can allow dissociative electron attachment to dominate in low electron temperature plasmas [12].

$$e + A_2 \rightarrow A + A^- \tag{1.3.25}$$

Elastic Collisions

Ionisation, excitation and dissociation use the kinetic energy of the species to overcome the potential barrier and therefore decrease the kinetic energy of the particles after the interaction, which makes them inelastic. However, in some interactions, the species involved remain unchanged because the potential energy in both particles does not change. These collisions are called elastic collisions, as shown in equation 1.3.26. These collisions simply scatter and change the velocities of the particles involved. Also, because the threshold energy is zero, there is no exponential function in the rate constant and, depending on the reaction, there can be no dependence of T_e [32].

$$e + A \rightarrow e + A \tag{1.3.26}$$

Electron Impact Detachment

Electron impact detachment is an important reaction in the consumption of negative ions within the plasma. It occurs when an electron and a negative ion interact and causes the extra electron of the negative ion to be realised into the plasma bulk, as can be seen in equation 1.3.27. This requires energy to occur, as the electron needs to have sufficient energy to overcome the repulsive Coulomb force [12].

$$e + A^- \rightarrow A + 2e \tag{1.3.27}$$

Electron Ion Recombination

On average, the flux of positively and negatively charged particles onto the surface is equal. To maintain quasineutrality, the particles need to be reflected off the surface in equal quantities or neutralised. In reality, on the surface, the vast majority of particles are neutralised and then diffuse back into the plasma or are absorbed by the surface [12]. This reaction is called electron ion recombination. Surface-based electron ion recombination is the only high-rate neutralisation reaction, as the gas-based electron ion recombination mechanism shown in equation 1.3.28 is forbidden. This is because momentum cannot be conserved in the formation of one body from two. Unless the particle becomes excited after electron ion recombination; however, this has a rate coefficient lower than that of other electron ion recombination mechanisms; therefore, their contribution is negligible [38]. Therefore, when electron ion recombination occurs in the gas, it usually occurs with a three-body collision, as they have higher rates than the two body process; however, these occur less frequently than surface-based electron ion recombination [12].

$$e + A^+ \rightarrow A \tag{1.3.28}$$

The surface-based electron ion recombination is able to maintain a high rate because the third body is provided by the surface and therefore allows the momentum to be conserved, as shown in equation 1.3.29.

$$e + A^+ + S \rightarrow A + S \tag{1.3.29}$$

Dissociative Recombination

Another way to conserve momentum in the recombination of an electron and ion is through the dissociation of a molecular ion. This allows momentum to be conserved by splitting the molecular ion into two particles as shown in equation 1.3.30. Additionally, the two particles produced in this reaction can not both be in the ground state because the potential energy of A_2^+ is larger than the two constituent parts [12].

$$e + A_2^+ \rightarrow A + A^* \tag{1.3.30}$$

1.3.5 Heavy Particle Collisions Inside Plasmas

In addition to electron collisions inside plasmas, we can have collisions between exclusively heavy particles. They have a larger cross-sectional area but lower temperatures and velocities. Therefore, for collisions with high threshold energies, such as ionisation and excitation, they often have a reaction rate constant lower than that for electron plasma collisions, since the rate constant is now dependent on the heavy particle's temperature. However, there are still some collisions that are inelastic and alter the chemistry of the plasma, causing ionisation, recombination and dissociation [32].

Charge Exchange

When an ion and neutral atom interact, there is a chance that an electron can be exchanged from the neutral particle to the ion. In a multi-species plasma this can happen between any species. Because of electromagnetic potentials inside the sheath that accelerate the ion before collision, the ion has a velocity significantly higher than that of a neutral atom. This high velocity of the particle is maintained after the charge exchange as shown in equation 1.3.31 whereby the neutral atom becomes the particle with higher velocity [12]. This is useful if you require an increase in neutral gas temperature, for example, in a neutral electrothermal plasma thruster on a spacecraft [25, 39].

$$A(slow) + B^+(fast) \rightarrow A^+(slow) + B(fast) \tag{1.3.31}$$

Associative Detachment

Another common reaction that can occur is the associative detachment of a heavy negative particle and a heavy neutral particle to form a heavier neutral molecular particle and eject an electron, as shown in equation 1.3.32. This can only occur in this way so that the momentum is conserved in the collision, as without the ejection of the electron momentum would not be conserved. This can take place in plasmas that contain molecular gases, i.e. oxygen, so that the covalent bonds between the atoms are reformed, but it can also occur in noble gases.

$$A^- + B \rightarrow AB + e \tag{1.3.32}$$

Positive-Negative Ion Recombination

Positive-negative ion recombination occurs when a positive and negative ion interacts and exchanges the extra electron from the negative ion to the positive ion forming two heavy neutral particles, as can be seen in equation 1.3.33. For negative ions in a low pressure plasma, this can become a dominant loss mechanism [12]. This reaction can also occur in the form of a three body reaction as seen in equation 1.3.34.

$$A^- + B^+ \rightarrow A + B \tag{1.3.33}$$

$$A^- + B^+ + C \rightarrow A + B + C \tag{1.3.34}$$

Dissociation

Dissociation can occur when two heavy particles interact and break the covalent bonds in a molecule, splitting the molecule as shown in equation 1.3.35. The particle being split must be molecular; however, the other particle involved can be atomic with no ability to form covalent bonds, i.e., argon. In addition, the particles produced from splitting the molecule do not need to be atomic; they can also still be molecules.

$$A + BC \rightarrow A + B + C \tag{1.3.35}$$

Ion-Neutral Elastic Scattering

Ion-neutral elastic scattering is similar to charge exchange collisions; however, the electron does not transfer from the neutral atom to the ion. Therefore, because no potential energy change has occurred, this is an elastic collision as shown in equation 1.3.36. This collision simply scatters the ion and neutral particles, changing their velocities. For example, inside the plasma sheath ions are accelerated towards the surface of the reactor through the electromagnetic potential. Ion-neutral elastic scattering can cause the ions inside the sheath to lose speed in the direction of the surface, therefore, potentially reflecting ions inside the sheath back into the plasma bulk, reducing the flux to the surface.

$$A + B^+ \rightarrow A + B^+ \tag{1.3.36}$$

Neutral-Neutral Elastic Scattering

Neutral-neutral elastic scattering collisions are elastic collisions in which the colliding particles are unchanged as shown in equation 1.3.37. These types of collisions only scatter the particles and transfer kinetic energy between the neutral particles.

$$A + B \rightarrow A + B \tag{1.3.37}$$

Sputtering

When heavy particles impact the surface with energies above the threshold energy, atoms can be sputtered from the surface as shown in equation 1.3.38. The threshold energy is different depending on the material; for example, germanium has a threshold energy of 20 eV. This is typically achieved by ions because of the potential that accelerates the particle through the sheath onto the surface. Etching rates can be increased by increasing the energy of these ions to greater than 500 eV [12]. However, for use in ALE processes, this is not possible, as it leads to poor selectivity between the mask, other layers and the desired material to be etched, and for the surface to become over-etched because these high energies are outside the ALE energy window of typical materials such as germanium [12].

$$A^+ + B_{Surface} \rightarrow A^+ + B_{Gas} \tag{1.3.38}$$

Neutral Particle Adsorption

When neutral particles diffuse onto a surface, they can be absorbed as shown in equation 1.3.39. This can be done in one of two ways: physisorption, where the atom or molecule is attracted to the surface by the weak van der Waals force, and chemisorption, where a chemical bond is formed between the atom or molecule and the surface [12].

$$A + S \rightarrow A : S \tag{1.3.39}$$

The fraction of atoms or molecules that stick to a surface is defined as the sticking coefficient s. The absorbed flux can be found in equation 1.3.40 [12].

$$\Gamma_{abs} = s\Gamma_s \tag{1.3.40}$$

Here, Γ_{abs} is the absorbed flux and Γ_s is the flux incident on the surface of the reactor. This is an important measure for analysing the neutral surface fluxes used in ALD. For efficient ALD, high fluxes are required, as well as a high sticking coefficient, to allow atoms and molecules to be readily absorbed.

1.4 Plasma Chemistry

The chemistry that occurs in a plasma is very complex with a large number of reactions occurring and can vary significantly depending on the composition of elements inside the plasma. At its most basic, a plasma formed from purely noble gases involves electron ionisation, electron excitation collisions, heavy-particle elastic collisions and surface collisions. This causes a complex system with continuous collisions between positive and negative charged particles, neutral ground and excited atoms and free electrons, and a continuous flux of positively and negatively charged particles to the surface. However, if we introduce a molecular gas that has an incomplete outer shell of valence electrons, i.e. oxygen. we get a large number of new species types that can form. Molecules can dissociate and recombine to form atomic particles or molecules with more atoms, such as O and O_3 from O_2 with each of these forming their own ions and excited states. In addition, atoms without a full outer shell of valence electrons can readily absorb electrons to fill the outer shells. This creates a heavy negative ion that affects the flux balance to the surface of the reactor and potential inside the plasma. Therefore, to model the complex nature of a plasma, a large number of reactions and species are imperative to accurately model the chemistry inside a plasma.

1.4.1 Argon-Oxygen Plasmas

In this thesis, the gas mixtures studied are either pure argon or an argon-oxygen mixture. Argon, as a noble gas, can only be excited or ionised and, as such, has a limited set of reactions and species. This simplicity means that the production of ions for ALE can be performed efficiently. Furthermore, because of the full outer shell of the valence electrons, argon is chemically inert, making it ideal for precise physical sputtering processes without altering the chemical composition of the surface or causing additional chemical reactions to other materials. As such, it is used extensively in biomedical applications and for ALE in microelectronics production, materials processing [33, 40–43]. In an oxygen-argon plasma, there is both an atomic and a molecular gas present when the plasma forms. This causes a vastly larger reaction and species set, which could lead to energy being wasted producing species which are not required for the desired process. In addition, because the outer shell of valence electrons is incomplete, oxygen is significantly more reactive than Argon. This allows surface effects such as absorption and oxidation to occur, allowing the chemical makeup of the surface to be altered and is widely used in biomedical applications and in ALD for industrial manufacturing [31, 44–47].

1.5 Thesis Outline

The remainder of the thesis is laid out as described below:

Chapter 2 (Method):
Plasma modelling is introduced with several methods discussed. The simulation model used in this thesis is introduced and the underlying equations described. Finally, the geometry of the modified Gaseous Electronics Conference (GEC) reference cell is discussed.

Chapter 3 (Argon Dynamics for ALD):
Investigation into the effect of changing the pressure and pulsed power waveform parameters of the frequency and duty cycle on argon ion production and flux in a pure argon plasma. This chapter culminates in an analysis of the change in energy per ion incident onto the surface.

Chapter 4 (Pressure Effect on ALD):
Investigation into the effect of changing the pressure on the production and flux of oxygen ions and atomic oxygen in a mixed argon-oxygen plasma. This chapter culminates in an analysis of the change in energy per ion and atomic oxygen incident onto the surface.

Chapter 5 (Conclusion):
Concludes key results and their impact on the energy per ion incident onto the surface and their affect on atomic layer processing.

Chapter 2

Method

In this chapter, the principles of plasma modelling are introduced, and the nuances between particle and fluid models are discussed. After this, the global model for argon-oxygen inductively coupled plasmas that is used throughout this thesis is introduced. The method employed to initialise and undertake a five-step cycle to update the simulation in time is discussed, and the principles equations behind the physics in each step are introduced. Finally, the reactor being modelled is introduced, the validity of the model is discussed, and the methods used to analyse the data and calculate the efficiency of surface fluxes are discussed.

2.1 Plasma Numerical Models

Plasma numerical models are useful tools for testing hypotheses and possible reactor parameters cheaply and quickly without investing time and money into an experimental prototype. Plasma numerical models are systems of equations along with boundary conditions that iterate through a number of steps to converge onto a solution. These models are typically non-analytical as, due to the collective behaviour of plasma, they typically cannot be resolved analytically without large assumptions that will restrict the type of systems that can be simulated. Numerically modelling plasmas comes with a lot of challenges, with a large number of particles, in the order of $> 10^{20}$ for neutral particles, collision and non-collisional effects, and reactions constantly occurring, which affect the plasma gas chemistry. This, combined with the varied time scales of plasma numerical models (10 ns - 10 s), allows us to easily see that there is no completely accurate method for simulating a plasma in its entirety [25, 48, 49]. The remainder of this section will discuss the three main types of technique used to model plasmas; kinetic models, fluid models and global modals.

2.1.1 Kinetic and Fluid Models

Kinetic models consider each particle or group of 'superparticles' inside the volume of the simulation separately, where each particle's motion is determined by Newton's law of motion with forces applied by physical and electromagnetic sources experienced by that particle inside the plasma. Superparticles are a group of $10^5 - 10^7$ particles that represent the characteristics of a particle species in time and space. The most common types of kinetic models are the particle in cell (PIC) model and the Monte Carlo collisional model [50, 51]. PIC models use a continuous mesh to treat the dynamics of a particle while using Poisson's equation to calculate the associated electric field on a discrete mesh [52]. The Monte Carlo collision model is used to determine when and what type of collision occurs between different groups of superparticles using a stochastic method. The two models are often used in conjunction with each other with PIC models modelling the motion of superparticles and the Monte Carlo algorithm handling the collisions. These are considered to be the highest standard of models available as they require a small amount of assumptions to be placed on the plasma. However, with particle counts exceeding 10^{20}, these simulations have a large computational expense, and as such there exists a trade-off between the time taken to run a simulation and the complexity of the model.

Fluid models consider the macroscopic properties of the plasma such as densities, fluxes and temperatures rather than the individual particles [53, 54]. The macroscopic properties are determined by taking moments of the Boltzmann equation to obtain conservation equations for the particle mass, flux and energy from the zeroth, first and second moments, respectively [55]. This requires an additional assumption or knowledge of the electron energy distribution function before determining the electron transport coefficients and reaction rate, which is commonly obtained by using a zero-dimensional Boltzmann solver iteratively throughout the simulation or beforehand or, assuming the shape of the energy distribution for each species beforehand [25, 53, 54, 56]. The benefit of fluid models is the reduced computational expense of simulations; this allows a larger number of simulations to be run within a specific time frame or higher-dimensional (2D or 3D) simulations to be run, improving the spatial accuracy of the model. However, since the electron energy distribution function is based on the local value of mean energy and the electric field, the model begins to breakdown as pressure decreases. This is due to particle kinetics becoming increasingly non-local at lower pressure as lower pressure leads to a higher mean free path and lower collision frequency, which allows electrons to travel further within the reactor before colliding [54].

2.1.2 Zero-Dimensional (OD) Chemical Kinetic Global Models (GM)

Global models solve the same governing equations as fluid models where the spatial derivative's are neglected within the moments of the Boltzmann equation. Although spatial dependence has been neglected, global models can still use assumed spatial gradients to aid in calculations in the model, such as the density gradient through a sheath [57]. The spatially averaged values of these plasma properties mean that they represent the plasma as a whole and not a

particular point in the plasma unlike higher-dimension simulations, and this is why they are often considered to be OD models. The temporally dependent particle and energy rate balance equations typically solved by GM's remove the momentum balance equation, as the momentum is not resolved when the spatial component is neglected [58]. The balance equations for particles and energy are made up of source and loss terms for the specific particle species being tracked. These source and loss terms are dependent on the specific chemical reactions included in the model, the transport effects modelled, and any assumptions used within the model. The terms for particle balance are typically the gain or loss of particles caused by reactions occurring inside the plasma and the flux of charged particles to the surface walls of the system. The terms for the energy balance equation are typically the energy absorbed from the power coupling method, energy changes from elastic, superelastic and inelastic collisions, and energy lost through the flux of charged particles to the surface walls of the system [32]. The energy balance equation is often only solved for electrons inside low-temperature plasmas because heavy species are at a much lower temperature than electrons with low amounts of energy coupled to them. The electron source equations are usually dependent on an electron energy distribution function that is usually assumed to be Maxwellian, but the model can be coupled with a zero-dimensional Boltzmann solver to obtain the electron energy distribution function, as in a fluid model [32, 57]. The decreased number of dimensions needed to be solved decreases computational expense and leads to faster generation of spatially averaged values of the density and temperatures of systems that would otherwise be difficult to model. In addition, due to reduced computational expense, these models typically include a larger number of species and types of reactions, allowing greater insight into the chemical kinetics within a plasma [32, 57, 58]. However, the larger chemical reaction scheme included in global models requires accurate rate coefficients and cross sections, which often have large uncertainties with different sources producing values that vary from source to source and are also only valid for certain pressure or temperature regimes. Therefore, when constructing global models, it is difficult to produce a complete reaction set with accurate values of rate coefficients and cross sections that are within the desired operating regime so that these do not affect the accuracy of the results [59].

2.2 Argon Oxygen Global Model

This thesis uses a GM for low pressure Ar/O_2 inductively coupled plasmas that has been developed by Michel Osca Engelbrecht et al. (2024) and the explanation of the GM in the following sections of this thesis is based on the explanation given in their paper [32]. This GM has been extended by Michel Osca Engelbrecht et al. into a plasma chemical-kinetic model from the collisional radiative model developed by M. Fiebrandt et. al. (2020) and is built with methods developed and used by J. T. Gudmundsson and E. G. Thorsteinsson (2007) [60, 61]. In addition, the basic construction of equations used within the GM is adapted from J. T. Gudmundsson and E. G. Thorsteinsson (2007) and Hurlbatt et al. (2017) [58, 61]. In this work, the GM is used without modification and is applied to perform a parameter study in which gas composition, input power, pressure, duty cycle and frequency are varied, and the resulting plasma properties

are analysed.

The GM has been developed to model a cylindrical container that contains a plasma in a volume of length L and radius R where the power P_{in} is coupled into the plasma inductively, using the Julia programming language [32, 62]. Several input parameters can be changed to alter the simulation with both a constant power option and a pulsed square-shaped power waveform. For both the constant and pulsed square waveform, the input parameters consist of total pressure p_T, input power P_{in} and oxygen mixture fracton χ_{O_2} which is the fraction of the initial gas made up of O_2. For the pulsed square waveform, there are additional input parameters of frequency f, duty cycle D and power amplitude P_{amp}, which is the value of power when the power is turned on and replaces the input power where the input power is calculated instead using $P_{in} = DP_{amp}$. The pulsed square waveforms repeat in pulses at a frequency f. At the beginning of each pulse, the power changes nearly instantaneously to the constant value equal to the power amplitude. It remains at constant power for a period of time determined by the duty cycle D, which represents the fraction of the cycle in which the power is on. After this period of time, the input power changes nearly instantaneously to zero and remains at zero until the next cycle to form a square shape. The square pulsed waveform shape has been chosen as it is a very common waveform shape for pulsed etching and deposition processes [63]. The numerical order of operations of the GM consists of an initialisation of the simulation base conditions, and then a five-step cycle that updates the simulation by time Δt as shown in figure 2.1 [32]. The initial simulation base conditions required to be defined in advance are the length L and radius R of the cylindrical reactor and the length of time of the simulation T_{end}. In addition to the initial temperature of electrons T_e and heavy particles T_N, the density n_s of each species and the plasma input parameters. After initialisation of the simulation base conditions, the model iterates in a five-step cycle. It computes plasma properties and a new electron temperature and species density value and then advances time by Δt until the simulation time length is reached $t \geq t_{end}$, after which the simulation ends. The five steps of the cycle are described briefly below, and steps 2-4 are expanded in section 2.2.4 and step 5 is expanded in sections 2.2.2 and 2.2.3. The equations used to calculate the system parameters in Step 1 are described where they are first used in Steps 2-5.

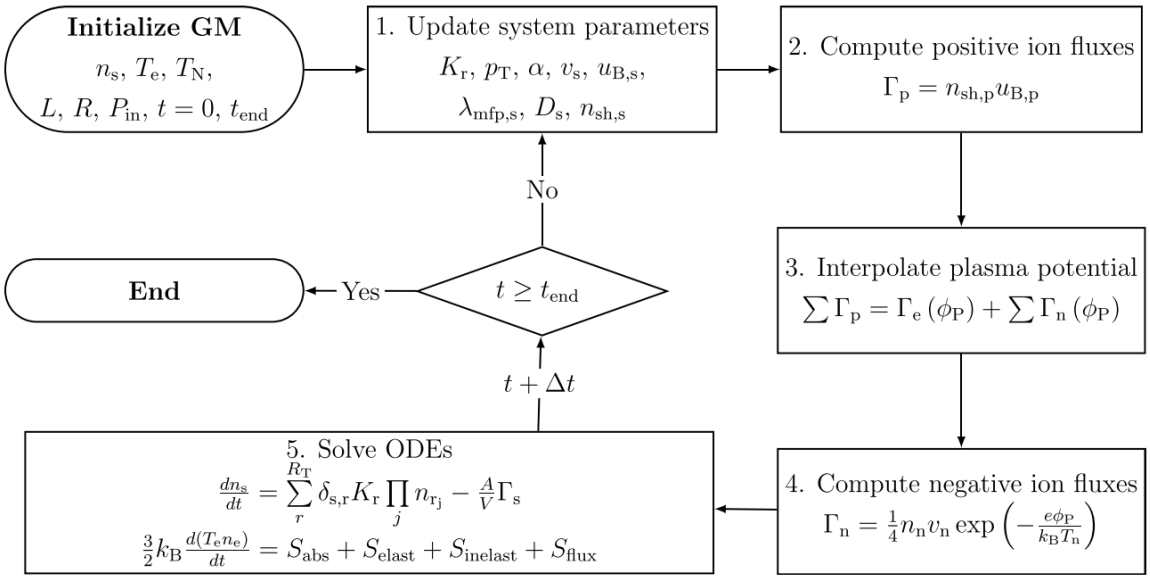

Figure 2.1: Flow chart that depicts the order of operations of the 0D plasma chemical kinetic GM. Reproduced from Engelbrecht Et Al. (2024) [32], Plasma Sources Science and Technology, licensed under CC by 4.0

Step one consists of the calculation of the system parameters used in the later steps. These include reaction rate coefficients K_r, total pressure p_T, electronegativity α, thermal speed v_s, and species specific: Bohm velocity $\mu_{B,s}$, mean free path $\lambda_{mfp,s}$, diffusion coefficient D_s and number density at the edge of the plasma sheath $n_{sh,s}$ [32]. Steps two to four consist of the calculation of positive and negative ion surface fluxes Γ and the plasma potential ϕ_P, these steps are described further in section 2.2.4. Step five uses the ordinary differential equation (ODE) solver Rosenbrock23 in the DifferentialEquations library to solve a system of ODEs formed by mass and energy continuity equations, these are discussed further in sections 2.2.2 and 2.2.3 [32, 64].

2.2.1 Plasma Species and Important Chemical Reactions

The species list used in the GM was collected by Michel Osca Engelbrecht et al. (2024), based on previous simulation work of plasmas containing argon and oxygen, as can be seen in table 2.1 [32, 60, 61, 65].

Table 2.1: Species used inside the GM [32]

Species	Atomic Level
e	
Ar	
Ar^+	
Ar(4P)	$3s^2 3p^5(2P^0_{3/2})4p, 3s^2 3p^5(2P^0_{1/2})4P$
Ar^m	$3s^2 3p^5(2P^0_{3/2})4s_2, 3s^2 3p^5(2P^0_{1/2})4s_0$
Ar^r	$3s^2 3p^5(2P^0_{3/2})4s_1, 3s^2 3p^5(2P^0_{1/2})4s_1$
O_2	
O_2^+	
O_2^-	
$O_2(a^1\Delta_u)$	
$O_2(b^1\Sigma_u^+)$	
O	$2s^2 2p^4(^3P_{2,1,0})$
O^+	
O^-	
$O(^1D)$	$2s^2 2p^4(^1D_0)$
$O(^1S)$	$2s^2 2p^4(^1S_0)$
$O(^3S)$	$2s^2 2p^3(^3S^0)3s(^3S^0_1)$
$O(^5S)$	$2s^2 2p^3(^3S^0)3s(^5S^0_2)$
$O(^3P)$	$2s^2 2p^3(^3S^0)3p(^3p_{1,2,0})$
$O(^5P)$	$2s^2 2p^3(^3S^0)3p(^5p_{1,2,3})$
O_3	
$O_3(v)$	
O_3^+	
O_3^-	
O_4	
O_4^+	
O_4^-	

The excited states of argon have been grouped into 3 separate groups, the 4p radiative states and the s-level radiative and metastable states. The only difference between the two states in each group is the total angular momentum. However, they behave chemically identically and can easily be grouped together [32]. The main reactions involved in the results from the plasmas modelled in this thesis are listed in table 2.2, where the complete list of plasma reactions is collected by Michel Osca Engelbrecht et al. (2024) as a compendium of reactions

from various sources [32, 58, 60, 61, 65, 66].

Table 2.2: Main Reactions Involved in the Plasmas Modelled in this Thesis [32]

#	Reaction	$E_{thr}(eV)$	$K_r(m^{3+3(N_r-2)}s^{-1})$	References
1	$e+O \rightarrow 2e+O^+$	13.6	$4.93\cdot10^{-15}T_e^{0.723}exp(-13.2/T_e)$	[65, reaction 12][67]
2	$e+O \rightarrow e+O(^1D)$	1.96	$8.45\cdot10^{-15}T_e^{-0.306}exp(-3.13/T_e)$	[65, reaction 13][67]
3	$e+O \rightarrow e+O(^1S)$	4.18	$1.04\cdot10^{-15}T_e^{-0.134}exp(-4.19/T_e)$	[65, reaction 14][67]
4	$e+O(^1D) \rightarrow 2e+O^+$	11.65	$4.93\cdot10^{-15}T_e^{0.723}exp(-11.64/T_e)$	[65, reaction 15]
6	$e+O(^1S) \rightarrow 2e+O^+$	9.43	$4.93\cdot10^{-15}T_e^{0.723}exp(-9.42/T_e)$	[65, reaction 17]
10	$e+O_2 \rightarrow 2e+O_2^+$	12.06	$2.32\cdot10^{-15}T_e^{0.990}exp(-12.51/T_e)$	[65, reaction 21][68, 69]
11	$e+O_2 \rightarrow e+O+O(^1D)$	8.5	$3.12\cdot10^{-14}T_e^{0.017}exp(-8.05/T_e)$	[65, reaction 22][70]
82	$e+O_2^+ \rightarrow O+O(^1D)$	0	$9.1\cdot10^{-15}T^{-0.7}$	[65, reaction 151] [71–73]
83	$e+O_2^+ \rightarrow O(^1D)+O(^1S)$	0	$6\cdot10^{-15}T^{-0.7}$	[65, reaction 152] [71–73]
107	$e+Ar \rightarrow 2e+Ar^+$	15.76	$2.3\cdot10^{-14}T_e^{0.59}exp(-17.44/T_e)$	[61, 74]
271	$O_2+Ar^+ \rightarrow O_2^++Ar$	0	$4.9\cdot10^{-17}(300/T_N)^{0.78}$	[61, 75]
274	$O+Ar^+ \rightarrow O^++Ar$	0	$6.4\cdot10^{-18}$	[61, 76]
301	$O^++O^- \rightarrow 2O$	0	$3.1\cdot10^{-14}(300/T_N)^{1.1}$	[65, reaction 186][77]

Table 2.3: Main Plasma Surface Reactions Involved in the Plasmas Modelled in this Thesis. Here, γ is the Sticking Coefficient

#	Reaction	γ	$K_r(s^{-1})$	References
343	$O^+ \rightarrow O$	N/A	$2u_{B,O^+}\frac{R^2h_{L,O^+}+RLh_{R,O^+}}{R^2L}$	[61]
344	$O_2^+ \rightarrow O_2$	N/A	$2u_{B,O_2+}\frac{R^2h_{L,O_2^+}+RLh_{R,O_2^+}}{R^2L}$	[61]
347	$Ar^+ \rightarrow Ar$	N/A	$2u_{B,Ar^+}\frac{R^2h_{L,Ar^+}+RLh_{R,Ar^+}}{R^2L}$	[61]
352	$2O \rightarrow O_2$	$0.1438e^{\frac{2.5069}{p_{O_2}}}$, $p_{O_2}>2$ mTorr $1-\frac{p_{O_2}}{4}$ otherwise	$\left[\frac{\Lambda^2}{D_O}+\frac{2V(2-\gamma_0)}{Av_0\gamma_0}\right]^{-1}$	[61]
353	$O(^1D) \rightarrow O$	1.0	$\left[\frac{\Lambda^2}{D_{O(^1D)}}+\frac{2V(2-\gamma_{O(^1D)})}{Av_{O(^1D)}\gamma_{O(^1D)}}\right]^{-1}$	[60]
354	$O(^1S) \rightarrow O$	1.0	$\left[\frac{\Lambda^2}{D_{O(^1S)}}+\frac{2V(2-\gamma_{O(^1S)})}{Av_{O(^1S)}\gamma_{O(^1S)}}\right]^{-1}$	[60]

In total, there are 393 reactions included. The reaction rate coefficients for the electron impact reactions are described as functions of the electron temperature assuming a Maxwellian electron energy distribution function [32]. The reactions between charged particles and the surface of the system are discussed in detail in section 2.2.4 and the reactions between neutral particles and the surface of the system are discussed in detail in section 2.2.6. The atomic energy level

transitions and radiative processes are discussed in section 2.2.7 and in more detail in Michel Osca Engelbrecht et al. (2024) [32].

2.2.2 Mass Balance Equations

To achieve mass continuity within the GM, a mass balance equation is used for each species s, in table 2.1 [32]. The mass balance equation calculates the rate of change in time of the density of each species s, as can be seen in equation 2.2.1 [32].

$$\frac{dn_s}{dt} = \sum_{r}^{R_T} \delta_{s,r} K_r \prod_{j} n_{r_j} - \frac{A}{V}\Gamma_s \tag{2.2.1}$$

The rate of change in time for the density of each species s, is represented by the left-hand side of the equation. The gain or loss of particles as a result of the total reactions R_T included in the reaction set is represented by the first term on the right-hand side. The mass variation caused by the rth reaction is the product of the densities of the j reacting species n_{r_j} with the rate coefficient K_r and the integer factor $\delta_{s,r}$. The integer factor represents the particle balance of species s in reaction r where $\delta_{s,r} > 0$ represents a mass gain of species s, $\delta_{s,r} < 0$ represents a mass loss of species s and $\delta_{s,r} = 0$ represents an equilibrium in the mass of species s in reaction r [32]. For example, in reaction 301 $O^+ + O^- \rightarrow 2O$ found in table 2.2, $\delta_{O^+,301} = -1$, $\delta_{O^-,301} = -1$ and $\delta_{O,301} = 2$, as one positive and negative oxygen ion is effectively lost as they exchange charges to create two neutral atomic oxygen particles. The second term on the right-hand side accounts for the mass variation caused by the flux and subsequent neutralisation of charged particles to the surface walls of the system Γ_s where A is the surface area and V is the volume of the cylindrical system [32].

2.2.3 Energy Balance Equations

To achieve energy continuity within the GM, an energy balance equation is used to calculate the rate of change in time of the electron temperature, where the temperatures of heavy particles are assumed to be constant in time. The rate of change in time of the electron temperature can be seen in equation 2.2.2, where the shape of the energy distribution function is assumed to be Maxwellian [32].

$$\frac{3}{2}k_B \frac{d(T_e n_e)}{dt} = S_{abs} + S_{elast} + S_{inelast} + S_{flux} \tag{2.2.2}$$

Here in the left hand side of the equation k_B is the Boltzmann constant, T_e is the electron temperature and is the metric used to represent energy and n_e is the electron density. In the

right hand side S_{abs} is the absorbed input power per unit volume, S_{elast} are the energy changes caused by elastic collisions, $S_{inelast}$ are the energy changes caused by superelastic and inelastic collisions and S_{flux} is the kinetic energy lost by fluxes of electrons and ions through the sheath. The rate of absorption of the input power is shown in equation 2.2.3 [32].

$$S_{abs} = \frac{P_{in}}{V} \tag{2.2.3}$$

Here, P_{in} is the power coupled to the electrons through the inductive power source. The energy changes caused by elastic collisions between neutral heavy particles N and electrons in the form of $e + N \rightarrow e + N$ are shown in equation 2.2.4 [32].

$$S_{elast} = -3 \sum_{l}^{Relast} \frac{m_e}{m_{N_l}} k_B (T_e - T_N) K_l n_e n_{N_l} \tag{2.2.4}$$

Here, R_{elast} is the number of elastic collisions between electrons and neutrals included inside the GM, m_e is the mass of an electron. Additionally, m_{N_l}, T_{N_l} and n_{N_l} are the mass, temperature and density of the neutral species N_l, respectively, and K_l is the reaction rate coefficient of the collision between electrons and neutral species N_l. The electron energy changes caused by superelastic and inelastic collisions are shown in equation 2.2.5 [32].

$$S_{inelast} = -\sum_{r} E_{thr,r} K_r \prod_{r_j} n_j \tag{2.2.5}$$

Here, $E_{thr,r}$ is the energy absorbed or released by the rth collision, K_r is the reaction rate coefficient of the rth collision and n_j is the density of jth reacting species in collision r. The kinetic energy lost by the electrons and ions that pass through the sheath and are subsequently lost at the surfaces is shown in equation 2.2.6 as described in [12, 32].

$$S_{flux} = -\frac{A}{V}\left[2k_B T_e \Gamma_e + \sum_{p}\left(\frac{1}{2}k_B T_e + q_p \phi_P\right)\right] \tag{2.2.6}$$

Here, Γ is the flux of particles to the surface walls of the system, where the subscripts p and e are for positive ions and electrons, respectively, q_p is the electric charge of the positive ion and ϕ_P is the plasma potential. The kinetic energy lost at the surfaces by the particles that pass through the sheath is split into two terms on the right-hand side. The first term is for electrons and the second term is for positive ion particles. The method used by the GM to treat and calculate these particle fluxes is described in the section 2.2.4 below.

2.2.4 Ion Flux to the Surface Walls of the System

Ion fluxes through the plasma sheath and onto the surface are an important factor in plasma processing. Ion flux also has an imperative role in the balance of mass and energy inside the plasma simulation continuity equation as well as in calculating the plasma potential, which is required to compute the fluxes of negative ions and the electron energy equation. The first portion of this section discusses positive ion surface fluxes denoted by a subscript of p and the second portion of this section discusses negative ion surface fluxes, denoted by a subscript e for electrons and the subscript n for negative ions and the plasma potential.

Positive Ions

The surface flux of positive ions is calculated using equation 2.2.7 [32].

$$\Gamma_p = n_{sh,p} u_{B,p} \quad \text{where} \quad u_{B,p} = \sqrt{\frac{k_B T_e}{m_p}} \tag{2.2.7}$$

Here, $n_{sh,p}$ is the density of positive ion species p at the edge of the sheath and $u_{B,p}$ is the Bohm velocity, which is the velocity required for the ions to enter the sheath. The density of ions at the edge of the sheath is calculated using equation 2.2.8 [12, 32, 78].

$$n_{sh,p} = \frac{R^2 h_{L,p} + RL h_{R,p}}{R^2 + RL} n_p \tag{2.2.8}$$

Here, n_p is the bulk plasma density for positive ion species p, R is the radius and L is the height of the cylindrical system, as well as the parameters $h_{L,p}$ and $h_{R,p}$ which are depicted in equation 2.2.9 [32, 79, 80].

$$h_{\{R,L\},p} = \left[\left(\frac{h_{\{R,L\}0}}{1 + 3\alpha/2} \right)^2 + h_c^2 \right]^{1/2} \tag{2.2.9}$$

Here, factors $h_{R0,p}$, $h_{L0,P}$ and h_c enable the calculation of the density at the edge of the sheath at both low and high pressure and low and high electronegativity as described in a paper by E. G. Thorsteinsson et al. (2010) and the references within [79]. The h factors are calculated using the equations 2.2.10, 2.2.11 and 2.2.12 [32].

$$h_{R0,p} = 0.8\left[4 + \frac{\eta R}{2\lambda_{mfp,p}} + \left(\frac{0.8Ru_{B,p}}{\chi_{01}J_{1(\chi 01)}D_{a,p}}\right)^2\right]^{-1/2} \tag{2.2.10}$$

$$h_{L0,p} = 0.86\left[3 + \frac{\eta L}{2\lambda_{mfp,p}} + \left(\frac{0.86Lu_{B,p}}{\pi D_{a,p}}\right)^2\right]^{-1/2} \tag{2.2.11}$$

$$h_c = \frac{1}{\gamma_-^{1/2} + \gamma_+^{1/2}\left[n_{*,p}^{1/2}n_+/n_-^{3/2}\right]} \tag{2.2.12}$$

Here, $_{\chi_{01}} \simeq 2.405$, J_0 is the first zero of the zero order Bessel function and J_1 is the Bessel function 1 of the first kind [32]. The electronegativity of the plasma is the ratio of the densities of negative ions and electrons inside the plasma as described in equation 2.2.13 [32].

$$\alpha = \frac{1}{n_e}\sum_n n_n \tag{2.2.13}$$

Here, n_e is the density of electrons and n_n is the density of all species of negative ions. The estimate of the mean free path of each species inside the model is shown in equation 2.2.14 [32].

$$\lambda_{mfp,p} = \frac{1}{\sum_s n_s\sigma_{ps}^T} \tag{2.2.14}$$

Here, n_s is the density of species s and σ_{ps}^T is the total collision cross section between species p and s where the superscript T denotes the total. The mean free path between a specific species s and species p is: $\lambda_{mfp,ps} = 1/n_s\sigma_{ps}^T$. The species' s are only heavy mass species, and therefore the mean free path includes only ion-ion and neutral-ion collisions and other processes such as coulomb collision, elastic scattering and charge exchange. The cross section values used when calculating the mean free path for collisions are approximated using equation 2.2.15 [32].

$$\sigma_{ps} \simeq \frac{K_r}{\nu_{ps}} \quad \text{where} \quad \nu_{ps} = \sqrt{\frac{8k_BT_N}{\pi\mu_{ps}}} \tag{2.2.15}$$

Here, ν_{ps} is the mean speed of relative motion, μ_{ps} is the reduced mass and T_N is the temperature of heavy mass species [12]. For the processes of elastic scattering and charge exchange, if the cross section is available, then it is extracted from the following references [12, 61, 81]. If cross sections are not available, they are calculated using the hard-sphere model using the following radius of atomic and molecular radii: $r_{Ar} = 188\ pm$, $r_O = 152\ pm$, $r_{O_2} = r_{O_3} = r_{O_4} = 197\ pm$ and equation 2.2.16 [32].

$$\sigma_{ps} = \pi(r_p + r_s)^2 \tag{2.2.16}$$

Here, r_p and r_s are the radius of species p and s repetitively. Additionally, the cross section estimate used for Coulomb collisions has a constant value of 5×10^{-19} m^2 [79]. The ratio between the temperatures of the positive and negative ions η is described in equation 2.2.17 [32].

$$\eta = \frac{2T_+}{T_+ + T_-} \tag{2.2.17}$$

Here, T_+ is the average temperature of all positive ion species and T^- is the average temperature of all negative ion species. The ambipolar diffusion coefficient $D_{a,p}$ is described in equation 2.2.18 [32].

$$D_{a,p} = D_p \frac{1 + \gamma_p + \gamma_p \alpha}{1 + \gamma_p \alpha} \tag{2.2.18}$$

Here, D_p is the diffusion coefficient for ions and neutrals and γ_p is the temperature ratio between electrons and the positive ion species p as described in equation 2.2.19 [32].

$$\gamma_p = \frac{T_e}{T_p} \tag{2.2.19}$$

Here, T_e is the electron temperature and T_p is the temperature of the specific positive ion species p, where for negative ions this will become $\gamma_n = T_e/T_n$ where T_n is the temperature of the specific negative ion species. The diffusion coefficient for ions and neutrals is described in equations 2.2.20, 2.2.21 and 2.2.22 [32].

$$D_p = \frac{1}{\sum_s \frac{1}{D_{ps}}} \tag{2.2.20}$$

$$\text{where,} \quad D_{ps} = \frac{K_B T_N}{\mu_{ps} \nu_{ps}} \tag{2.2.21}$$

$$\text{and} \quad \nu_{ps} = n_s \sum_r K_r \tag{2.2.22}$$

Here, D_{ps} is the binary diffusion coefficient between positive ion species s and the sth heavy mass species, and ν_{ps} is the total collision frequency between species p and species s. The parameter h_c uses temperature ratios $\gamma_- = T_e/T_-$ and $\gamma_+ = T_e/T_+$, which for the simulations used in this thesis the temperature of the ions and neutrals are equal and therefore $T_+ = T_- = T_N$ and $\gamma_- = \gamma_+$. The factor $n_{*,p}$ is calculated as described in equation 2.2.23 [32].

$$n_{*,p} = \frac{15}{56} \frac{\eta^2}{K_{rec} \lambda_{mfp,p}} \nu_p \tag{2.2.23}$$

Here, K_{rec} is the effective rate coefficient based on the recombination reactions that can be seen in table A6 inside Michel Osca Engelbrecht et al. (2024) [32].

2.2.5 Negative Ions and Plasma Potential

The flux of negative ions is described in equation 2.2.24 [32, 82].

$$\Gamma_n = \frac{1}{4} n_n v_n exp\left(-\frac{e\phi_P}{k_B T_N}\right) \quad \text{where,} \quad v_n = \sqrt{\frac{8k_B T_N}{\pi m_n}} \tag{2.2.24}$$

Here, the subscript n stands for negative ion species n and this equation is also valid for electrons where the subscript n can be replaced by an e to gain the surface flux of electrons Γ_e. Furthermore, ϕ_P is the plasma potential, e is the elementary charge and v_n and m_n are the thermal speed and mass of the negative ion species n, respectively. Because the plasma potential contains negatively charged species inside the plasma bulk, the flux of negative species to the surface is restricted to the particles with energy high enough to overcome the potential barrier of the plasma potential. Therefore, to calculate the flux of electrons and negative ions, the plasma potential must be known, which is calculated by solving a flux balance equation. The flux balance equation states that the total flux of electrons and all positive and negative ion species to the surface must be balanced to maintain quasineutrality of the charge inside the plasma. The flux balance equation is shown in equation 2.2.25 [32].

$$\sum_p q_p \Gamma_p + q_e \Gamma_e + \sum_n q_n \Gamma_n = 0 \tag{2.2.25}$$

Here, q_p, q_n and q_e is the charge of positive ion species p, negative ion species n and electrons, respectively. The flux balance equation is solved for the plasma potential ϕ_P using an iterative method which can then be used for the flux term in the energy balance equation 2.2.6 and the negative flux equation 2.2.24 [32]. In the GM both positive and negative ions that make contact with the surface wall of the system become neutralised to maintain mass conservation [61]. The reactions are listed in table 2 inside Michel Osca Engelbrecht et al. (2024) [32] which has been extended from J. T. Gudmundsson 2007 [61] with the important reactions for this thesis listed at the bottom of table 2.2. The rate of these reactions is such that the equation 2.2.26 is balanced [32, 61].

$$\frac{A}{V}\Gamma_s = \delta_{s,r} n_s K_r \tag{2.2.26}$$

Here, the rates are included in the mass balance equation 2.2.1 for both reactants and products of the neutralisation reactions.

2.2.6 Neutral Diffusion to the Surface Walls of the System

The diffusion of neutral particles within the plasma is important for plasma processes such as ALD, as it determines the surface flux of neutral species to the surface walls of the system [12, 78]. This is important because reactions at the surface de-excite metastable species and recombines atomic oxygen into diatomic molecular oxygen, and therefore neutral wall reactions, like the one used in ALD, depend heavily on the specific species diffusion properties. These reactions are shown in table 3 within Michel Osca Engelbrecht et al. (2024), where the important reactions for this thesis are at the bottom of table 2.2 [32]. The effective loss rate coefficient to the surface walls of the system for the neutral species N is shown by equation 2.2.27, where the equations for the effective diffusion length, Λ and the thermal speed of the neutral species N, ν_N are shown in equation 2.2.28 [32, 83, 84].

$$K_{D,N} = \left[\frac{\Lambda^2}{D_N} + \frac{2V(2-\gamma_N}{A\nu_N\Gamma_N}\right]^{-1} \quad \text{where,} \tag{2.2.27}$$

$$\Lambda = \left[\left(\frac{\pi}{L}\right)^2 + \left(\frac{2.405}{R}\right)^2\right]^{-\frac{1}{2}} \quad \text{and,} \quad \nu_N = \sqrt{\frac{8k_BT_N}{\pi m_N}} \tag{2.2.28}$$

Here, Λ is the effective diffusion length within a cylindrical reactor, D_N, γ_N and ν_N are the diffusion coefficient, sticking coefficient and thermal speed of the neutral species N, respectively [83]. Furthermore, the diffusion coefficient and the mean free path equations are identical to equations 2.2.14 and 2.2.20 but for the neutral species N. The sticking coefficient depends on several factors, two of particular importance being the surface wall material and the operating pressure of the reactor [61, 78]. The GM uses values taken from simulations conducted with similar operating conditions where all sticking coefficients except ground state atomic oxygen are constant parameters [32, 60, 61]. The sticking coefficient of ground state atomic oxygen is dependent on pressure as shown in equation 1.3.40 [32]. The values of the sticking coefficient that are important for the results in this thesis can be found at the bottom of table 2.2, and the sticking coefficients for all the neutral species included within the GM in table 3 inside Michel Osca Engelbrecht et al. (2024) [32].

$$\gamma_O = \begin{cases} 1 - p_{O_2}[mTorr]/4, & p_{O_2} < 2mTorr \\ 0.1438exp(2.5069/p_{O_2}[mTorr]), & otherwise \end{cases} \tag{2.2.29}$$

Here p_{O_2} is the pressure of O_2 within the reactor in $mTorr$ and the expressions have been derived for stainless steel reactors [61]. Please note that for all simulations used within this thesis, the pressure is greater than 2 $mTorr$.

2.2.7 Atomic Energy Transitions

The radiation process of the dexcitation of excited states from energy level a to a lower energy level b through the emission of radiation at a wavelength of λ_{ab} is included in this GM with rates described by Einstein coefficients for spontaneous emission. The reactions that include a radiative component are shown in figure 2.2 and in table 4 inside Michel Osca Engelbrecht et al. (2024) [32]. For higher energy-level transitions, a cascade process is used to simplify the transitions to reduce the complexity of the collisional radiative scheme [32, 60].

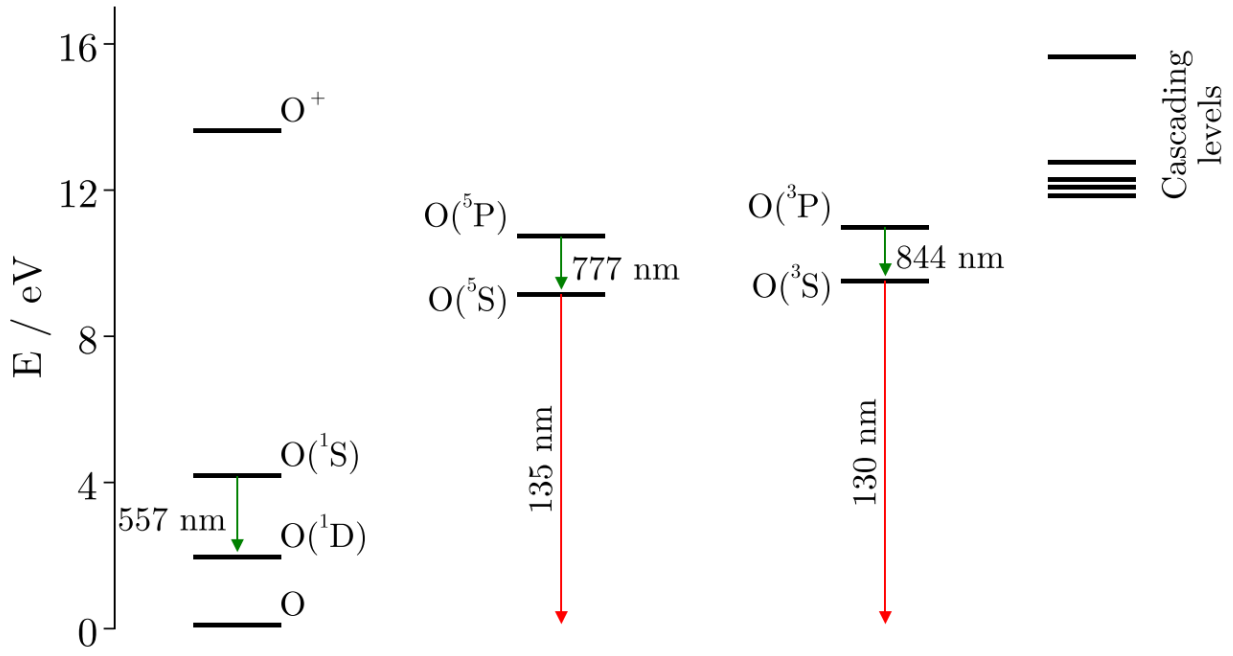

Figure 2.2: Energy level diagram of atomic oxygen with the radiative transitions included inside the GM shown. The cascading levels shown are a representative subset of existing high energy levels. [85]. Reproduced from Engelbrecht et al. (2024) [32] Plasma Sources Science and Technology, licensed under CC by 4.0. Figure originally adapted from Fiebrandt et al. (2020) [60], Plasma Sources Science and Technology, licensed under CC by 4.0.

Cascading processes collect several energy transitions into a single reaction without the need to know the intermediate states in-between. Typically, reactions that require the use of cascading processes are electron excitation of atomic oxygen or dissociative exciton of O_2, which can excite to a high energy level before quickly decaying to a lower state that is included in the GM [32]. This is included in the GM as a simplification as modelling each step in the cascading decay down to the lower state with Einstein coefficients would significantly increase the complexity of the collisional radiative scheme [32]. Several reactions are included in the GM that include cascades; these include electron excitation of atomic oxygen, as well as a number of reactions that are based on emission cross sections that include cascade processes. Such as the electron

dissociation of O_2 in reaction number 381 in table A7 within Michel Osca Engelbrecht et al. (2024) [32] $e + O_2 \rightarrow e + 2O + \lambda_{130.4}$ where a wavelength of 130.4 nm is released due to the contribution of cascading processes. A more in-depth explanation of these processes and how they are incorporated into the GM is provided by Michel Osca Engelbrecht et al. (2024) [32].

Another physical mechanism captured by the GM is self absorption [32]. Self absorption is an effect where a particle in the lower energy state of an energy transition reabsorbs the emitted photon from the energy transition and therefore excites back to the higher energy state. This is important to be included in the model due to its impact on the densities of the emitting species as well as the intensity of radiation leaving the plasma [32]. This is achieved in the GM by adding an escape factor γ_{ab} as a correction to the spontaneous emission Einstein coefficient A_{ab}, which is done following an approach by M. Fiebrandt et. al [60]. The emission rate K_{ab} is shown in equation 2.2.30 and the intensity per unit volume I_{ab} is shown in equation 2.2.31 for atomic transitions where self absorption is a factor [32].

$$K_{ab} = \gamma_{ab} A_{ab} \tag{2.2.30}$$

$$I_{ab} = K_{ab} n_a \tag{2.2.31}$$

Here, A_{ab} is the Einstein coefficient for spontaneous emission, n_a is the density of the upper energy level a and γ_{ab} is the escape factor calculated using an empirical formula from R. Mewe (1967) and as shown in equation 2.2.32 [32, 86].

$$\gamma_{ab} = \frac{2 - exp(-10^{-3} \kappa_{ab,0} R)}{1 + \kappa_{ab,0} R} \tag{2.2.32}$$

Here, this factor is correct where Doppler broadening is the dominant line boarding mechanism as is true for the low pressure conditions inside the plasmas used in this thesis. Furthermore, $\kappa_{ab,0}$ is the absorption coefficient at the centre of the emission line, which is calculated as shown in equation 2.2.33, which is from T. Holstein (1947) [32, 87].

$$\kappa_{ab,0} = n_b A_{ab} \frac{g_a}{g_b} \frac{\lambda_{ab,0}^3}{8\pi} \sqrt{\frac{m_N}{2 k_B T_N \pi}} \tag{2.2.33}$$

Here, n_b is the density of the lower energy level b, g_a is the statistical weight of the energy level a, g_b is the statistical weight of the energy level b and $\lambda_{ab,0}$ is the central wavelength of the emission line.

The species used in this GM as shown in table 2.1 consists of a number of species that are made up of grouped states. This is useful for the plasma-chemical model due to their similar energies; however, the fact that their radiation is emitted at different wavelengths needs to be accounted for. Therefore, the density distribution of the states within each grouped state must

be estimated following the approach in [60]. The density of each multiplet level n_m is shown in equation 2.2.34 [32].

$$n_m = \frac{g_m}{\sum_i g_{m_i}} n_g \tag{2.2.34}$$

Here, g_m are the statistical weights of each multiplet level within the group state, n_g is the density of the grouped state, and $\sum_i g_{m_i}$ is the sum of the statistical weights of each multiplet level in the grouped state. For more details on the effect of grouped states and their statistical weights on the species in table 2.1, see the paper by Michel Osca Engelbrecht et al. (2024) [32].

2.3 Simulation Geometry and Operating Parameters

The geometry of the reactor used for the simulations inside this thesis is based on a modified version of the gaseous electronics conference (GEC) reference cell [88]. The modified GEC reference cell is a cylindrical inductively coupled plasma reactor which consists of a five-turn circular coil on the top of the reactor and a grounded electrode on the bottom of the reactor. The dimensions of the reactor consist of a distance of 43 mm between the coil and the electrode and a radius of 51 mm as shown inside the red dashed box in figure 2.3, however, this has been approximated in the simulations carried out in this thesis to 4 and 5 cm, respectively [89]. The rest of the figure depicts the design of the real reactor, including the electrodes and gas flow.

The plasma input parameters used in this thesis vary from a base case, with each chapter investigating the effect on the efficiency of surface fluxes with a different parameter variation. The base case is depicted in table 2.4 where the parameters being varied are frequency, duty cycle average power, pressure and whether the oxygen mixture fraction is 0.1 or 0, with the rest being a constant in all simulations. The oxygen mixture fraction is the proportion of the plasma that is made up of O_2 so that $n_{Ar} = (1-\chi_{O_2})n_T$ and $n_{0_2} = \chi_{O_2} n_T$ where χ_{O_2} is the oxygen mixture fraction and n_T is the total neutral gas density determined from the initial pressure, temperature and volume. The initial density of the ions is divided between the argon and O_2 ions in proportion to the oxygen mixture fraction with the initial electron density equal to the total initial ion density to maintain quasineutrality so that $n_e = n_{O_2^+} + n_{Ar^+} = n_p$ where n_p is the total initial density of ions. The rest of the neutral and charged species start with an initial density of zero.

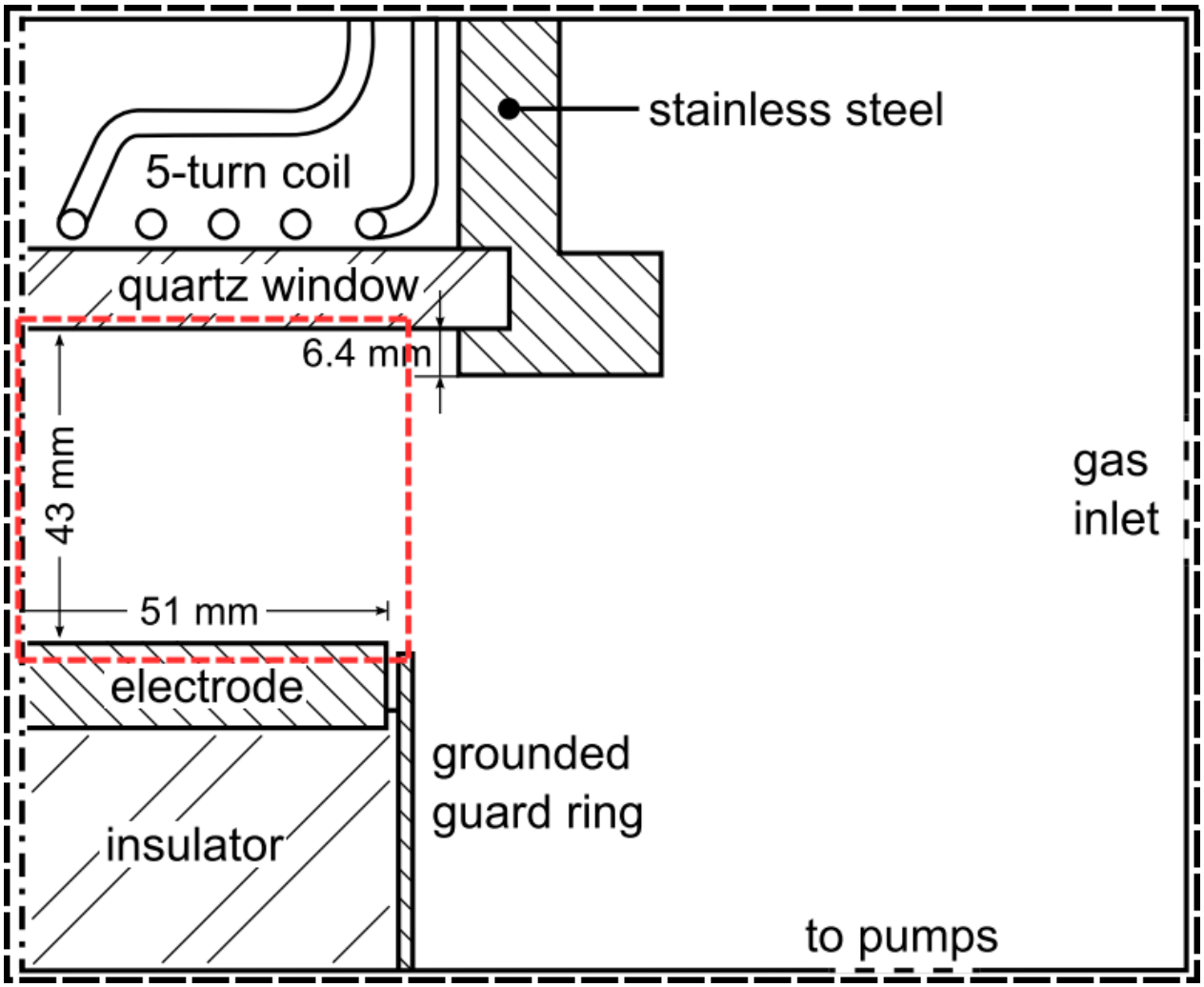

Figure 2.3: Depicts the geometry of the modified GEC reference cell where the cylindrical reactor simulated in this thesis is the region inside the red dashed box. Adapted from A. Greb (2013) [89]. Licensed under CC by 2.5.

Table 2.4: Depicts the Initial Simulation Parameters of the Base Case

Oxygen Gas Mixture Fraction	Frequency (kHz)	Duty Cycle	Average Power (W)	Pressure (Pa)
0.1	10	0.5	400	5

Neutral Gas Temperature (K)	Initial electron Temperature (eV)	Simulation End Time (s)
1000	1.5	0.005

Initial Density of Ions (m^{-3})	Initial Density of Electrons (m^{-3})
1×10^{10}	1×10^{10}

In chapter 4 a pressure variation from 1 to 25 Pa is applied at multiple average powers between 200 and 1000 W to a gas with an oxygen mixture fraction of 0.1. In chapter 3 the oxygen mixture fraction is set 0 to create a pure argon plasma, and a frequency variation of 5 to 50

Khz and a duty cycle variation from 0.1 to 0.9 is applied at multiple average powers between 200 and 600 W. Furthermore, a pressure variation of 0.5 to 25 Pa is applied at multiple average powers between 200 and 1000 W.

2.4 Validity of Results

This GM has been extensively compared to experimental measurements using a similar inductively coupled cylindrical reactor with geometry of a radius of 20 cm and distance between the coil and grounded electrode of 20 cm which possesses electron and Ar^m density's and electron temperatures similar to those found in the plasmas simulated in this thesis by Michel Osca Engelbrecht et al. (2024) [32]. The comparison shows that the simulation results follow experimental measurements qualitatively over a wide range of pressures, average powers and oxygen mixture fractions, and since the reactor geometry and properties are similar, results from modified GEC reference cell have a strong likelihood to follow qualitatively to experimental measurements. An additional caveat to note is that the experimental comparison by Michel Osca Engelbrecht et al. (2024) was performed with plasmas simulated using a constant power deposition, whereas plasmas simulated in this thesis are using pulsed power deposition [32]. The experimental comparison of pulsed power deposition plasmas is something that should be done in the future; however, it is expected to still follow qualitatively to experimental measurements. Therefore, this GM can be used accurately to control and improve the efficiency of flux in atomic layer processes inside the modified GEC reference cell. Furthermore, the assumption of a constant heavy particle temperature of 1000 K is shown to not have a strong influence on the qualitative trend and therefore will not have an effect on the results in this thesis [32].

2.5 Power Pulse and Data Analysis Methods

The shape of the power pulse can vary based on the input parameters. The pulsed power cycle repeats at a frequency f where at the beginning of the cycle the input power goes to the power amplitude calculated by $P_{amp} = D \cdot P_{avg}$ for the proportion of the cycle defined by the duty cycle D before returning to a power of 0 W. This type of waveform is known as a square waveform and can be seen in figure 2.4 where figure 2.4a represents the base case power waveform, and figure 2.4b shows how the waveform is affected by changing the duty cycle to 0.2. Please note that the average power is kept the same between each different duty cycles by changing the maximum amplitude as well as the length of time the power is on.

The rapidly changing power in the pulsed power regime creates densities and other plasma parameters that form a dynamic equilibrium throughout the time of the simulation. This dynamic equilibrium forms where shortly after the breakdown of the plasma the properties of the plasma begin to cycle around a point of equilibrium with the period of the frequency of the power cycle as can be seen in figure 2.5. Therefore, the simulation timespan is long enough

for the data to be representative of the plasma properties even if the power is coupled into the plasma for longer.

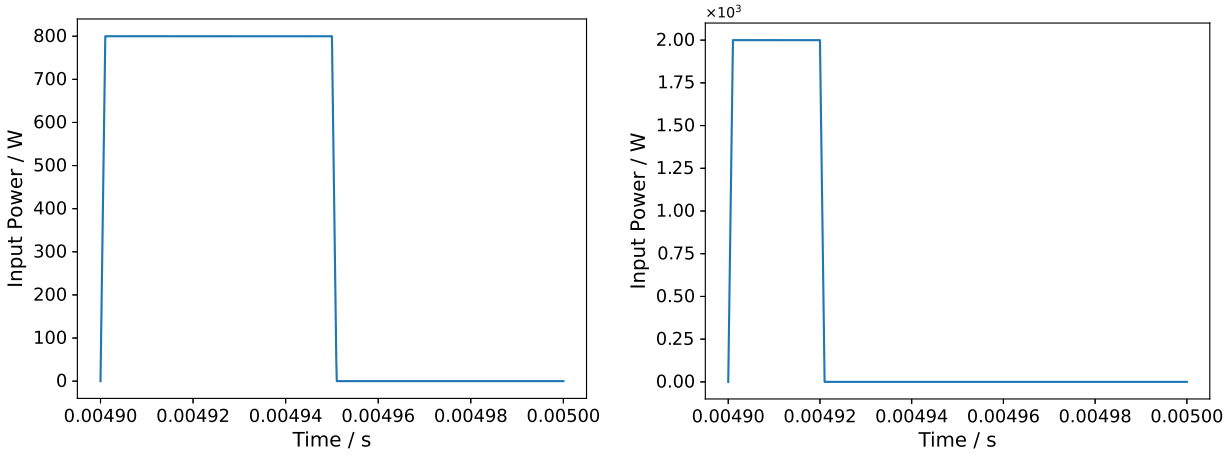

(a) (b)

Figure 2.4: Depicts the Input Power of the Last Pulse as a Function of Time with a Frequency of 10 Khz and an Average Power of 400 W. Here (a) has a Duty Cycle of 0.5 and Peak Power of 800 W and (b) has a Duty Cycle of 0.2 and Peak Power of 2000 W

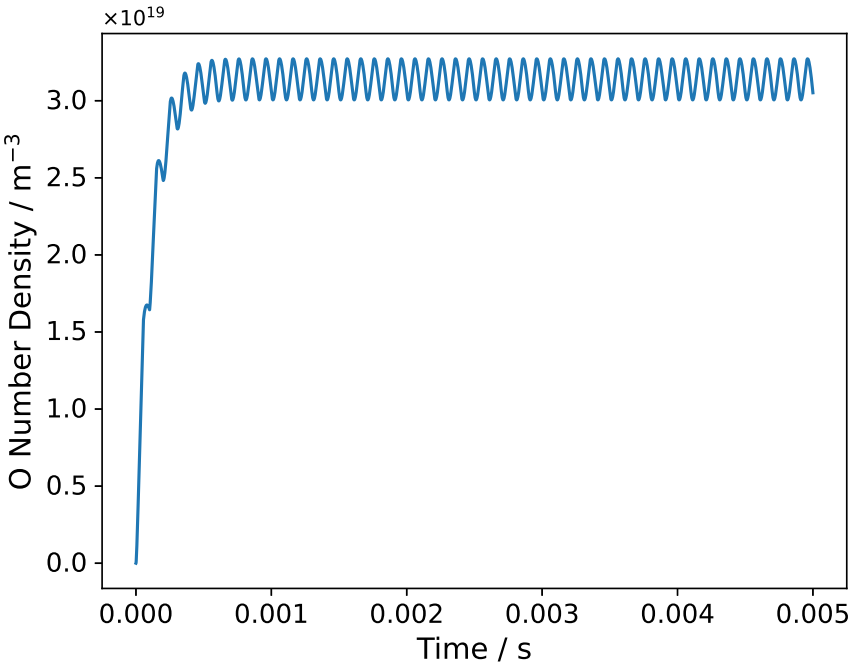

Figure 2.5: Depicts the Number Density of Atomic Oxygen as a Function of Time across the Whole Timespan of the Simulation

Since each pulse is identical, an average of the data during the last pulse of the dynamic equilibrium can be used to create a data point that is representative of the whole plasma. This is

achieved by using the NumPy trapz function in python to average the values in the last pulse [90]. This function computes a time integrated value of the data that accounts for the difference in time steps between, then the time integrated value is divided by the time span of the last pulse to gain an averaged value. To average the values of the argon only simulations for the purpose of ALE processing, the shape of the plasma potential across the final pulse needs to be taken into account. This is because only the surface flux of argon ions inside the energy window of the surface material to be etched should be considered. The vast majority of the energy of ions that impact the surface is gained by accelerating across the plasma potential of the sheath. Therefore, only the region of time where the plasma potential is inside the energy window of the surface material that is being etched should be considered. The shape of the plasma potential during the last pulse of the base case can be seen in figure 2.6.

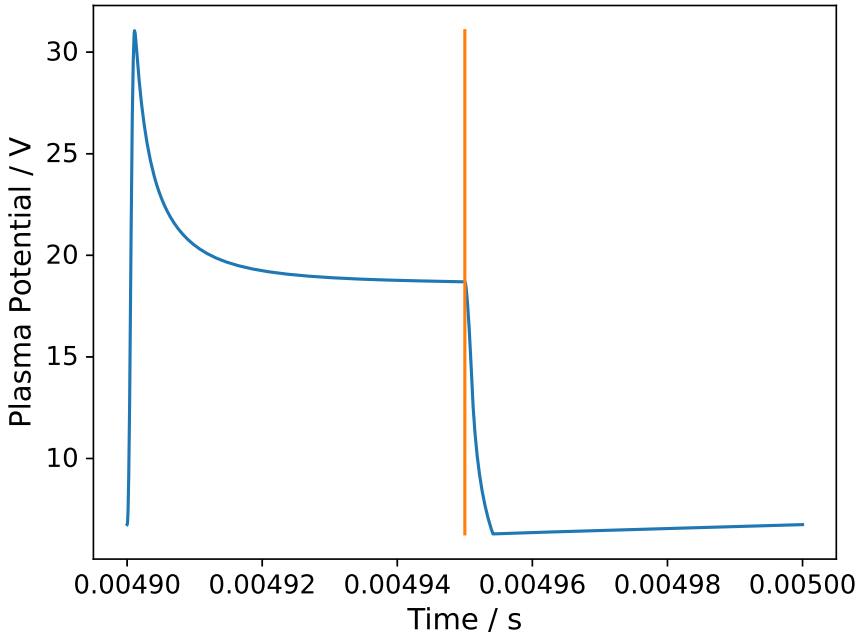

Figure 2.6: Depicts the Plasma Potential during the Last Pulse of the Base Case as a Function of Time, where the orange line denotes where the power is turned off during the last pulse. Here, the Frequency is 10 Khz, the Duty Cycle is 0.5, the Pressure is 5 Pa, the Average Power is 400W and the Oxygen Mixture Fraction is 0.1

In figure 2.6 the plasma potential spikes when the power is initially turned on and then decays to a consistent value, which changes based on the plasma input parameters. Once the power is turned off, the potential decreases significantly to less than 10 eV. This is important as the energy window for germanium is between 20 and 30 eV. Germanium is chosen because inductively coupled plasmas typically produce plasma potentials that lie in this range for pressure values used in the simulations in this thesis, and other materials possess an energy window higher than this plasma potential [40, 82]. Therefore, the time frame where the plasma potential is sufficient for etching germanium is only the beginning of the pulse where the power is on. So, to average the argon-only simulation values, which are used when investigating plasmas for the purpose of ALE processes, the same method is applied, but only over the portion of the

pulse when the power is on, and then divided by that amount of time. Please note that whilst the spike in the beginning of the pulse can be outside of the energy window, the duration of the spike is brief and is unlikely to affect the results.

An important equation for the results is how the efficiency of the flux of particles to the surface walls of the reactor is calculated. The efficiency is defined as the energy per particle fluxed to the surface and is calculated as seen in equation 2.5.1 by dividing the energy inputted into the plasma in the last pulse by the surface fluence in the last pulse.

$$E_{\Phi_s} = \frac{E_P}{\Phi_s} \tag{2.5.1}$$

Here, E_{Φ_s} is the energy per particle fluxed to the surface measured in Joules J, E_P is the energy of the last pulse where $E_P = \frac{P_{avg}}{f}$ and Φ_s is the surface fluence in the last pulse. The surface walls fluence is calculated by using the same method to average surface flux values as above, however, not dividing by the length of time of the pulse to get a total particle count fluxed to the surface instead, where for argon only plasmas in chapter 3 it is the total particle count fluxed to the surface inside the time the power is on.

Additionally, the flux used in the discussion of the effects on atomic oxygen ground and excited states, which informs the energy per particle fluxed to the surface of atomic oxygen, is the flux of particles that recombine or de-excite at the surface walls of the reactor. This is calculated slightly differently, as the output from the simulation is a per volume reaction rate of the recombination or neutralisation reactions where the reactions are reactions 352, 353 and 354 in table 2.2 with the units of $m^{-3}s^{-1}$. This is normalised to the surface area like the rest of the surface fluxes by multiplying the value $\frac{V}{A}$ where V is the volume of the reactor and A is the surface area of the reactor. Then after the data are normalised, the surface flux of atomic oxygen ground and excited states is analysed in the same way as the other surface fluxes as shown above.

Chapter 3

Production and Flux of Argon Ions in a Pure Argon Plasma for ALE

In this chapter, the effect of changing the pressure, frequency and duty cycle at multiple average powers on the production of argon ions and the input energy per argon ion fluxed to the surface in a completely argon plasma is investigated for the purpose of ALE processes. Argon is important for ALE processes, as argon is a noble gas with a full outer shell of valence electrons. As such, argon is chemically inert and, therefore, is ideal for the physical sputtering process without altering the chemical composition of the surface. Additionally, argon has a limited set of reactions, being able to be excited and ionised only. Therefore, the production of argon ions, which are needed so that they can accelerate across the plasma potential to sputter the material in ALE, can be undertaken with less energy being used to produce other particles. The base case for this chapter can be seen in table 2.4 where the mixture fraction has been set to 0 so that the initial density of the argon ions is 1×10^{10}. The pressure is varied between 1 and 25 Pa at multiple average powers between 200 and 1000 W, the frequency is varied between 5 and 50 Khz and the duty cycle is varied between 0.1 and 0.9, both at multiple average powers between 200 and 600 W.

3.1 Temporal Variation of Plasma Properties

During each power pulse, the important plasma properties that affect the production and flux of ionised argon vary temporally in a non-uniform manner. The way in which the plasma properties vary depends on the amount of power applied to the plasma and the amount of time within the pulse that the power is applied. Therefore, as plasma input parameters, such as the frequency and duty cycle, are varied, the plasma properties temporally vary differently, which affects the averaged values of the properties during the pulse. As such, this section investigates how the plasma properties important to the production and flux of Ar^+ vary temporally during the last pulse of the base case simulation. The temporal variation of the plasma properties can

be seen in figure 3.1. Here, the temporal variation of the number densities of Ar^+ and electrons can be seen in figure 3.1a and the temporal variation of the temperature of the electrons and plasma potential can be seen in figure 3.1b. Additionally, in both figures 3.1a and 3.1b the orange line denotes when the power is switched off during the last pulse where the waveform of the input power for the base case can be seen in figure 2.4a.

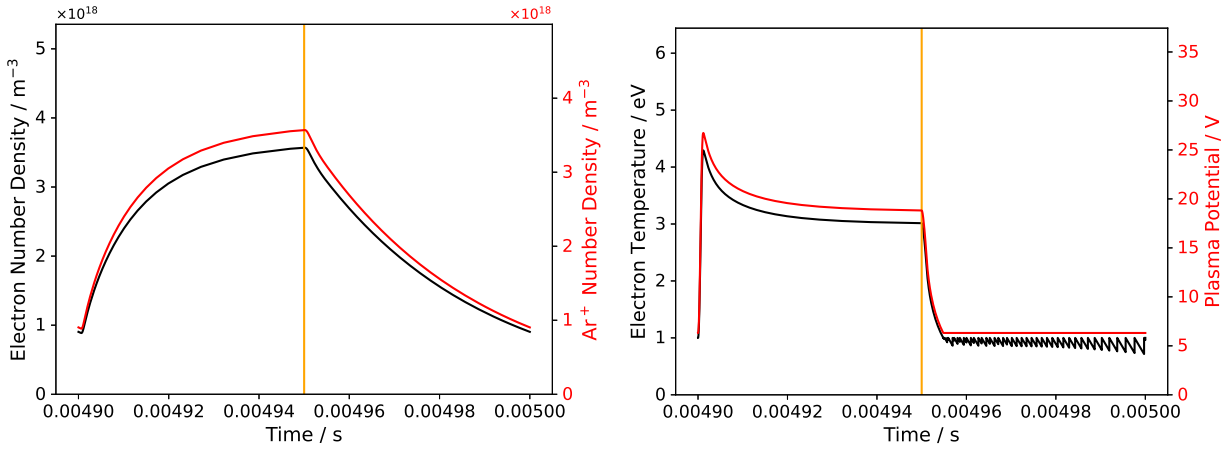

(a) (b)

Figure 3.1: (a) Number Density of Electrons and Ar^+ and (b) Temperature of the Electrons and Plasma Potential as a Function of Time during the Last Pulse of the Base Case

In figure 3.1a the number densities of electrons and Ar^+ increase during the power-on phase, with the rate of increase decreasing over time approaching a steady value. This is because the applied power increases the rate of electron impact ionisation, leading to an increase in the number density of electrons and Ar^+. The increase in the number density of the particles increases loss mechanisms, such as electron ion recombination and surface flux, which decrease the rate of increase in the number densities. This leads to a dynamic equilibrium where the production and loss mechanisms balance to produce a steady state, causing the number density of charged particles to approach a steady value. After the power is turned off in figure 3.1a the number densities of electrons and Ar^+ decrease with the rate of decrease decreasing over time. This is because when the power is off, the electrons lose energy rapidly, which decreases electron impact ionisation. Therefore, the loss mechanisms will dominate, causing the number density of electrons and Ar^+ to decrease. Additionally, the density of charged particles decreases approximately exponentially as a result of the timescale of diffusion to the reactor walls. In figure 3.1b the temperature of the electrons and the plasma potential increase rapidly when the power is turned on, reaching a maxima and then decreasing to a steady value. This is because when the power is turned on the deposited power is distributed between relatively few electrons, and therefore the temperature of electrons increases rapidly. However, over time the number density of electrons increases; therefore, the power deposited into the plasma is split between more electrons, reducing the energy per electron, causing the temperature to decrease from the maxima. As time increases, the temperature of electrons enters a dynamic equilibrium as the power absorbed by the plasma balances with energy losses from elastic and

inelastic collisions and electron flux to the surface. After the power is turned off in figure 3.1b the temperature of the electrons and the plasma potential quickly decrease before approaching a steady value for the remainder of the pulse. This is because in the absence of power being deposited into the plasma, electrons lose energy rapidly due to collisions and electron surface flux, causing the temperature of electrons to decrease rapidly. Then around 1 eV the rate of decrease slows significantly because the temperature of electrons becomes too low to sustain significant amounts of inelastic collisions due to the threshold energies of many inelastic collisions. This decreases the amount of energy lost inside the plasma, causing the temperature of the electrons to approach a steady value. The plasma potential follows the trend in the temperature of electrons as the plasma potential is approximately proportional to the temperature of electrons. Additionally, the oscillatory behaviour of the temperature of electrons after the power is turned off is likely due to a numerical artefact of the GM rather than a physical process.

3.2 Plasma Electron Properties

The density and temperature of electrons are vital to understanding the rate of production and flux of argon ions to the surface, as can be seen in equations 1.3.4 and 1.3.15. In addition, the electron temperature is important to the calculation of the plasma potential across the sheath, which determines how much energy the ions possess and therefore whether they are inside the ALE window. This is because the electron temperature is the main parameter that will require the plasma potential to shift to satisfy the flux balance equation 2.2.25. As such, this section investigates and discusses how electron properties vary as the input parameters of duty cycle, frequency and pressure are changed.

3.2.1 Duty Cycle

A change in the duty cycle of the waveform of the input power controls the intensity at which the power is applied to the plasma and the proportion of time in each pulse period of which the power is applied. As such, this can affect the rate of heating of electrons and the ionisation rate inside the plasma, affecting the density and temperature of electrons. The effects on electron properties caused by changing the duty cycle from 0.1 to 0.9 can be seen in figure 3.2. Here, the effect of a duty cycle change between 0.1 and 0.9 at multiple average power levels between 200 and 600 W on the temperature of electrons is shown in figure 3.2a and on the number density of electrons is shown in figure 3.2b.

In figure 3.2a the temperature of electrons as the average power increases stays at a roughly constant value, this coincides with a constant linear increase in the number density of electrons as the duty cycle increases as seen in figure 3.2b. This is caused by the increasing average power, causing an increase in ionisation proportional to the increase in average power rather than any increase in the electron thermal energy.

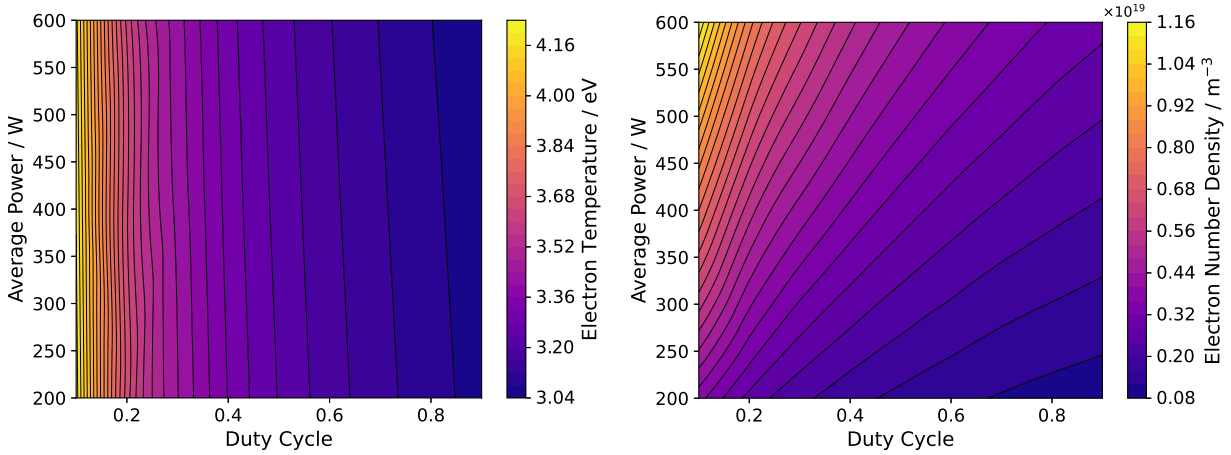

(a) (b)

Figure 3.2: (a) Temperature of Electrons (eV) and (b) Number Density of Electrons (m^{-3}) as a Function of Duty Cycle and Average Power

As the duty cycle increases in figure 3.2a, the temperature of the electrons decreases with the rate of change decreasing exponentially as the duty cycle increases. This is due to the decrease in the amplitude of the power pulse as the duty cycle increases. This causes less intense heating of the electrons during the period of the pulse when the power is first turned on because the rate of change in the temperature of the electrons is dependent on the power absorbed by the plasma, as can be seen in equation 2.2.2. This leads to a smaller peak in the temperature of electrons as the duty cycle increases, therefore decreasing the overall average temperature of electrons during the power pulse (Figure not shown). In figure 3.2b, as the duty cycle increases, the number density of electrons decreases with the rate of decrease slowing as the duty cycle increases. This is caused by the particle balance inside the plasma. As the duty cycle increases, the temperature of the electrons drops because of the decrease in the amplitude of the power pulse, which decreases both the ionisation and loss mechanisms such as the electron surface flux. Due to the high ionisation potential of argon at 15.76 eV, the rate of decrease in ionisation is higher than the decrease in the electron surface flux. Therefore, to maintain a pulsed periodic steady state, the number density of electrons decreases.

3.2.2 Frequency

A change in the frequency of the waveform of the input power controls the length of time in each cycle that electrons have to be ionised into the plasma bulk and for electrons to gain energy. However, it also controls the length of time in each cycle that particles have to lose energy and be lost to surface flux. As such, the frequency of the waveform can affect the average temperature and density of electrons throughout the power pulse. The effects on electron properties caused by changing the frequency from 5 to 50 Khz can be seen in figure 3.3. Here, the effect of the frequency change between 5 and 50 Khz at multiple average power levels between 200 and

600 W on the temperature of electrons is shown in figure 3.3a and on the number density of electrons is shown in figure 3.3b.

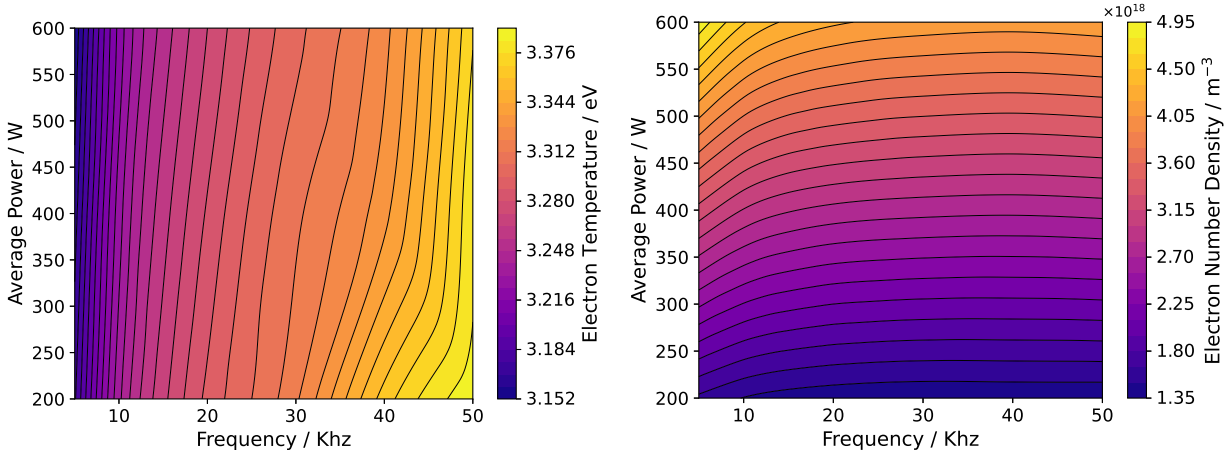

(a) (b)

Figure 3.3: (a) Temperature of Electrons (eV) and (b) Number Density of Electrons (m^{-3}) as a Function of Frequency and Average Power

In figure 3.3a the temperature of the electrons stays roughly constant as the average power increases, and in figure 3.3b the number density of electrons increases linearly as the average power increases due to the reasons discussed above for figure 3.2. The temperature of electrons in figure 3.3a increases slightly with frequency roughly linearly. This is because as the frequency increases the time that the power is on in each pulse becomes smaller, which gives the temperature of electrons less time to reach the steady-state (Figure not shown). As such, at higher frequencies the temperature of the electrons has less time to decrease from the initial peak when the power is first turned on, therefore the overall temperature is higher at higher frequencies. In figure 3.3b the number density of electrons decreases slightly as the frequency increases with the rate of decrease slowing as the frequency increases. This is because as the time that the power is on in each pulse becomes shorter, the plasma has less time to ionise and reach the steady-state number density of electrons (Figure not shown). Therefore, during the time the plasma pulse is on, the maximum number density of electrons is lower at higher frequencies, which decreases the average density during the power pulse.

3.2.3 Pressure

A change in the pressure of the neutral gas that makes up the plasma affects the initial density of the particles within the reactor. This can change the frequency of plasma collisions such as ionisation which requires energy and also releases electrons, affecting the number density and temperature of electrons. As such, the pressure of the plasma can significantly affect the properties of electrons. The effect on the properties of electrons by changing the plasma pressure

from 1 to 25 Pa can be seen in figure 3.4. Here, the effect of the pressure change between 1 and 25 Pa at multiple average power levels between 200 and 1000 W on the temperature of electrons is shown in figure 3.4a and on the number density of electrons is shown in figure 3.4b.

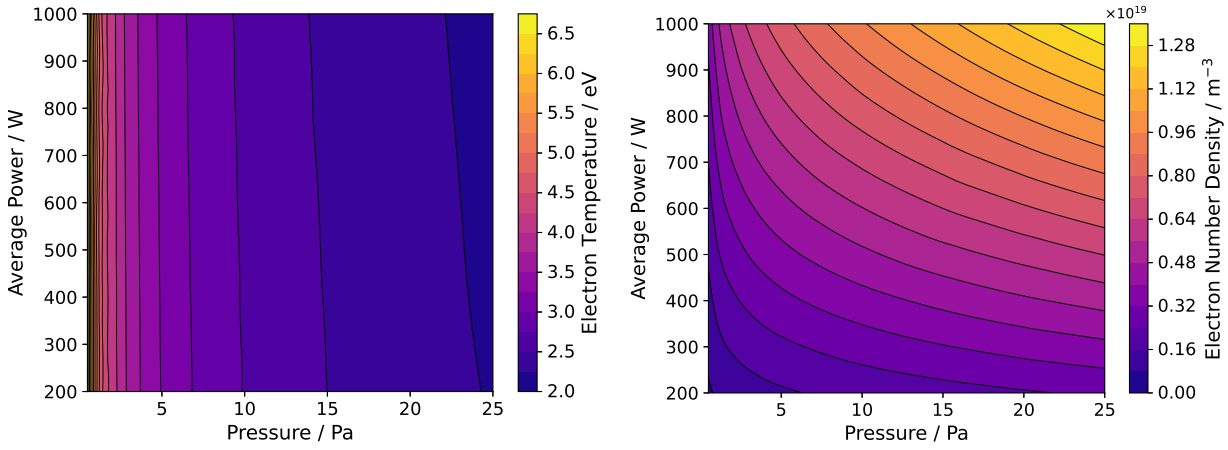

(a) (b)

Figure 3.4: (a) Temperature of Electrons (eV) and (b) Number Density of Electrons (m^{-3}) as a Function of Pressure and Average Power

Similarly to frequency and duty cycle the effect of increasing the average power in figure 3.4 causes the temperature of electrons to remain constant and the number density of electrons to increase linearly with average power. This is due to the same reasons as stated above for figure 3.2. In figure 3.4a the temperature of electrons decreases with an increase in pressure with the rate of decrease decreasing exponentially. This is because as the gas pressure increases, the number of elastic collisions with neutral particles increases because of the higher density of neutral particles. This transfers energy from the electrons to other particles, which decreases the temperature of the electrons. Additionally, at low pressures the flux of particles, in particular argon ions, to the surface of the reactor increases; therefore, for the plasma to maintain a pulsed periodic steady state the temperature of electrons increases to maintain sufficient ionisation rates. In figure 3.4b the number density of electrons increases with pressure, with the rate of increase decreasing slightly at higher pressures. This is because as pressure increases the higher gas pressure requires a higher number density of electrons to maintain a pulsed-periodic steady-state where the production and consumption of electrons are equal.

3.3 ALE Energy Window

To ensure that the argon ions have sufficient energy to etch the material, an investigation into the average plasma potential over the time frame of the last pulse in which the power is applied is necessary. Subsequently, only the range of input parameters that generate a plasma potential

inside the energy window of germanium, which is 20 -30 eV, is used for further investigation. The results from all other input parameters are not included because they do not produce a plasma with sufficient plasma potential for the ALE process of germanium. Here, germanium has been chosen as inductively coupled plasmas in the pressure ranges used in simulations in this chapter produce plasma potentials in the range of the energy window of germanium, where other materials have an energy window higher than these plasma potentials [40, 82]. The effect on the plasma potential as the frequency is varied between 1 and 50 Khz and the duty cycle is varied between 0.1 and 0.9 both at multiple average powers between 200 and 600 W is shown in figures 3.5b and 3.5a, respectively. And the effect on the plasma potential as the pressure is varied between 1 and 25 Pa at multiple average powers between 200 and 1000 W is shown in figure 3.5c.

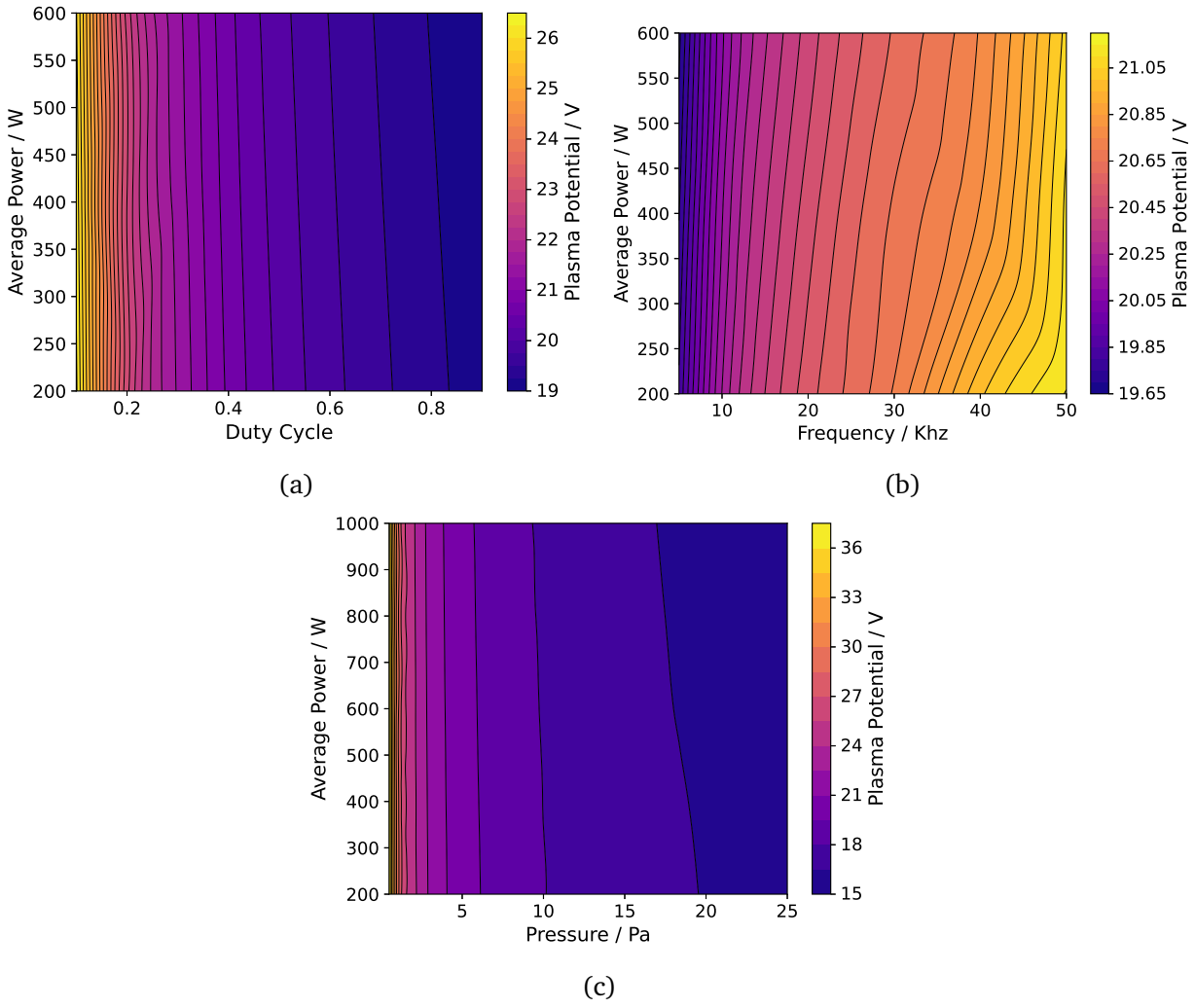

Figure 3.5: Plasma Potential (V) (a) as a Function of Duty Cycle and Average Power, (b) as a Function of Frequency and Average Power and (c) as a Function of Pressure and Average Power

In all three graphs in figure 3.5 the plasma potential is roughly constant as the average power increases. This is because the temperature of electrons is roughly constant with average power increase and since the plasma potential scales roughly linearly to the temperature of electrons, the plasma potential is constant as the average power increases. In figure 3.5a the plasma potential decreases as the duty cycle increases with the rate of change slowing as the duty cycle increases. This decrease in plasma potential as the duty cycle increases is due to the decrease in the amplitude of the power pulse, which decreases the temperature of electrons, which subsequently causes the plasma potential to decrease. The region at which the plasma potential is within the energy window for germanium etching is found between duty cycles of 0.1 and 0.5. In figure 3.5b the plasma potential increases with frequency roughly linearly. This is because as frequency increases, there is an increase in the average temperature of electrons because of a decreased amount of time for electron elastic collisions to occur during each pulse (Figure not shown). This increase in the average electron temperature then subsequently increases the plasma potential sightly as the frequency increases. The region in which the plasma potential is within the energy window for germanium etching is found between 10 and 50 Khz. In figure 3.5c the plasma potential decreases as the pressure increases, with the rate of decrease decreasing exponentially as the pressure increases. This is caused by the higher gas density, which increases the number of elastic collisions with neutral particles, decreases the temperature of electrons, and causes the plasma potential to decrease. The region in which the plasma potential is within the energy window for germanium etching is found between 0.5 and 5.0 Pa. All graphs in the rest of the chapter are therefore only inside the input parameter ranges of 0.1 to 0.5 for the duty cycle 10 to 50 khz for frequency and 0.5 to 5.0 Pa for pressure to ensure that the energy of the argon ions is inside the energy window of germanium. Additionally, it can be seen that decreasing the overall density of the gas and increasing the intensity of the pulses are effective methods to raise the plasma potential and can be utilised if you wanted to etch a different material that has an energy window with higher energy values. It is important to note that whilst the averaged plasma potential values for a duty cycle of 0.5, a frequency of 10 Khz and a pressure of 5 Pa are inside the energy window for germanium, these values are very close to being outside this window. Therefore, for these input parameters the plasma potential is lower than 20 eV for a portion of the power pulse. However, the global model only follows experiments qualitatively and, therefore, these values have an error associated with them. These averaged values are still included because they are on average still inside the energy window for germanium; therefore, the effect of this is likely to be minimal.

3.4 Production of Ar^+

Argon ions inside the plasma are constantly produced and consumed through various mechanisms when inside the plasma. The main mechanisms of production of argon ions are electron ionisation of Ar, Ar($4P$) and Ar^m, where ionisation of ground state argon is the most significant reaction. The only significant consumption mechanism is the flux to the surface, as all other significant loss mechanisms require oxygen to be present in the plasma. The flux of argon ions

is dependent on the diffusion coefficient of argon ions because this determines the rate at which argon ions diffuse to the edge of the sheath. We can treat these plasmas in a pulse period steady state, where the density of argon ions is such that it balances the production and loss rate of itself so that they are equal to each other.

3.4.1 Duty Cycle

How the plasma properties are affected by changing the duty cycle and the effect the plasma properties have on the balance of the pulsed periodic steady state of argon ions and therefore the number density of argon ions can be seen in figure 3.6. The temperature and number density of electrons and the diffusion coefficient of argon ions in the duty cycle range between 0.1 and 0.5 at a constant average power of 400 W can be seen in figure 3.6a. The same plasma properties in the average power range of 200 to 600 W at a constant duty cycle of 0.1 can be seen in figure 3.6c. Additionally, the number density of argon ions for these respective input parameters is also shown in figures 3.6b and 3.6d, respectively.

In figure 3.6a the number density and temperature of electrons decrease proportionally to D^{-1}, where D represents the duty cycle; as the duty cycle increases, the diffusion coefficient of argon ions is roughly constant at all values of the duty cycle. In figure 3.6b the number density of argon ions decreases proportionally to D^{-1} as the duty cycle increases. This is because as the duty cycle increases, the amplitude of the power is lower, which lowers the temperature and number density of electrons, as discussed in section 3.2.1. Additionally, because the duty cycle has no effect on the initial density of neutrals inside the plasma, the diffusion coefficient of the argon ions stays constant. This means that the production and consumption of argon ions as the duty cycle increases becomes less effective; however, the decrease in consumption is less significant than the decrease in production because the consumption decreases only from a decrease in the Bohm velocity. This necessitates a decrease in the number density of argon ions to maintain a pulsed periodic steady state, so the production and consumption of argon ions are balanced. In figure 3.6c the temperature of the electrons and the diffusion coefficient of the argon ions remain roughly constant as the average power increases and the number density of electrons increases linearly as the average power increases. In figure 3.6d the number density of argon ions increases linearly as the average power increases. This is because as the average power increases, the number density of electrons increases but does not cause an increase temperature of the electrons as discussed in section 3.2.1. Additionally, an increase in average power has no effect on the density of heavy particles inside the plasma; therefore, the diffusion coefficient stays constant, as there is no change in the number of heavy particle collisions. This means that the production of argon ions becomes more effective as a result of a larger number of electrons inside the plasma, while the consumption of argon ions stays the same because there is no change in the diffusion or Bohm velocity. This necessitates a proportional increase in the number density of argon ions to maintain a pulsed periodic steady state inside the plasma.

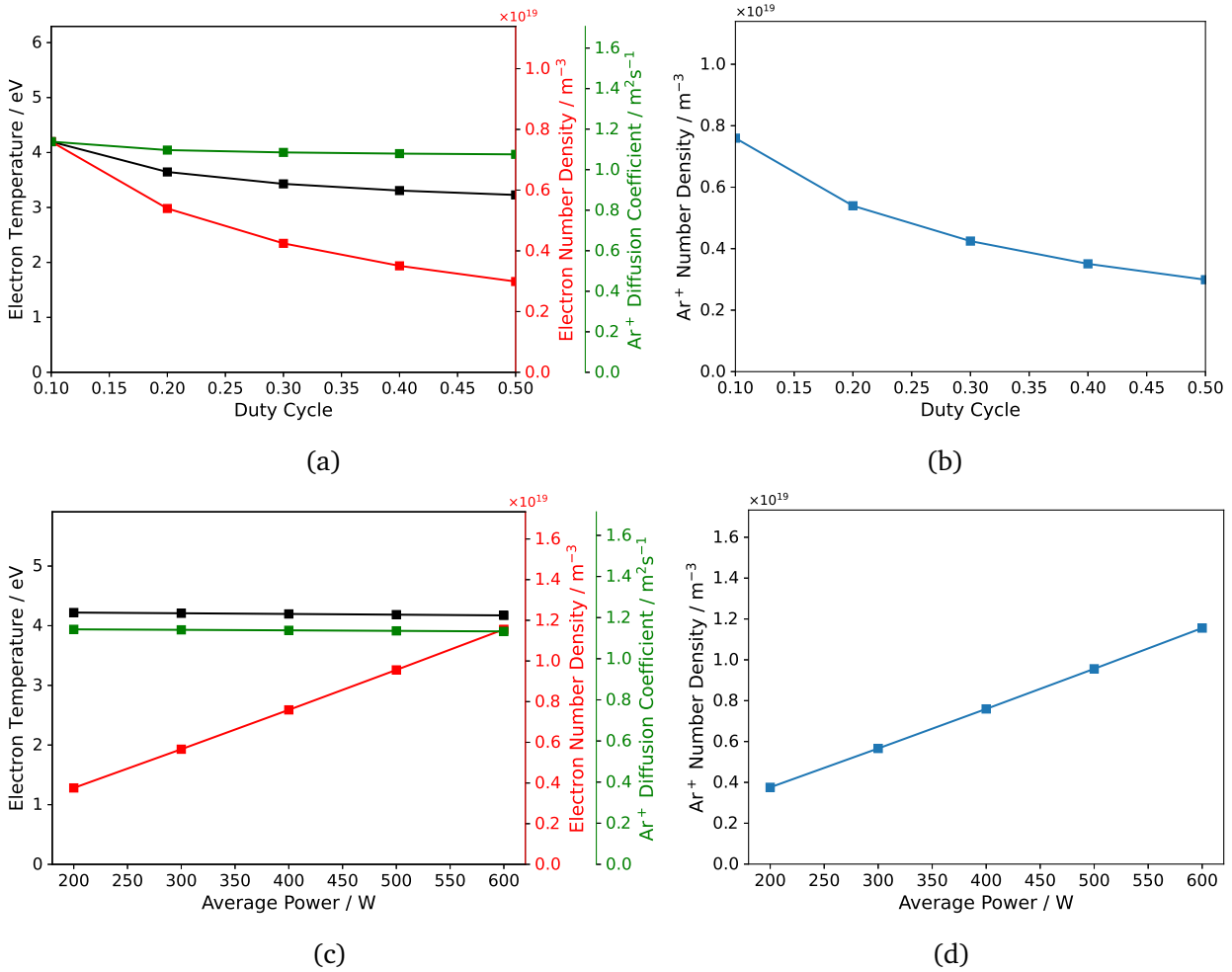

Figure 3.6: Temperature (eV) and Number Density (m^{-3}) of electrons and the Diffusion Coefficient (m^2s^{-1}) of Argon Ions (a) as a Function of Duty Cycle at an Average Power of 400 W and (c) as a Function of Average Power at a Duty Cycle of 0.1. Number Density of Argon Ions (m^{-3}) (b) as a Function of Duty Cycle at an Average Power of 400 W and (d) as a Function of Average Power at a Duty Cycle of 0.1

3.4.2 Frequency

The effect of a frequency variation on the plasma properties that affect the consumption and production of argon ions as well as the effect on the number density of argon ions can be seen in figure 3.7. The temperature and number density of the electrons and the diffusion coefficient of the argon ions in the frequency range between 10 and 50 Khz at a constant average power of 400 W can be seen in figure 3.7a. The same plasma properties in the average power range of 200 to 600 W at a constant frequency of 10 Khz can be seen in figure 3.7c. Additionally, the number density of argon ions for these respective input parameters is also shown in figures 3.7b and 3.7d, respectively.

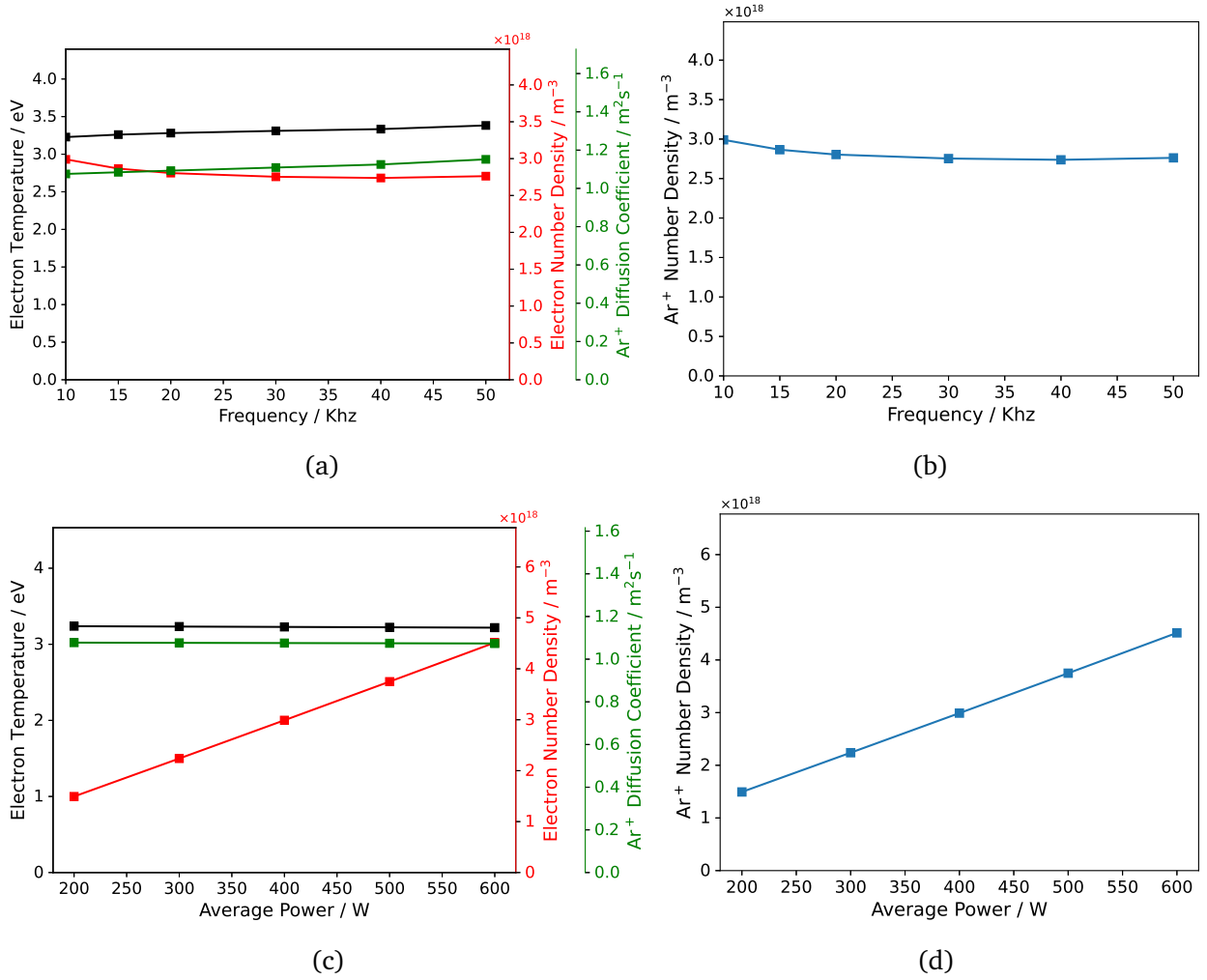

Figure 3.7: Temperature (eV) and Number Density (m^{-3}) of electrons and Diffusion Coefficient (m^2s^{-1}) of Argon Ions (a) as a Function of Frequency at an Average Power of 400 W and (c) as a Function of Average Power at a Frequency of 10 Khz. Number Density of Argon Ions (m^{-3}) (b) as a Function of Frequency at an Average Power of 400 W and (d) as a Function of Average Power at a Frequency of 10 Khz

In figure 3.7a the temperature of the electrons and the diffusion coefficient of the argon ions increases slightly and the number density of the electrons decreases proportionally to f^{-1}. The reason why the electron properties change is discussed in section 3.2.2. Also in figure 3.7b the number density of argon ions decreases slightly with frequency. This means that because of a decreased electron density, production of argon ions is hindered, with consumption of argon ions becoming more effective because of the higher diffusion coefficient and Bohm velocity. This necessitates a decrease in the density of argon ions to maintain the balance of production and consumption of argon ions in a pulsed periodic steady state. In figure 3.7c the temperature of the electrons and the diffusion coefficient of the argon ions are constant at all values of average power and the number density of electrons increases linearly with average power. Also, in figure 3.7d the number density of argon ions increases linearly with the average power. This is the

same trend observed at a duty cycle of 0.1 as discussed above, so the effect of the average power between 200 and 600 W on the production of argon ions is not dependent on the frequency or duty cycle. This effect is caused by the average power increasing the ionisation of the plasma without increasing the electron temperature, as discussed in section 3.2.2. This means that the production of argon ions is more effective, whereas the effectiveness of consumption remains unchanged. This necessitates an increase in the number density of argon ions to balance the production and consumption to maintain a pulsed periodic steady state.

3.4.3 Pressure

The effect of a change in the pressure of the plasma on the properties that affect the consumption and production of argon ions, affect on the number density of argon ions can be seen in figure 3.8. The diffusion coefficient of argon ions as a function of pressure and average power can be seen in figure 3.8a The temperature and number density of electrons and the number density of argon ions in the pressure range between 0.5 and 5.0 Pa with a constant average power of 400 W can be seen in figure 3.8b. The same plasma properties in the average power range of 200 to 600 W at a constant pressure of 5.0 Pa can be seen in figure 3.8d. Additionally, the number density of argon ions for these respective input parameters is also shown in figures 3.8c and 3.8e, respectively.

In figure 3.8a the diffusion coefficient of argon ions decreases proportionally to P^{-1} but remains constant as the average power changes. This is because as the gas pressure increases, a larger number of collisions occur inside the plasma due to the density of the gas increasing, whereas increasing the average power does not increase the overall gas density, and therefore has no effect on the diffusion coefficient. In figure 3.8b the temperature of electrons decreases proportionally to P^{-1}, the number density of argon increases linearly as the pressure increases and the number density of the electrons increases as the pressure increases with the rate of increase decreasing as the pressure increases. Also, in figure 3.8c the number density of argon ions increases with pressure, with the rate of increase decreasing slightly at higher pressures. This is because as the gas pressure increases, the density of heavy argon particles inside the plasma increases and therefore decreases the electron temperature due to increased elastic collisions and increases the electron number density, as discussed in section 3.2.3. When combined with the decreased diffusion coefficient, the consumption of argon ions is hindered, with the production of argon ions also being hindered because of the strong dependence on the temperature of electrons. However, consumption is hindered more significantly because of the increase in the number density of argon and electrons, which serve to increase the production. Therefore, this necessitates an increase in the number density of argon ions to maintain a pulsed periodic steady state within the plasma. In figure 3.8d the temperature of the electrons and the number density of argon remain constant at all values of average power and the number density of electrons increases linearly as average power increases, as discussed in section 3.2.3. Also, in figure 3.8e the number density of argon ions increases linearly as the average power increases.

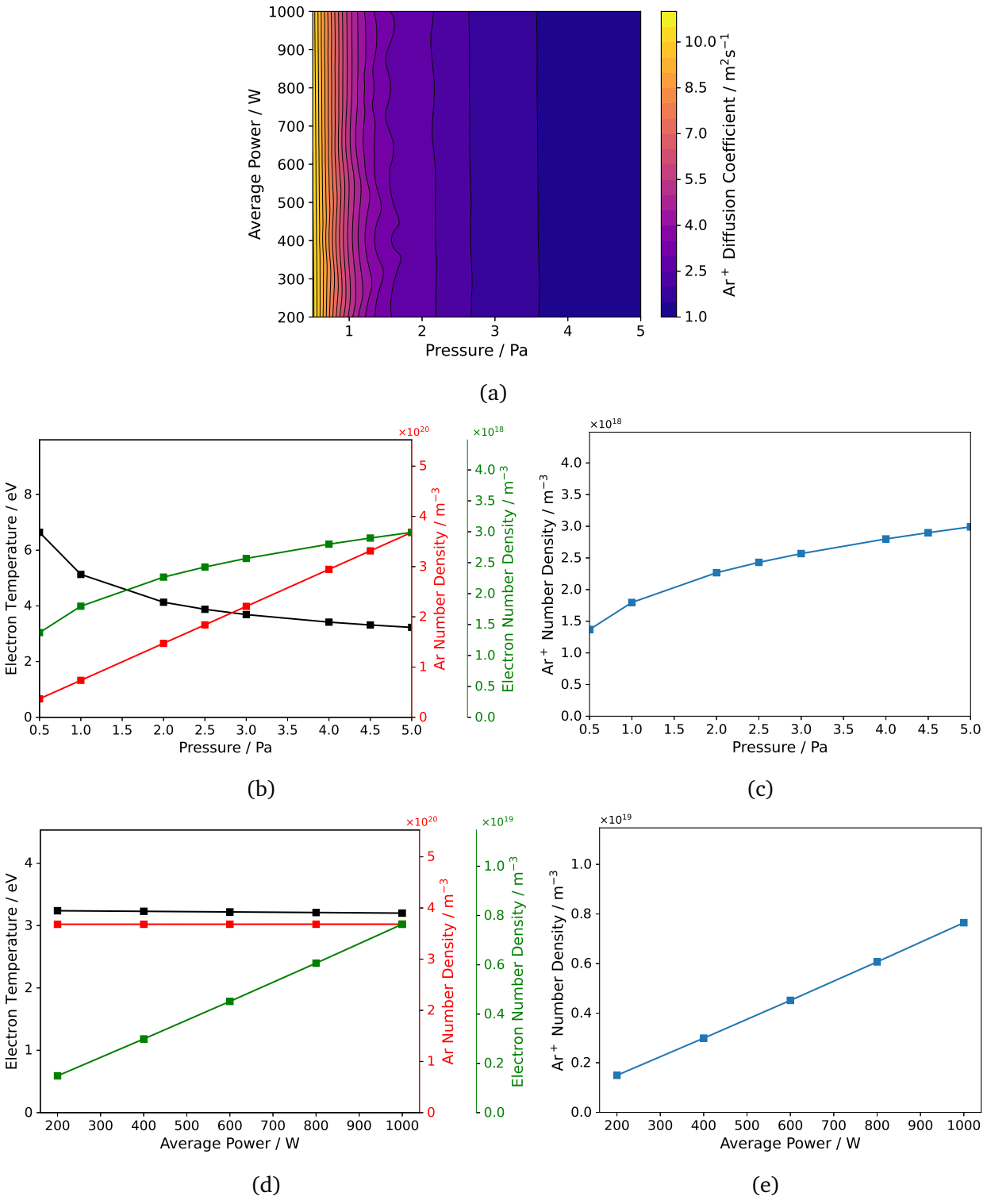

Figure 3.8: Diffusion Coefficient of Argon Ions (m^2s^{-1}) (a) as a Function of Pressure and Average power, Temperature (eV) and Number Density (m^{-3}) of electrons and Number Density of Argon (m^{-3}) (b) as a Function of Pressure at an Average Power of 400 W and (d) as a Function of Average Power at a Pressure of 5.0 Pa. Number Density of Argon Ions (m^{-3}) (c) as a Function of Pressure at an Average Power of 400 W and (e) as a Function of Average Power at a Pressure of 5.0 Pa

This makes the production of argon ions more effective while the effectiveness of consumption remains unchanged, necessitating an increased number density of argon ions to maintain a pulsed periodic steady state. This is the same trend as observed at a duty cycle of 0.1 and at 10 Khz as discussed above. Therefore, the effect of the change in average power on the number density of argon ions is independent of the input parameters of the pressure of the gas or the frequency and duty cycle of the power waveform.

3.5 Argon Ion Surface Flux

The flux of ions onto the surface of the reactor is driven by the potential difference inside the sheath where ions entering the sheath are accelerated onto the surface of the reactor. Therefore, when determining the surface flux, we need to determine the flux of ions into the sheath from the plasma bulk. The flux into the sheath and, therefore, the flux onto the surface walls can be seen in equation 1.3.4 where the diffusion coefficient and number density of argon ions determine the number density at the sheaths edge and the temperature of electrons determine the Bohm velocity which an increase in all factors leads to a higher surface flux. Finding a regime with an optimal combination of those factors for the energy inputted into the plasma is vital to reduce the energy required for ALE.

3.5.1 Duty Cycle

The effect of the change in duty cycle and average power on the plasma parameters that determine the surface flux of argon ions and the effect on the surface flux and surface fluence of argon ions is shown in figure 3.9. The temperature of electrons and the number density and diffusion coefficient of argon ions as a function of duty cycle between 0.1 and 0.5 at an average power of 400 W can be seen in figure 3.9a. The same plasma properties as a function of average power between 200 and 600 W at a duty cycle of 0.1 can be seen in figure 3.9c. Additionally, the surface flux of argon ions for these respective input parameters can be seen in figures 3.9b and 3.9d, respectively. The surface fluence of argon ions, defined as the total number of argon ions that is fluxed to the surface during the power-on period of the last cycle, is shown in figure 3.9e. The surface fluence is calculated by multiplying the surface flux per second by the duration for which the power is on in the final cycle. This duration depends on the duty cycle, since the duty cycle represents the fraction of the cycle during which the power is on, with each simulations last cycle in this section having the same total duration, since they all have the same frequency. Here, the graphs for the number density and diffusion coefficient of argon ions and the temperature of electrons are included again to help illustrate why the trends in the surface flux of argon ions appear.

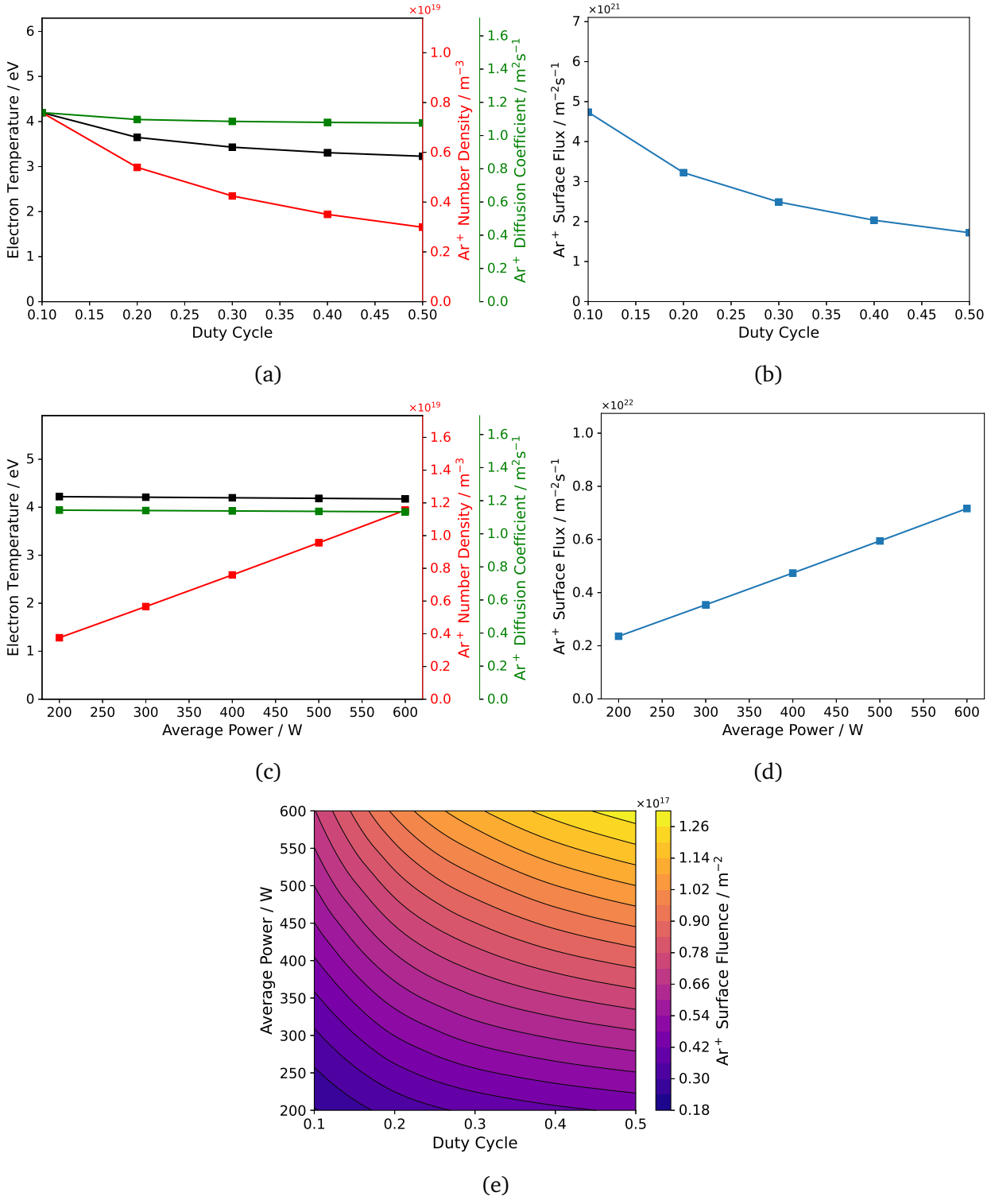

Figure 3.9: Temperature (eV) of electrons and the Number Density (m^{-3}) and Diffusion Coefficient (m^2s^{-1}) of Argon Ions (a) as a Function of Duty Cycle at an Average Power of 400 W and (c) as a Function of Average Power at a Duty Cycle of 0.1. Surface Flux of Argon Ions ($m^{-2}s^{-1}$) (b) as a Function of Duty Cycle at an Average Power of 400 W and (d) as a Function of Average Power at a Duty Cycle of 0.1 and the Surface Fluence of Argon Ions (m^{-2}) (e) as a Function of Duty Cycle and Average Power

In figure 3.9a the temperature of the electrons and the number density of the argon ions decreases proportionally to D^{-1} and the diffusion coefficient remains constant at all values of duty cycle. Also in figure 3.9b the surface flux of argon ions decreases proportionally to D^{-1}. This is because as the duty cycle increases, the decrease in the amplitude of the power decreases the temperature of the electrons, hindering the production of argon ions and therefore causing a decrease in the density of argon ions, as discussed in sections 3.2.1 and 3.4.1. The constant diffusion coefficient means that the effectiveness of the argon ions diffusing to the edge of the sheath is not affected. Therefore, in combination with a decrease in the number density of argon ions in the plasma bulk, this means that the density of argon ions at the edge of the sheath decreases. This, combined with the lower temperature of the electrons that lowers the Bohm velocity into the sheath, causes the surface flux of argon ions to decrease by 64% as the duty cycle increases from 0.1 to 0.5. In figure 3.9c the temperature of the electrons and the diffusion coefficient of the argon ions remain constant at all values of duty cycle and the number density of the argon ions increases linearly as the average power increases, as discussed in sections 3.2.1 and 3.4.1. Also in figure 3.9d the surface flux of argon ions increases linearly as the average power increases. This means that the Bohm velocity stays the same at all values of average power with the density at the edge of the sheath increasing because the density in the plasma bulk increases and the diffusion coefficient remains constant. Therefore, this creates a linear dependence on the average power for the surface flux of argon ions because of a linear increase in the density of argon ions at the edge of the sheath. In figure 3.9e the surface fluence of argon ions decreases as the duty cycle increases with the rate of decrease slowing as the duty cycle increases and increases linearly with average power. The trend in surface fluence, as the duty cycle changes, is opposite to the trend in surface flux because the values of the flux are inside the period of time where the power is on. This is because the difference in the time that the power is on, as can be seen in figure 2.4 reverses the trend. The surface flux increases by 175% from 0.5 to 0.1 duty cycle; however, the time the power pulse is on decreases by 80%. This means that more total particles are fluxed to the surface during the last pulse at higher duty cycles, which means that the fluence increases as the duty cycle increases. However, surface fluence follows the same trend with average power as surface flux because there is no length of time difference between each different average power at a specific duty cycle; therefore, fluence will follow the same trend as the flux.

3.5.2 The Effect of Duty Cycle on the Input Energy per Argon Ion Fluxed to the Surface

Reducing the input energy per argon ion fluxed to the surface is important for reducing the energy usage during ALE processes commonly used in semiconductor manufacturing. As such, the input energy per argon ion fluxed to the surface is calculated using equation 2.5.1 as a function of the duty cycle and the average power is shown in figure 3.10.

In figure 3.10 the input energy per particle fluxed to the surface of argon ions decreases as the duty cycle increases with the rate of decrease slowing as the duty cycle increases and stays constant as the average power increases. The reason why increasing the duty cycle decreases

the input energy per argon ion is that the length of time the power is on in each pulse increases more than the flux per second decreases as the duty cycle increases. This allows more argon ions to be fluxed to the surface at the given power level, hence decreasing the input energy per argon ion fluxed to the surface. The input energy per argon ion stays constant as the average power changes as the flux of argon ions increases proportionally to the average power as it increases. The flux increases are due to the number density of argon ions also increasing linearly in proportion to average power due to the additional energy provided to the plasma directly increasing ionisation proportional to the average power increases instead of using the energy to increase the temperature of electrons. Therefore, in the range of average powers and duty cycle tested, the average power can be changed to control the rate at which argon ions are incident with the surface material with no effect on the input energy per argon ion fluxed to the surface.

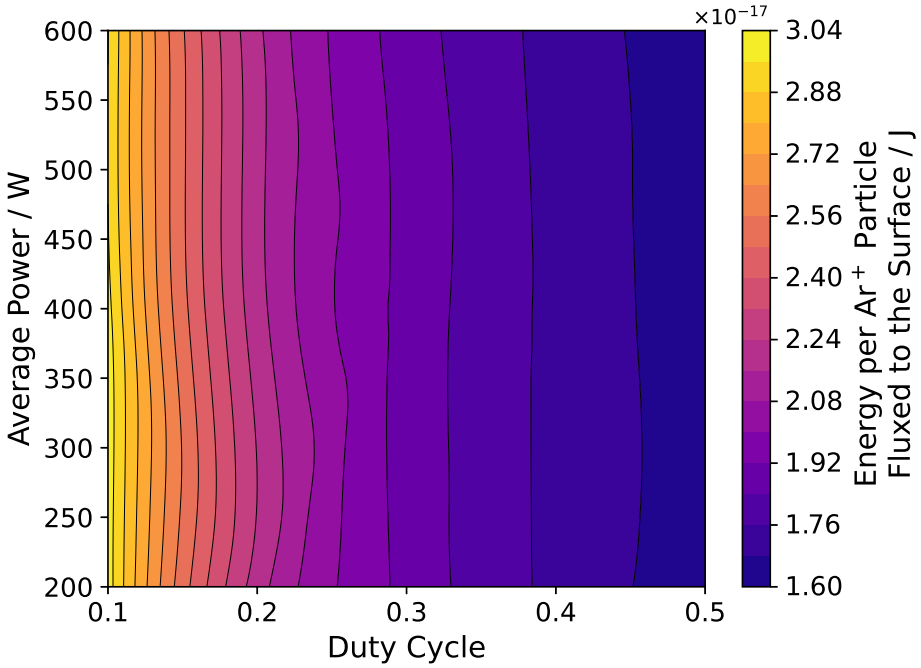

Figure 3.10: Input Energy per Argon Ion Particle fluxed to the surface (J) as a Function of Duty Cycle and Average Power

3.5.3 Frequency

The effect of the change of frequency and average power on the plasma parameters that determine the surface flux of argon ions and the effect on the surface flux of argon ions, is shown in figure 3.11. The temperature of the electrons and the number density and diffusion coefficient of the argon ions as a function of frequency between 10 and 50 Khz at an average power of 400 W can be seen in figure 3.11a. The same plasma properties as a function of average power between 200 and 600 W at a frequency of 10 Khz can be seen in figure 3.11c. Additionally,

the surface flux of argon ions for these respective input parameters can be seen in figures 3.11b and 3.11d, respectively.

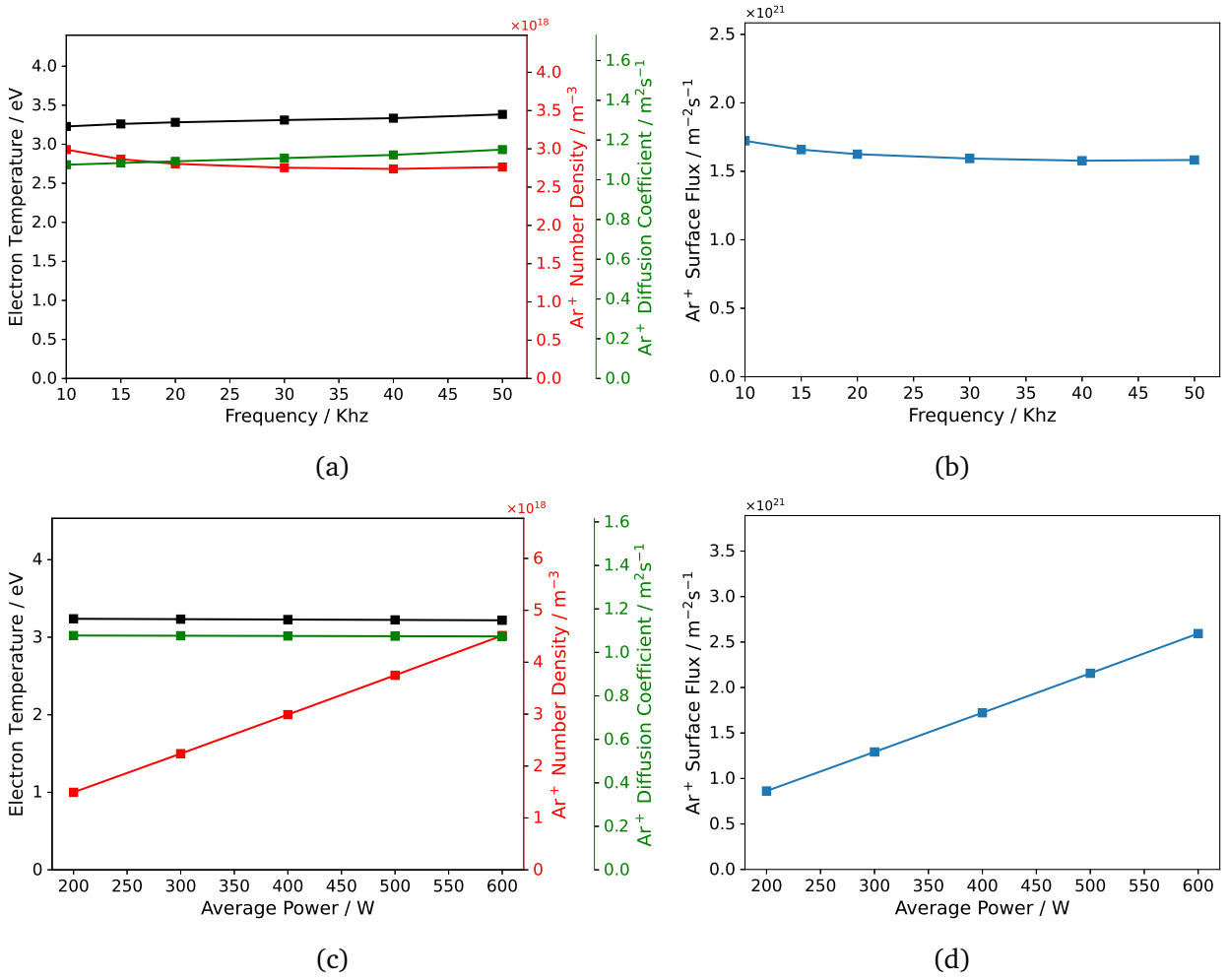

Figure 3.11: Temperature (eV) of electrons and the Number Density (m^{-3}) and Diffusion Coefficient (m^2s^{-1}) of Argon Ions (a) as a Function of Frequency at an Average Power of 400 W and (c) as a Function of Average Power at a Frequency of 10 KHz. Surface Flux of Argon Ions ($m^{-2}s^{-1}$) (b) as a Function of Frequency at an Average Power of 400 W and (d) as a Function of Average Power at a Frequency of 10 KHz

Here, the graphs for the number density and diffusion coefficient of argon ions and the temperature of electrons are included again to help illustrate why the trends in the surface flux of argon ions appear.

In figure 3.11a the temperature of the electrons and the diffusion coefficient of the argon ions increases slightly and the number density of argon ions decreases proportionally to f^{-1}. Also in figure 3.11b the number density of argon ions decreases proportionally to f^{-1}. This is because as frequency increases, more energy is deposited into electron heating rather than being used to cause ionisation, which decreases the number density of argon ions whilst only causing a

slight increase in the temperature of electrons, as discussed in sections 3.2.2 and 3.4.2. This means that the number density of argon ions at the edge of the sheath decreases because of a lower density in the plasma bulk, which is not counteracted by the slight increase in the diffusion coefficient. The lower number density of argon ions at the edge of the sheath, as the frequency increases, is not mitigated by the increase in Bohm velocity from the slight increase in the temperature of electrons, and therefore, reduces the surface flux of argon ions as frequency increases. In figure 3.11c the temperature of the electrons and the diffusion coefficient of the argon ions remain constant at all values of the average power, and the number density of argon ions increases linearly as the average power increases, as discussed in sections 3.2.2 and 3.4.2. Also in figure 3.11d the surface flux of argon ions increases linearly as the average power increases. This increases the number density of argon ions at the edge of the sheath combined with a constant Bohm velocity because of the constant temperature of the electrons, and this causes an increase in the surface flux. This is the same trend in the surface flux as the average power changes observed in the duty cycle variation, and therefore, the effect of average power on the surface flux of argon ions is not affected by duty cycle or frequency differences.

3.5.4 The Effect of Frequency on the Input Energy per Argon Ion Fluxed to the Surface

How the input energy per argon ion fluxed to the surface which is calculated using equation 2.5.1 changes as a function of frequency and the average power is shown in figure 3.12.

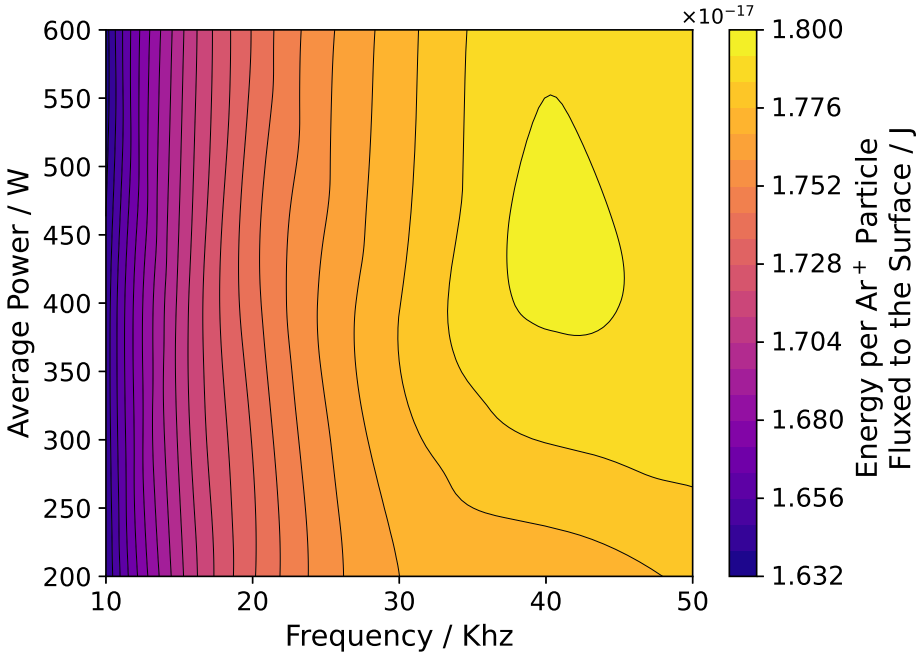

Figure 3.12: Input Energy per Argon Ion Particle fluxed to the surface (J) as a Function of Frequency and Average Power

In figure 3.12 the input energy per argon ion fluxed to the surface increases as the frequency increases and stays constant as the average power changes. However, at higher frequencies, there is a maximum with average power; however, the change is small enough to be caused by rounding or run to run variance. The reason why the input energy per argon ion fluxed to the surface increases with frequency is that more energy is deposited into electron heating rather than being used in ionisation reactions. This causes a lower number density of argon ions at the edge of the sheath and therefore a lower surface flux of argon ions for the same energy inputted into the plasma at higher frequencies. However, the effect in increasing the input energy per argon ion fluxed to the surface as the frequency increases is minimal at a change of only 1.68×10^{-18} J compared to the change of 1.35×10^{-17} J in the duty cycle variation. Furthermore, increasing the frequency increases the plasma potential slightly, which would let the plasma operate at a higher duty cycle whilst still being inside the ALE energy window. The effect on the input energy per argon ion of the increased duty cycle could potentially offset the increase in input energy per argon ion caused by the increased frequency; however, this is not tested here. The input energy per argon ion fluxed to the surface stays constant as the average power changes because increasing the average power causes increased ionisation reactions proportional to the increase in the average power rather than increasing the temperature of the electrons. This is the same trend as observed with a duty cycle variation; therefore, the effect of average power on the input energy per argon ion fluxed to the surface is unaffected by the shape of the waveform. Furthermore, in the range of average powers and frequency tested, the average power can be changed to control the rate at which argon ions are incident with the surface material with no effect on the input energy per argon ion fluxed to the surface.

3.5.5 Pressure

The effect of changing the pressure and average power on plasma parameters that determine the surface flux of argon ions and the effect on the surface flux of argon ions is shown in figure 3.13. The temperature of electrons and the number density and diffusion coefficient of argon ions as a function of pressure between 0.5 and 5.0 Pa at an average power of 400 W can be seen in figure 3.13a. The same plasma properties as a function of average power between 200 and 1000 W at a pressure of 1 Pa can be seen in figure 3.13c. Additionally, the surface flux of argon ions for these respective input parameters can be seen in figures 3.13b and 3.13d, respectively. Here, the graphs for the number density and diffusion coefficient of argon ions and the temperature of electrons are included again to help illustrate why the trends in the surface flux of argon ions appear.

In figure 3.13a the temperature of the electrons and the diffusion coefficient of the argon ions decrease with pressure proportionally to P^{-1} and the number density of argon ions increases with pressure, but the rate of increase decreases as pressure increases. This is because as pressure increases, the average density of heavy particles inside the plasma increases. This causes an increased number of collisions to occur in the plasma, which reduces the temperature of electrons and the diffusion coefficient of argon ions. Meanwhile, the number density of argon ions increases to maintain the pulsed periodic steady state within the plasma, as discussed in

sections 3.2.3 and 3.4.3.

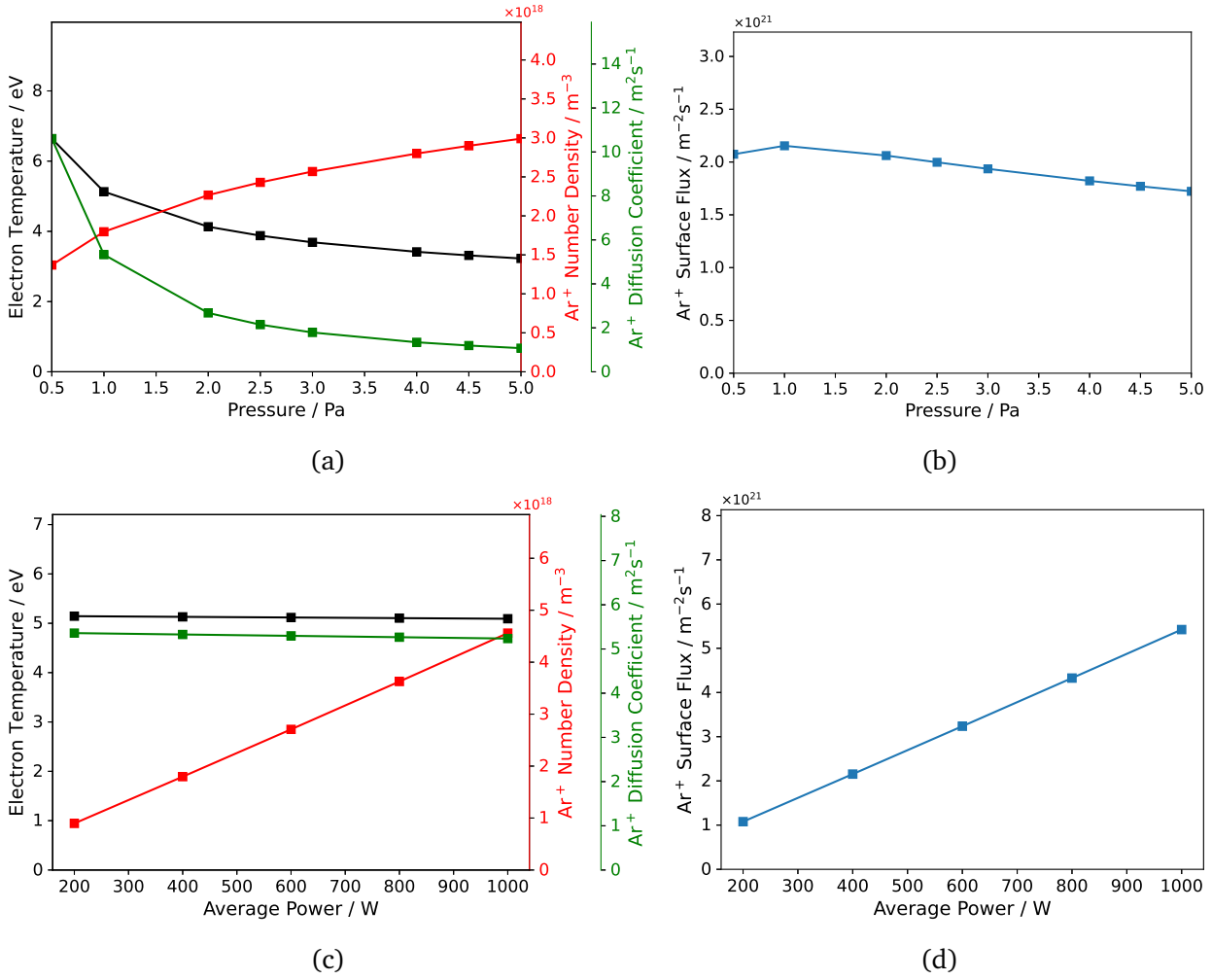

Figure 3.13: Temperature (eV) of electrons and the Number Density (m^{-3}) and Diffusion Coefficient (m^2s^{-1}) of Argon Ions (a) as a Function of Pressure at an Average Power of 400 W and (c) as a Function of Average Power at a Pressure of 1 Pa. Surface Flux of Argon Ions ($m^{-2}s^{-1}$) (b) as a Function of Pressure at an Average Power of 400 W and (d) as a Function of Average Power at a Pressure of 1 Pa

The effects of these factors combine to effect the surface flux of argon ions as seen in figure 3.13b. The surface flux of argon ions increases slightly as pressure increases from 0.5 Pa to 1 Pa, however, after 1 Pa the surface flux decreases linearly as pressure increases. This is because as pressure increases from 0.5 Pa to 1 Pa the effect of the increased number density of argon ions outweighs the effects of the diffusion coefficient, reducing the effectiveness of diffusion to the edge of the sheath and the temperature of electrons decreasing the Bohm velocity of ions into the sheath. However, past 1 Pa the effect of the reduced diffusion coefficient causes the diffusion to the edge of the sheath from the plasma bulk to become less effective, reducing the effect on the flux of the increased number density of argon ions. This, combined with the

decreased temperature of the electrons, which reduces the Bohm velocity, causes the surface flux of argon ions to decrease. In figure 3.13c the temperature of the electrons and the diffusion coefficient of the argon ions remain constant at all values of the average power, and the number density of argon ions increases linearly as the average power increases, as discussed in sections 3.2.3 and 3.4.3. Also in figure 3.13d the surface flux of argon ions increases linearly as the average power increases. This increases the number density of argon ions at the edge of the sheath, and combined with a constant Bohm velocity because of the constant temperature of the electrons this causes an increase in the surface flux. This is the same trend in surface flux as the average power increases, as observed in the variation of duty cycle and frequency, and therefore, the effect of average power on the surface flux of argon ions is not affected by duty cycle, frequency, or pressure differences for the average powers simulated.

3.5.6 The Effect of Pressure on the Input Energy per Argon Ion Fluxed to the Surface

How the input energy per argon ion fluxed to the surface which is calculated using equation 2.5.1 changes as a function of pressure and average power is shown in figure 3.14.

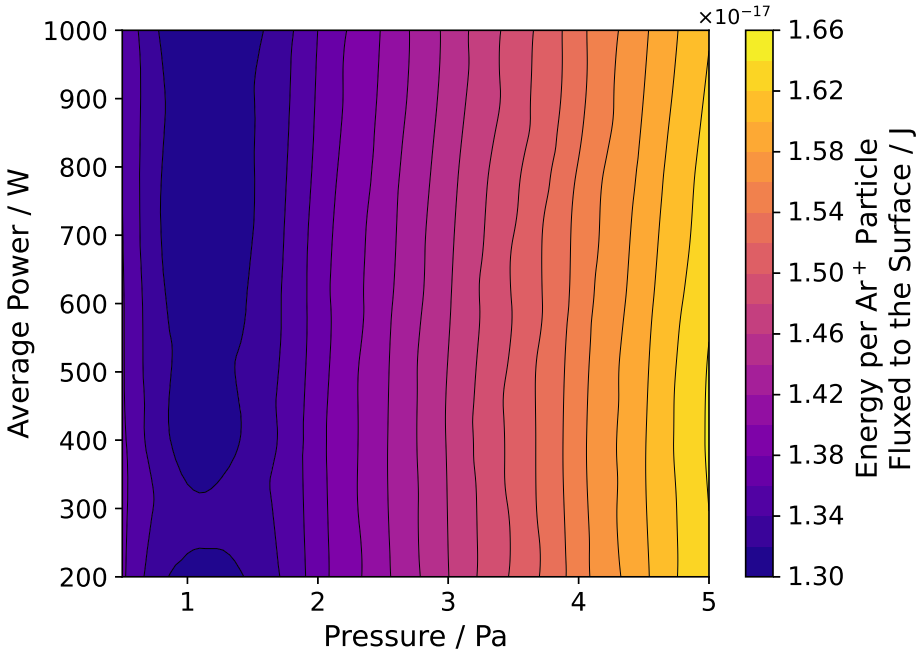

Figure 3.14: Input Energy per Argon Ion Particle fluxed to the surface (J) as a Function of Pressure and Average Power

In figure 3.14 the input energy per argon ion fluxed to the surface decreases with pressure until a minimum at 1 Pa and then increases linearly with pressure, and also the input energy per argon ion fluxed to the surface is constant as the average power increases. The input energy per argon

ion fluxed to the surface reaches a minimum at 1 Pa because as the pressure increases from 0.5 Pa to 1 Pa the effect of the increasing number density of argon ions, on the flux of argon ions, outweighs the effect of the decrease in the temperature of electrons and the diffusion coefficient of the argon ions. However, after 1 Pa the effect of the decreasing temperature and diffusion coefficient is larger than the effect of the increase in the number density of argon ions; therefore, the flux decreases past 1 Pa, and thus the input energy per ion fluxed increases. Therefore, to decrease the input energy per argon ion fluxed to the surface in an ICP reactor, the pressure needs to be chosen to maintain the optimal combination of those opposing factors. The input energy per argon ion fluxed to the surface stays constant with average power because of the increased energy inputted into the system, causing increased ionisation reactions proportional to the increase in average power rather than increasing the temperature of electrons. This is the same effect as observed in the duty cycle and frequency variations, and as such, for the average power ranges tested in this thesis, the duty cycle, frequency and pressure can be adjusted to achieve the lowest input energy per ion fluxed to the surface for the average power chosen. There is potential for the effects of changing the pressure, frequency and duty cycle to be combined together to produce a plasma operating regime with an even lower input energy per argon ion fluxed to the surface. For example, due to the increase in plasma potential as we decrease the pressure to the optimum pressure of 1 Pa, we can combine this pressure with a frequency lower than 10 Khz and a duty cycle above 0.5, which were excluded due to their plasma potential being lower than the energy window. Provided the trend in fluence with frequency and duty cycle continues at the lower pressure, this could lead to a further decrease in the energy used per ion fluxed to the surface. However, this has not been tested in this thesis.

Chapter 4

Pressure effect on ALD

In this chapter, the effect of changing the pressure and the average power on the production, flux, and input energy per particle fluxed to the surface of atomic oxygen and oxygen and argon ions is investigated for the purpose of ALD processes. Oxygen is important for the ALD process because the outer shell of valence electrons is incomplete. This makes oxygen more reactive than noble gases, such as argon, which allows surface effects such as the absorption of oxygen to occur at a lower surface temperature. These surface effects allow the chemical makeup of the surface to be altered, effectively depositing a new material on the surface. The new materials deposited onto the surface, such as low-k dielectrics and doped layers, are thermally sensitive [18, 20]. Therefore, they require the low temperature deposition enabled by atomic oxygen and ions to ensure that these materials do not degrade. Furthermore, it is important to investigate how the production and flux of oxygen species in argon-oxygen plasmas can be affected by changing plasma input parameters. This is because there are both atomic and molecular species inside the mixed plasma, which means that there is a larger number of species and reactions present in the plasma. This could lead to wasted energy used to produce species that are undesired for the purpose of ALD. In addition, the pressure of the plasma affects the initial density of the particles within the reactor. This affects the frequency of plasma collisions such as ionisation, which changes the mean free path of particles and alters the temperature of electrons. This affects the balance of production, consumption and the flux of atomic oxygen and oxygen and argon ions. We can treat these plasmas as they are in a pulsed periodic steady state. As such, the density of the particles is determined to be the density that balances the production and consumption rates of themselves. This means that pressure can affect the number density and flux of atomic oxygen and oxygen and argon ions. Therefore, investigating how pressure affects the number density, flux and the input energy per particle fluxed to the surface of atomic oxygen and oxygen and argon ions can reduce the energy used in ALD processes. The base case for this chapter can be seen in Table 2.4. The pressure is varied between 1 and 25 Pa at multiple average powers between 200 and 1000 W where the gas that makes up the plasma has an oxygen mixture fraction of 0.1.

4.1 Plasma Electron Properties

The temperature and number density of the electrons are important both for the rate of production and the flux of ions, as shown in equations 1.3.4 and 1.3.15. This is because increasing the temperature and number density of electrons increases the rate of ionisation reactions. The higher temperature of electrons means that on average the electrons have more energy available to ionise an electron from a atom. Also, increasing the number density of electrons means that there are more electrons per unit volume, which means that there is a higher likelihood for an ionisation collision to occur. Additionally, the temperature of electrons determines the Bohm velocity, which affects the rate of flux of ions to the surface. The effect of changing pressure from 1 to 25 Pa and average power from 200 to 1000 W on the temperature and number density of electrons can be seen in figures 4.1a and 4.1c, respectively. In addition, the effect of changing the pressure from 1 to 25 Pa at a constant average power of 400 W is shown in figure 4.1b

In figure 4.1a the electron temperature has a negligible change with average power, this coincides with a constant increase in the number density of electrons with average power for all pressures, as shown in figure 4.1c. This can be attributed to a higher average power causing an increase in ionisation proportional to the increase of average power rather than an increase in the electron thermal energy. In figure 4.1b the electron temperature can be seen to drop from 3.1 eV to 1.6 eV with the rate of decrease diminishing exponentially as pressure increases. This is caused by the higher gas density, which lowers the temperature of electrons due to increased electron elastic collisions, which transfer the energy from electrons to neutrals. The electron number density, as the pressure changes, increases until a peak then decreases slightly with higher pressure as shown in figure 4.1c. This is caused by the opposing production and consumption mechanisms of electrons within the plasma. The number density of electrons is determined to be the number density at which the plasma is in a pulsed periodic steady state where the production and consumption rates are equal. As pressure increases and the electron temperature drops, the consumption rate from the electron surface flux decreases; however, the consumption rate from dissociative electron attachment increases. In addition, the ionisation rate also decreases slightly as the pressure increases. This means that at low pressures the flux of electrons is dominant and therefore the density of electrons is required to be low to maintain the pulsed periodic steady state. However, as pressure increases, the consumption from the surface flux decreases sufficiently so that it is no longer dominant. Additionally, the increase in dissociative electron attachment has not increased significantly enough to be dominant over the production from ionisation. Therefore, to maintain a pulsed periodic steady state, a higher number density of electrons is required. However, past a certain pressure the decrease in ionisation and increase in dissociative electron attachment means that the consumption begins to dominate necessitating a lower number density of electrons. Therefore, as the pressure changes, a peak is formed in the number density of electrons. The peak in the number density of electrons moves with pressure from 10 to 19 Pa as the average power increases from 200 to 1000 W. The movement in the peak is due to the increased amount of energy deposited into the plasma, increasing the ionisation rate. This means that the pressure needs to increase further before the decrease in the ionisation is sufficient enough for the increase in dissociative

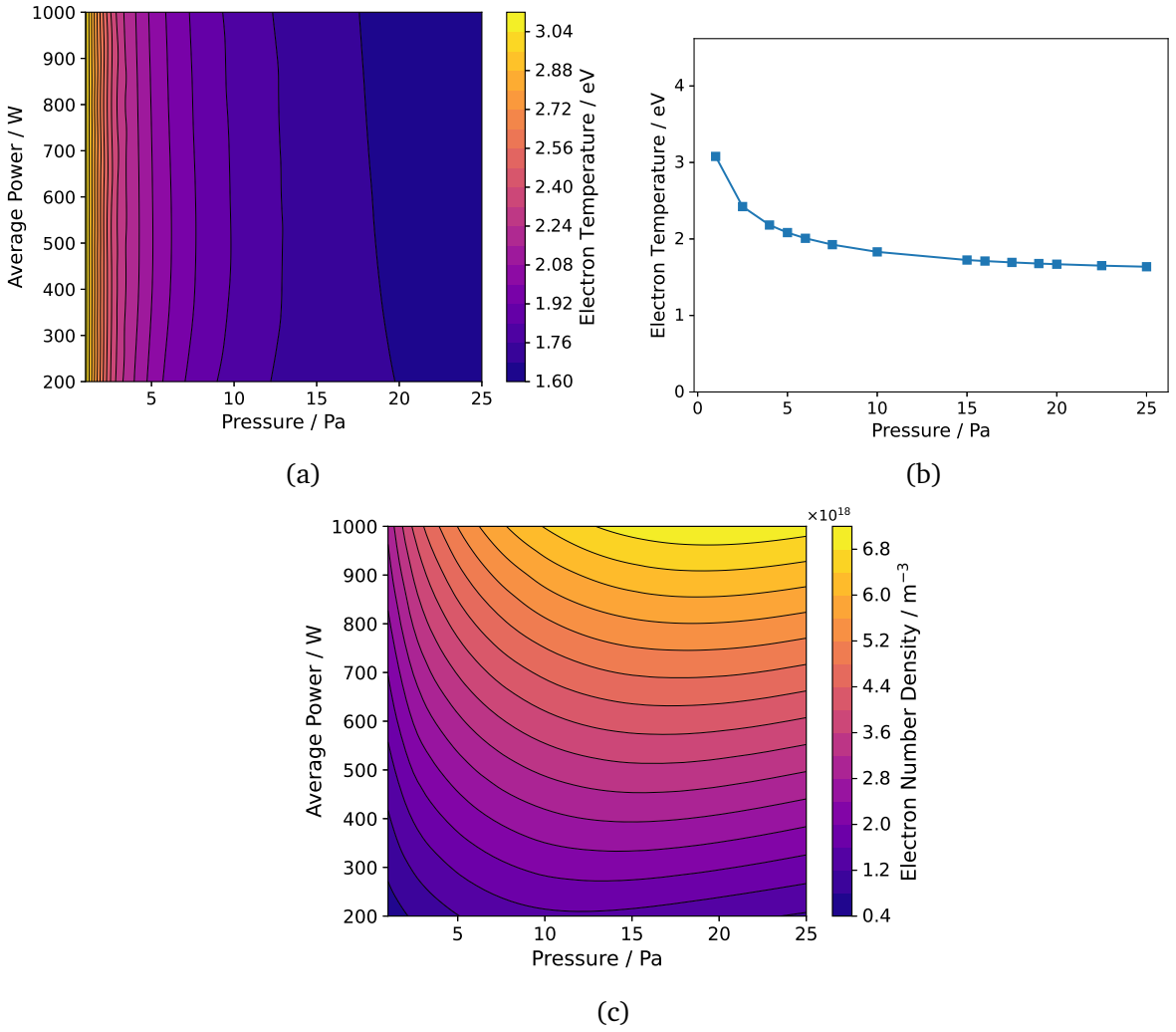

Figure 4.1: Electron Temperature (eV) (a) and Electron Number Density (m^{-3}) (c) as a Function of Pressure and Average Power and Electron Temperature (eV) (b) as a Function of Pressure at an Average Power of 400 W

electron attachment to begin to dominate over the production rate. Therefore, the peak occurs at a higher pressure.

4.2 Production of Atomic Oxygen

Atomic oxygen is constantly produced and consumed through various mechanisms within the plasma. Atomic oxygen is typically produced in one of three ways; dissociation of O_2, electron impact detachment of O^- and positive-negative ion recombination between O^- and Ar^+, however, there are many minor reactions that also produce atomic oxygen. Atomic oxygen is typically consumed in one of three ways; ionisation, charge exchange from Ar^+, recombina-

tion at the surface, and associative detachment with O^-. We can treat the plasma as a steady state which occurs when the loss rate is equal to the rate of production, where the density of atomic oxygen changes to balance the loss rate with the production rate. The most important reactions that determine the shape of the distribution of atomic oxygen number density are dissociation of O_2, ionisation of atomic oxygen and surface recombination, which are dependent on the number densities of O_2 and electrons, the diffusion coefficient of atomic oxygen that affects how readily the atoms diffuse towards the surface and the electron temperature that affects the rate constant. In addition, the population of atomic oxygen is constantly exciting and de-exciting, so the effect of pressure on $O(^1D)$ and $O(^1S)$ is also affected by these parameters. The properties that affect the production of atomic oxygen can be seen in figure 4.2. The number densities of O_2 and electrons and the diffusion coefficient of atomic oxygen in the pressure range of 1 - 25 Pa at an average power of 400 W are shown in figure 4.2a. The same plasma properties are also shown for the average power range of 200-1000 W at a pressure of 25 Pa in figure 4.2b. The number densities of O, $O(^1D)$ and $O(^1S)$ in the same power and pressure ranges are also compared in figures 4.2c and 4.2d, respectively. The number densities of ground state atomic oxygen and combined $O(^1D)$ and $O(^1S)$ excited states as a function of pressure and average power are shown in figures 4.2e and 4.2f, respectively. Here, the graphs for the number density of electrons are included again to help illustrate why the trends in the number density of atomic oxygen appear.

In figure 4.2a, the number density of O_2 increases linearly with pressure coinciding with a decrease in the diffusion coefficient of atomic oxygen proportional to P^{-1} and the number density of electrons peaks at 16 Pa. This causes a large increase in the number density of O, $O(^1D)$ and $O(^1S)$ as shown in Figure 4.2c as pressure increases, with the rate of increase of $O(^1D)$ and $O(^1S)$ decreasing at higher pressures due to increased collisional quenching of $e + O(^1D) \rightarrow e + O$, $O + O(^1D) \rightarrow 2O$ and similar reactions for $O(^1S)$. The cause behind the 1700% increase in the number density of O is that the increase in the number densities of O_2 and electrons increases the reaction rate of the production of atomic oxygen meanwhile, the diffusion coefficient decreases due to the increased pressure causing more collisions between atomic oxygen and other heavy particles. Therefore, to maintain a pulsed periodic steady state solution, the number density of O needs to increase. In figure 4.2b, the number density of O_2 decreases linearly by 57%, whilst the number density of electrons increases linearly by 1090% with average power and the diffusion coefficient of atomic oxygen changes negligibly. This causes an increase in the number density of O, $O(^1D)$ and $O(^1S)$ as shown in figure 4.2d, as the vastly greater increase in the number density of electrons outweighs the decreases in number density of O_2. This creates a larger reaction rate for the production of atomic oxygen which requires a higher number density of atomic oxygen to maintain a pulsed period steady state.

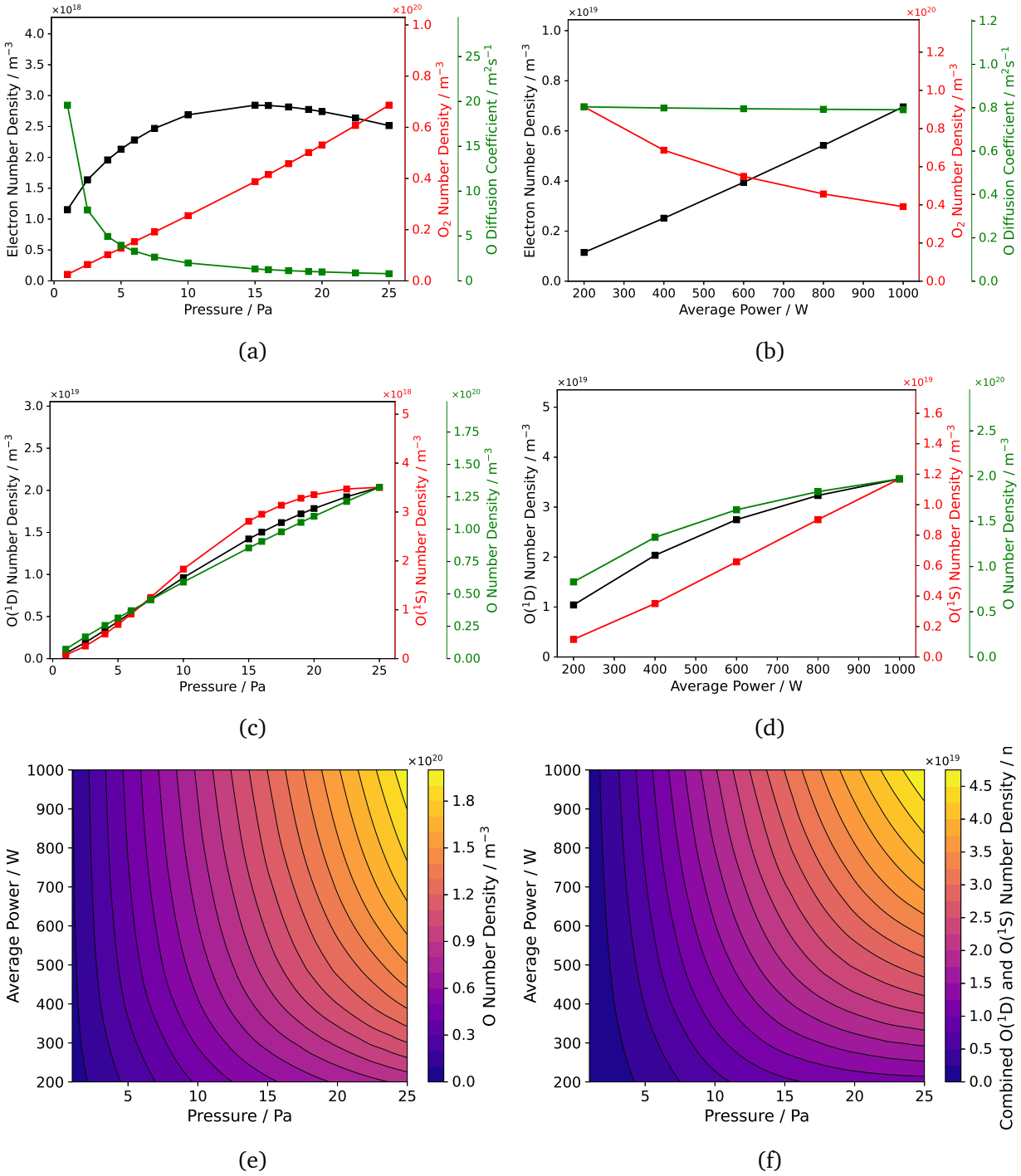

Figure 4.2: Number Density of O_2 and Electrons (m^{-3}) and Diffusion Coefficient of Atomic Oxygen (m^2s^{-1}) (a) as a Function of Pressure at an Average Power of 400 W and (b) as a Function of Average Power at a Pressure 25 Pa, Number Density of O, O(^1D) and O(^1S) (m^{-3}) (c) as a Function of Pressure at an Average Power of 400 W and (d) as a Function of Average Power at a Pressure of 25 Pa, Number Density of Ground State Atomic Oxygen (m^{-3}) (e) as a Function of Pressure and Average Power and the sum of the Number Density's of O(^1D) and O(^1S) Excited States (m^{-3}) (f) as a Function of Pressure and Average Power

The number density of ground state atomic oxygen in figure 4.2e and the sum of the excited atomic oxygen states; O(^1D) and O(^1S) in figure 4.2f show that the rate of increase with pressure in the number density of atomic oxygen at low average power is lower than that of higher average powers. This is caused by the earlier peak with pressure in the electron density at low average power, which causes the production rate of atomic oxygen to increase slower at high pressure and low powers. At high pressure, the number density increases with the average power; however, at low pressure, the change with the average power is small to negligible. This is caused by the large diffusion coefficient of atomic oxygen at low pressure, which requires a smaller change in the number density of atomic oxygen to maintain a pulsed periodic steady state. In figure 4.2f the rate of increase with pressure at high pressure and low average power is lower compared to the ground state atomic oxygen, due to increased collisional quenching. However, at higher average power the effect of collisional quenching becomes marginal in this regime, therefore the difference in the rate of increases is diminished.

4.3 Flux of Atomic Oxygen

The flux of atomic oxygen is defined as the flux of atomic oxygen particles to the surface walls that for the ground state atomic oxygen recombines or for the excited states de-excites at the wall and is a diffusion-driven flux regime. An increased diffusion coefficient and density will increase the drive of atomic oxygen to the surface. Furthermore, a higher sticking coefficient will give a higher probability for atoms to recombine to the surface; this increases the number of attachments per unit flux and also the density gradient from the plasma bulk to the surface driving an increase in flux of atoms to the surface. The sticking coefficient of ground-state atomic oxygen is shown in figure 4.3a, where the sticking coefficient of all excited states of oxygen in this model is set to 1 [32]. The number density, diffusion coefficient and surface flux of atomic oxygen for the pressure range of 1-25 Pa at an average power of 400 W and for an average power in the range of 200-1000 W at a pressure of 25 Pa are shown in figures 4.3b and 4.3c, respectively. Here in figure 4.3c the maximum axis values of the O number density and the O surface flux have been set differently to aid in visibility; without this the trends are identical. The surface flux of ground state atomic oxygen and the combined O(^1D) and O(^1S) excited states as a function of pressure and average power are shown in figures 4.2e and 4.2f, respectively. Here, the graphs for the number density and diffusion coefficient of atomic oxygen are included again to help illustrate why the trends in the flux of atomic oxygen appear.

In figure 4.3a the sticking coefficient for atomic oxygen decreases proportionally to P^{-1} from 0.2 to 0.15 [61]. This significantly affects the surface flux of ground-state atomic oxygen, as more than 80% of the flux interacting with the surface is reflected, and additionally this decreases the density gradient between the plasma bulk and the surface decreasing incident flux. This reduces the effectiveness of the ground-state atomic oxygen flux compared to the flux of O(^1D) and O(^1S) for the purpose of plasma processing.

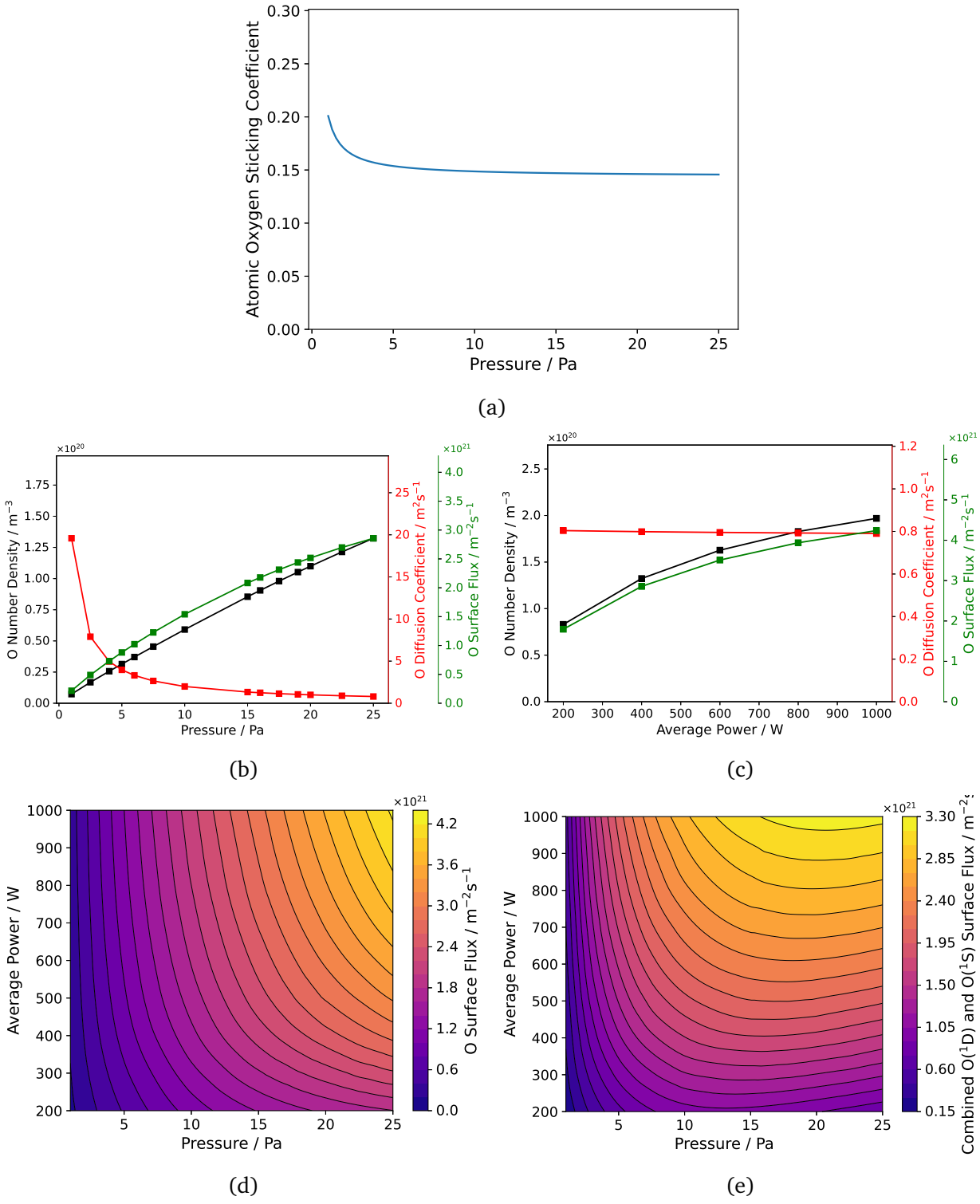

Figure 4.3: Sticking Coefficient of Atomic Oxygen (a) as a function of Pressure, Number Density (m^{-3}), Diffusion Coefficient (m^2s^{-1}) and Surface Flux (m^2s^{-1}) of Atomic Oxygen (b) as a function of Pressure at an Average Power of 400 W and (c) as a function of Average Power at a Pressure of 25 Pa, Ground State Atomic Oxygen Surface Flux (m^2s^{-1}) (d) and the sum of Excited O(^1D) and O(^1S) States, Surface Flux (m^2s^{-1}) (e) as a function of Pressure and Average Power

In figure 4.3b, the number density of atomic oxygen increases linearly, while the diffusion coefficient decreases proportionally to P^{-1}. This causes the flux of atomic oxygen to follow the trend of the number density with a boost to the low-pressure flux and hindrance to the high-pressure flux due to a decreasing diffusion coefficient. In figure 4.3c the number density and surface flux of atomic oxygen follow the exact same trend where they increase with the average power, with the rate of increase reducing with the average power. This is because of the negligible change in diffusion coefficient with average power and the constant nature of the sticking coefficient with average power; therefore, the surface flux of atomic oxygen as a function of average power depends only on the number density. This culminates in figure 4.3d, where the overall trend in surface flux follows the trend of the number density of atomic oxygen seen in figure 4.2e. However, with values of surface flux similar to the excited atomic oxygen surface flux in figure 4.3e, despite the higher number density of ground state atomic oxygen, due to the sticking coefficient. The surface flux of excited atomic oxygen increases with average power; however, this reaches a peak with the peak shifting with average power from a peak at 13 Pa at 200 W to 21 Pa at 1000 W. This is caused by the decreasing diffusion coefficient that coincides with the decreasing rate of increase in the number density of O(^1D) and O(^1S) at high pressure, causing the flux to reach a peak in pressure even though the number density is still increasing. The shift to peaks at higher pressure at higher average power is due to the increased rate of increase in the number density of O(^1D) and O(^1S) at higher average powers.

4.3.1 Input Energy per Atomic Oxygen Fluxed to the Surface

The input energy per atomic oxygen fluxed to the surface is defined as seen in equation 2.5.1, where the flux is the amount particles which react on the surface wall and the lower energy used per particle fluxed to the surface is a more efficient plasma operating regime. The input energy per O fluxed to the surface and the input energy per O(^1D) and O(^1S) fluxed to the surface as a function of pressure at an average power of 400 W and as a function of average power at a pressure of 25 Pa can be seen in figures 4.4a and 4.4b, respectively. Additionally, the input energy per O fluxed to the surface and the input energy per O(^1D) and O(^1S) fluxed to the surface as a function of pressure and average have been shown in figures 4.4c and 4.4d, respectively.

In figure 4.4a the input energy per atomic oxygen particle fluxed to the surface of both the ground state atomic oxygen and the sum of O(^1D) and O(^1S) excited states decreases with pressure proportional to P^{-1} however, at 16 Pa the input energy per O(^1D) and O(^1S) fluxed to the surface begins to increase marginally due to the peak in the number density of O(^1D) and O(^1S). In figure 4.4b the input energy per ground state atomic oxygen fluxed to the surface increases linearly with average power, while the input energy per O(^1D) and O(^1S) increases with the rate of increase, increasing marginally with average power. However, the overall increase is lower than that for the ground state. The increase in the input energy per particle fluxed to the surface means that even though at higher average power the surface attachment flux is higher, the rate of increase of the flux is lower than the increase in average power. Therefore, to decrease the input energy used per particle for atomic layer processing with atomic oxygen,

a low average power is preferred. This is likely caused by an increase in ionisation, recombination and collisional quenching at high average power regimes with the charge transfer of $O + Ar^+ \rightarrow O^+ + Ar$ increasing by 958% between 200 W and 1000 W at 25 Pa.

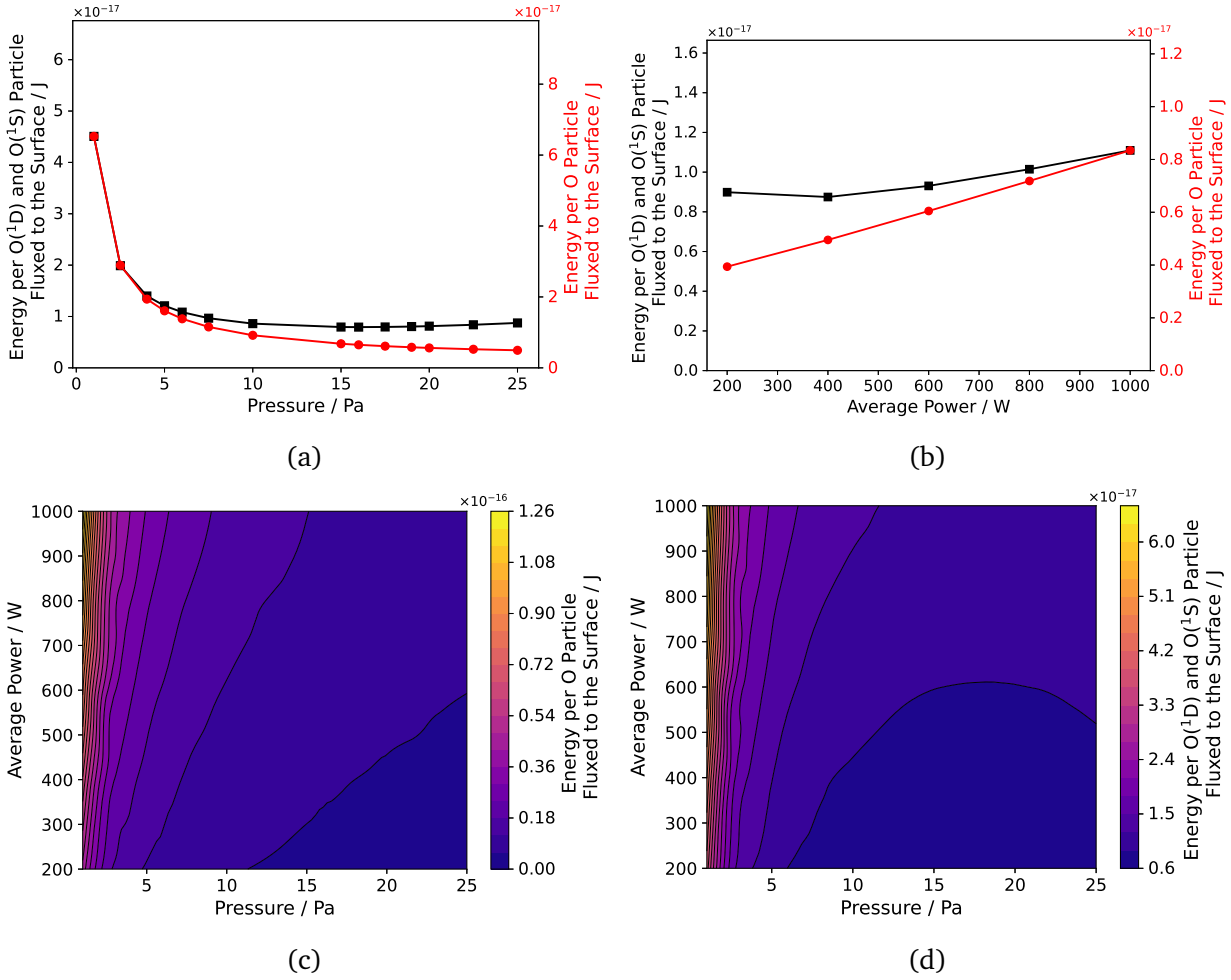

Figure 4.4: Input Energy per particle fluxed to the surface of Ground state Atomic Oxygen and the Sum of Excited O(^1D) and O(^1S) States (J) (a) as a function of Pressure at an Average Power of 400 W and (b) as a function of Average Power at a Pressure of 25 Pa, Input Energy per ground state Atomic Oxygen fluxed to the surface (J) (c) and Input Energy per Particle Fluxed to the Surface of the Sum of Excited O(^1D) and O(^1S) States (J) (d) as a Function of Pressure and Average Power

In figure 4.4c the input energy per ground state atomic oxygen fluxed to the surface decreases with pressure with a smaller rate of decrease at higher pressures. The input energy per ground state atomic oxygen fluxed to the surface increases with average power at the same rate at all pressures, with the rate of increase with average power becoming larger than the rate of increases from increasing the pressure at higher pressures. In figure 4.4d the input energy per O(^1D) and O(^1S) fluxed to the surface follows a trend similar to ground state atomic oxygen; however, past 5 Pa the rate of decrease in the input energy per O(^1D) and O(^1S) fluxed to the

surface with pressure slows with a minima located at 15 Pa at 200 W increasing to 22 Pa at 1000 W, caused by the peaks seen in the surface attachment flux. The input energy per O(^1D) and O(^1S) fluxed to the surface is similar to the input energy per ground state atomic oxygen fluxed to the surface oxygen, although the number density of ground state atomic oxygen is higher. This is because of the lower surface attachment flux of ground state atomic oxygen caused by the lower sticking coefficient and high excitation rates. This means that a portion of the flux to the surface is reflected or excited before it reaches the surface, therefore, lowering the surface attachment flux. At higher pressures and lower average powers, the input energy per ground state atomic oxygen fluxed to the surface is lower than that for the O(^1D) and O(^1S) excited states. Therefore, it is more efficient to use processes that make use of ground state atomic oxygen at high pressures, although the difference is marginal. In general, increasing pressure is an effective method of decreasing the input energy per atomic oxygen particle fluxed to the surface of atomic oxygen although beyond 15 Pa there are diminishing returns. In addition, decreasing the average power reduces the input energy per surface collision; however, it simultaneously reduces the surface flux. Therefore, to minimise the input energy per atomic oxygen fluxed to the surface, a high pressure, low average power regime is required; however, if high surface flux is required, increasing the average power at high pressures is still efficient, as there is a minimal increase in input energy per surface collision.

4.4 Production of Ions

The ions inside a plasma are constantly being produced and consumed. Similarly to the production of atomic oxygen, we can treat the plasma as it is in a pulsed periodic steady-state; this means that the loss rate of ions inside the plasma will be equal to the production rate. To achieve this, the number density of the ions will change, increasing if the production is stronger than the consumption and vice versa.

4.4.1 Production of Ar^+

For the production of argon ions the main sources of production are electron ionisation of Ar, Ar($4P$) and Ar^m, with the ionisation from ground state argon being the most significant reaction. The main loss mechanisms of argon ions are charge exchanges between Ar^+ and both O_2 and O and the surface flux of argon ions, which is affected by the diffusion coefficient of Ar^+ and the temperature of the electrons. The number density of ground state argon and electrons as well as the electron temperature are shown in figure 4.5a for the pressure range of 1 - 25 Pa at an average power of 400 W and in figure 4.5b for the average power range of 200 - 1000 W at a pressure of 16 Pa. The number densities of O_2 and O and the diffusion coefficient of Ar^+ for the same pressure and average power range are shown in figure 4.5c and 4.5d, respectively. The number density of Ar^+ as a function of pressure and average power is shown in figure 4.5e. Here, the graphs of the number density and temperature of electrons and the number density

of atomic oxygen are included again to help illustrate why the trends in the number density of Ar^+ appear.

In figure 4.5a the number density of ground state argon increases linearly with pressure, the electron temperature decreases proportionally to P^{-1} and the number density of electrons increases to a peak at 16 Pa and then slowly decreases afterward. However, in figure 4.5c the number densities of atomic oxygen and O_2 increases linearly, whilst the diffusion coefficient of Ar^+ decreases proportionally to P^{-1} due to increased collisions with heavy particles caused by increased pressure increasing the density of the gas. In figure 4.5e the number density of Ar^+ increases with pressure until a peak is reached with the number density slightly decreasing past that point. This is caused by the complex relationship between the production and consumption of Ar^+. As pressure increases, the production of Ar^+ decreases because the drop in electron temperature outweighs the increase in the number densities of ground-state argon and electrons. The consumption of Ar^+ through surface-based electron ion recombination decreases due to a decrease in the diffusion coefficient; however, the consumption due to charge exchange reactions with atomic oxygen and O_2 increases with pressure. At low pressure, the low number density of Ar^+ is caused by the high surface-based electron ion recombination that necessitates a low number density of Ar^+ to maintain a pulsed periodic steady state. As pressure increases, production decreases; however, consumption also decreases at a higher rate than production at medium pressures, causing an increase in the number density of Ar^+. As pressure rises, the consumption eventually begins to increase because of increased charge exchange reactions and diminishing rate of decrease of the diffusion coefficient, leading to a peak in the number density required to hold a pulsed periodic steady state. In figure 4.5b the number density of electrons increases linearly with average power whilst the electron temperature and the number density of ground state argon remain constant. In figure 4.5d the diffusion coefficient remains constant, whereas the number density of O_2 decreases with average power, and the number density of O increases with average power. This is caused by the increased energy deposited into the plasma allowing more dissociation events to occur, splitting O_2 into O. In figure 4.5e the number density of Ar^+ increases with average power due to the increased ionisation caused by the increase in the number density of electrons. The peak of the number density of Ar^+ in pressure moves from 12.5 Pa to 16 Pa as average power increases from 200 W to 1000 W, this is caused by the increased energy deposited into the plasma at higher average powers leading to higher ionisation rates which requires a higher pressure for the charge exchange consumption mechanism to increase enough to cause the number density to decrease to maintain a pulsed periodic steady state.

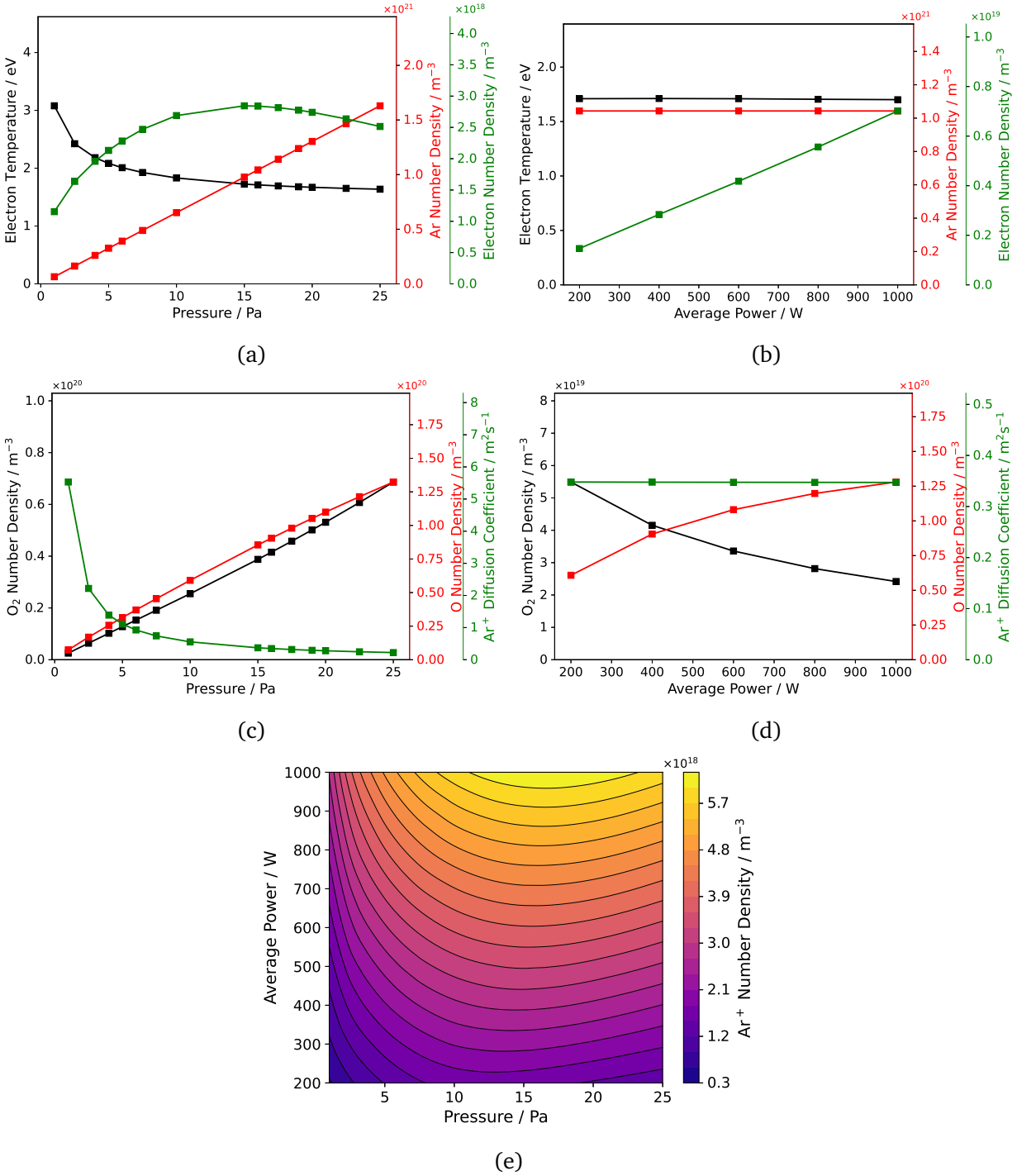

Figure 4.5: Number Density of Argon and Electrons (m^{-3}) and the Temperature of Electrons (eV) (a) as a function of Pressure at an Average Power of 400 W and (b) as a function of Average Power at a Pressure of 16 Pa, Number density of O_2 and Atomic Oxygen (m^{-3}) and the Diffusion Coefficient of Ar^+ (m^2s^{-1}) (c) as a function of Pressure at an Average Power of 400 W and (d) as a function of Average Power at a Pressure of 16 Pa and Number Density of Ar^+ (m^{-3}) (e) as a function of Pressure and Average Power

4.4.2 Production of O^+

For the production of O^+, the main production methods are the ionisation from the ground state of atomic oxygen or the excited states of $O(^1D)$ and $O(^1S)$, or charge exchange between Ar^+ and ground state atomic oxygen. The main consumption mechanisms are positive-negative ion recombination with O^- and electron ion recombination at the surface. The number densities of Ar^+, O and electrons are shown in figure 4.6a over the pressure range of 1 - 25 Pa at an average power of 400 W and in figure 4.6b over the average power range of 200 - 1000 W at a pressure of 25 Pa. The number density of O^- and the diffusion coefficient of O^+ for the same pressure and average power ranges are shown in figures 4.6c and 4.6d, respectively. The number density of O^+ as a function of pressure and average power is shown in figure 4.5e. Here, the graphs of the number densities of electrons, atomic oxygen and Ar^+ are included again to help illustrate why the trends in the number density of O^+ appear.

In figure 4.6a the number density of O increases linearly with pressure, the number densities of Ar^+ and electrons are roughly identical because the original plasma gas mixture being 90% argon, the number densities increase with pressure until a peak at 16 Pa then decrease slightly as discussed previously in sections 4.1 and 4.4.1. The increase in the number densities of Ar^+ and O increases the production of O^+ through charge exchange between the species. However, due to the decrease of electron temperatures, the rate of production of ionisation of O decreases with pressure; this culminates in the total production of O^+ remaining roughly constant with pressure at pressure and average power values greater than 5 Pa at 400 W. In figure 4.6c the diffusion coefficient of O^+ decreases proportionally to P^{-1} due to increased elastic collisions with other heavy species. The number density of O^- increases linearly with pressure due to the increase in the number densities of electrons and O_2 leading to increased dissociative electron attachment. The increase in the number density of O^- increases the consumption of O^+, however, because the low relative absolute value of the number density of O^- being around the value of 1×10^{17}, this requires a high pressure to become significant. On the other hand, the consumption of O^+ through surface-based electron ion recombination drops with pressure due to the diffusion coefficient reducing the flux to the surface. In figure 4.6b the number density of O increases with average power; however, the rate of increase drops at higher average power, the number densities of Ar^+ and electrons are roughly equal and increase linearly with average power; all can be attributed to the increased energy deposited into the plasma allowing more dissociation and ionisation events to occur as discussed in sections 4.2, 4.1 and 4.4.1. This significantly increases the production of O^+ as the increase in the number densities of Ar^+, O and electrons combined with the electron temperature remaining constant increases the reaction rates of the reactions that produce O^+. In figure 4.6d the diffusion coefficient of O^+ remains constant with the average power, which means that the surface-based electron ion recombination rate is unchanged, with the number density of O^- decreasing with the average power past 400 W due to increased rates of associative detachment. This decreases the consumption of O^+ as the decrease in the number density of O^- hinders positive-negative ion recombination with O^+.

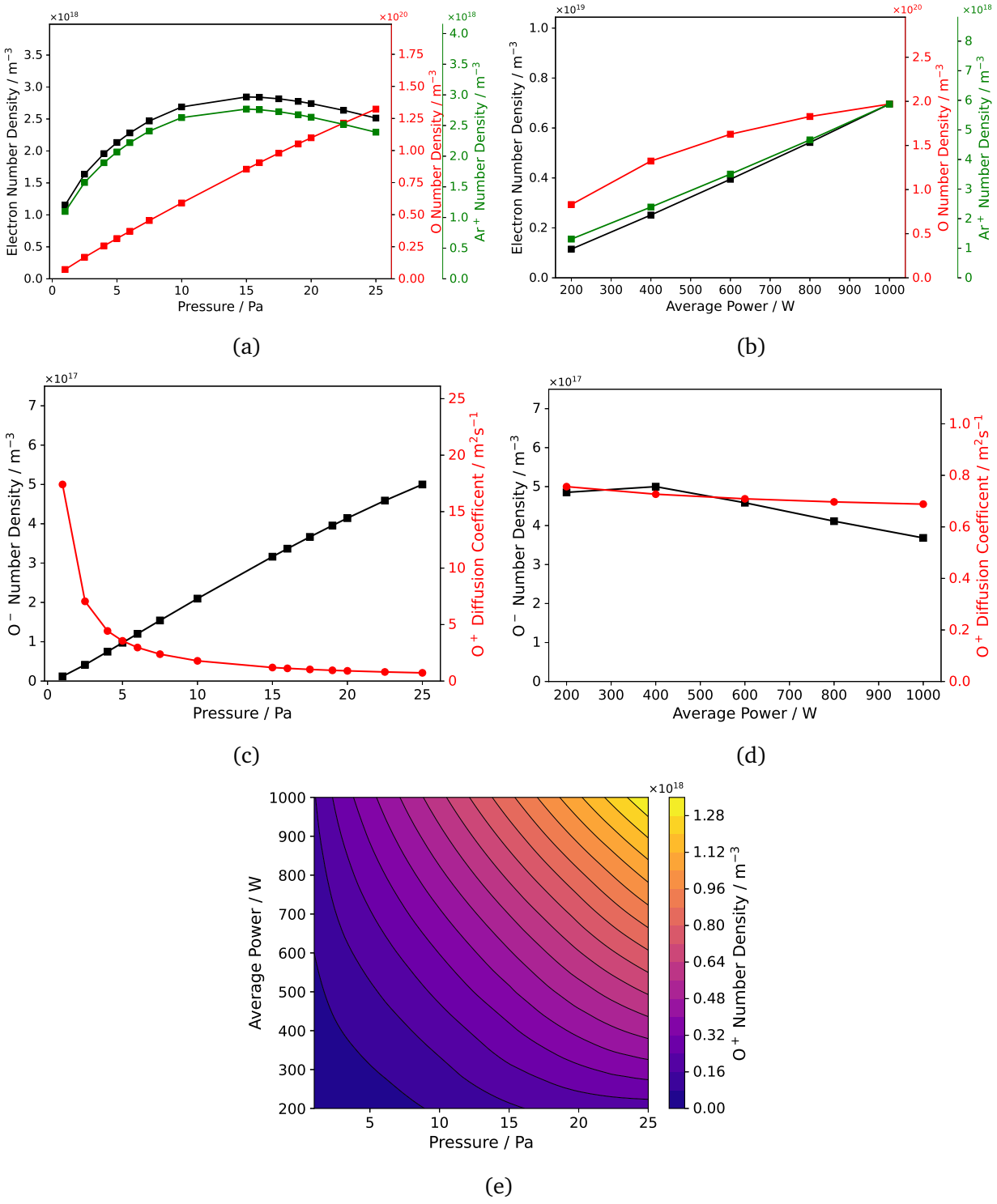

Figure 4.6: Number Density of O, Electrons and Ar^+ (m^{-3}) (a) as a function of Pressure at an Average Power of 400 W and (b) as a function of Average Power at a Pressure of 25 Pa, Number Density of O^- (m^{-3}) and the Diffusion Coefficient of O^+ (m^2s^{-1}) (c) as a function of Pressure at an Average Power of 400 W and (d) as a function of Average Power at a Pressure of 25 Pa and The Number Density of O^+ (m^{-3}) (e) as a function of Pressure and Average Power

In figure 4.6e the number density of O^+ increases with pressure, increasing faster at higher average powers, and increases with average power, increasing faster at higher pressure. The increase in the number density of O^+ with pressure is due to the decrease in the diffusion coefficient that hinders the consumption to surface-based electron ion recombination. With the increase in the number densities of O, Ar^+ and electrons causing the production of O^+ to remain roughly constant with pressure, these combined effects necessitate a higher number density of O^+ to maintain a pulsed periodic steady-state. The faster rate of increase at higher average power is due to the increased energy deposited into the plasma increasing the ionisation rates, whilst surface-based electron ion recombination remains unchanged. At low average power and high pressure, the rate of change with pressure of O^+ begins to stagnate. This is because the drop in the number density of Ar^+ and electrons and the electron temperature causes the production of O^+ to begin to drop. Therefore, starting to require a lower number density of O^+ to maintain a pulsed period steady-state and would likely result in a peak with pressure if the pressure regime is extended. The increase in the number density of O^+ with average power is due to increases in the number densities of O, Ar^+ and electrons with constant electron temperatures increasing the production rate of O^+, whilst the consumption rate is hindered by the drop in the number density of O^-. This means that a higher number density of O^+ is required to maintain a pulsed period steady-state. The rate of increase with average power is higher for higher pressure values due to the large diffusion coefficient at low pressures that increases surface-based electron ion recombination, requiring a lower change in the number density of O^+ to maintain a pulsed period steady-state.

4.4.3 Production of O_2^+

The main production mechanisms for O_2^+ are the ionisation of O_2 and charge exchange between Ar^+ and O_2. The main consumption mechanisms of O_2^+ are dissociative recombination and surface-based electron ion recombination. The number densities of O_2, Ar^+ and electrons are shown in figure 4.7a over the pressure range of 1 - 25 *Pa* at an average power of 400 *W* and in figure 4.7b over the average power range of 200 - 1000 *W* at a pressure of 25 *Pa*. The diffusion coefficient of O_2^+ as a function of pressure and average power is shown in figure 4.7c. The number density of O_2^+ as a function of pressure and power is shown in figure 4.7d. Here, the graphs of the number densities of electrons and Ar^+ are included again to help illustrate why the trends in the number density of O_2^+ appear.

In figure 4.7a the number density of O_2 increases linearly with pressure, the number densities of Ar^+ and electrons are roughly equal to each other, increasing until a peak is reached in pressure, then decreasing slightly as discussed previously in sections 4.1 and 4.4.1. This causes the production of O_2^+ to increase from charge exchange collisions, however, due to the electron temperature decreasing with pressure the production rate form ionisation drops slightly, although the total production rate increases with pressure. However, increasing the number density of electrons also increases the consumption of O_2 through dissociative electron attachment, negating some of the effect of increases in production.

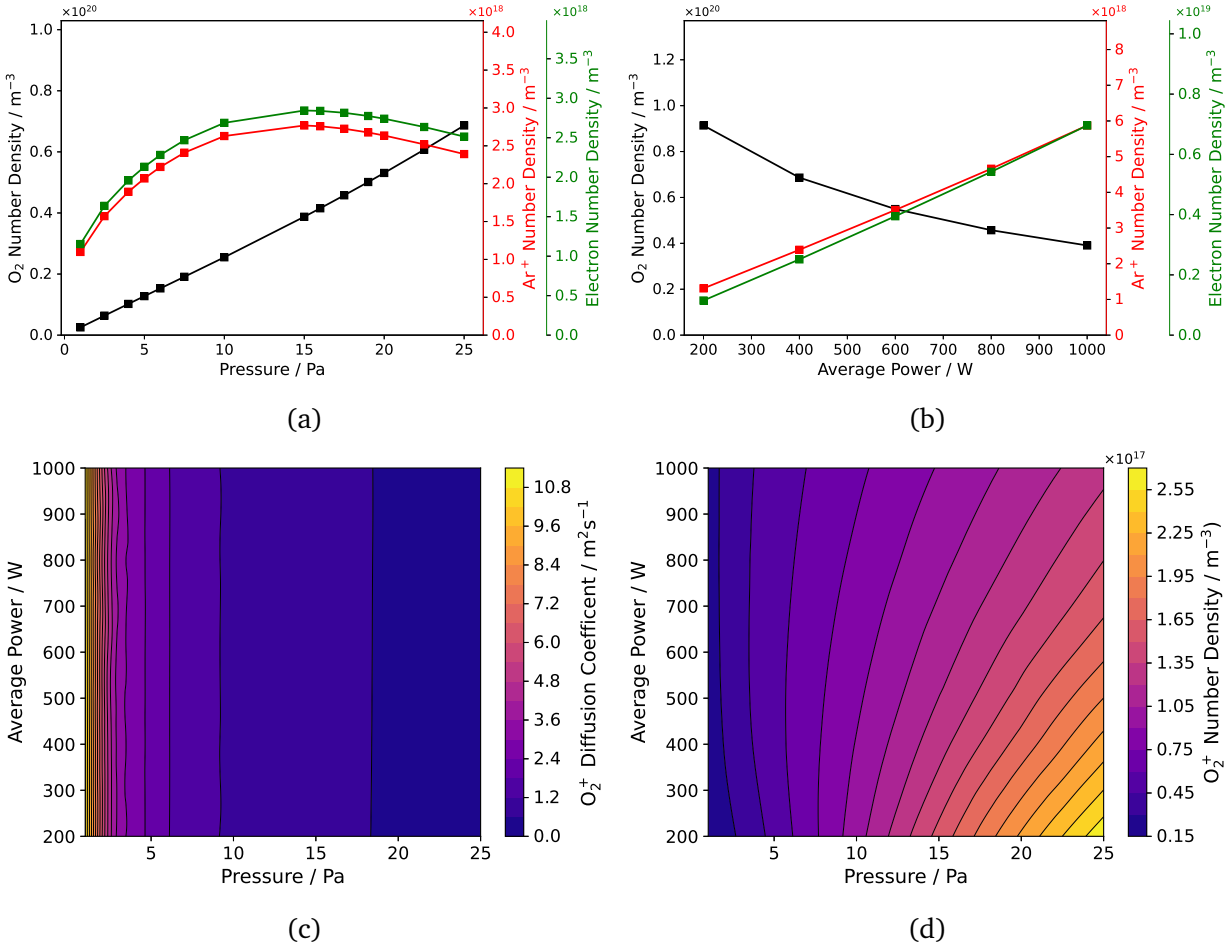

Figure 4.7: Number Density of O_2, Ar^+ and Electrons (m^{-3}) (a) as a function of Pressure at an Average Power of 400 W and (b) as a function of Average Power at a Pressure of 25 Pa, Diffusion coefficient of O_2^+ (m^2s^{-1}) (c) as a function of Pressure and Average Power and Number Density of O_2^+ (m^{-3}) (d) as a function of Pressure and Average Power

In figure 4.7b the number densities of Ar^+ and electrons increase linearly with the average power, whereas the number density of O_2 decreases linearly with the average power. This is because the increased energy deposited into the plasma causes increased ionisation and dissociation inside the plasma. The production of O_2^+ increases with average power because the number densities of Ar^+ and electrons increase faster than the decrease in the number density of O_2 with electrons and Ar^+ increasing by a factor of roughly 4 whereas O_2 only decreases by a factor of 0.42, with the electron temperature remaining constant. However, this also increases the consumption of O_2^+ through dissociative electron attachment due to the increased number density of electrons. In figure 4.7c the diffusion coefficient of O_2^+ decreases with pressure proportionally to P^{-1} and remains constant with average power, this is caused by increased heavy particle elastic collisions caused by the higher density of particles in the gas at higher pressure. This, combined with the decrease of electron temperature, causes the consumption from surface-based electron ion recombination to be hindered, which decreases the consumption rate. In figure 4.7d the number density of O_2^+ increases with pressure due to the increase

in production through ionisation and charge exchange, coinciding with a decrease in diffusion coefficient and electron temperature that hinders the consumption from surface-based electron ion recombination. However, the increase with pressure is hindered by the increase in dissociative electron attachment. The number density of O_2^+ is roughly constant as the average power changes at pressure bellow 5 *Pa* however, for pressures above this the number density decreases with the average power. This is because at low pressure the diffusion coefficient and electron temperature are high and the number density of O_2, Ar^+ and electrons are low; therefore, the rates of production are low compared to the consumption rate from surface-based electron ion recombination and as such any change in production rates has less of an affect. At high pressure, the drop in the number density of O_2^+ with average power is caused by the difference between the production and consumption rates. At high average power, consumption rates are closer to production rates requiring a lower number density of O_2^+ to maintain a pulsed periodic steady-state. However, as the average power is decreased, the consumption rate decreases faster than the production rate because the number density of electrons decreases more than the number density of O_2, causing a larger decrease in dissociative electron attachment than the decrease in ionisation and charge exchange. Therefore, to maintain a pulsed periodic steady-state, the number density of O_2^+ increases.

4.5 Flux of Ions

The flux of ions inside the plasma is driven by the sheath; however, when determining the flux, we need to determine the flux into the sheath. The flux into the sheath depends on the readiness of ions to diffuse to the edge of the sheath, the electronegativity which reduces the density of ions at the sheaths edge, the electron temperature and the number density of the ions. Finding a regime with the correct combination of factors that create a high flux for the energy imputed into the plasma is vital to increasing the efficiency of plasma processes.

4.5.1 The Flux of Ar^+

The flux of Ar^+ is important for the ALD process not because the ions help the process, but because they can hinder the process. This is because when the plasma potential is large enough, the ions when interacting with the surface will have enough energy to physically sputter the surface, lowering the quality of the end result of the process [31]. The energy required for this to occur depends on the material of the surface, however, is typically greater than 30 eV, which therefore requires a plasma potential of more than 30 eV. The plasma potential as it varies over time at an average power of 400 W and a pressure of 2.5 Pa is shown in figure 4.8a with the orange line signifying when the power is turned off in the cycle ends. The maximum value of plasma potential in the last cycle as a function of pressure and average power is shown in figure 4.8b.

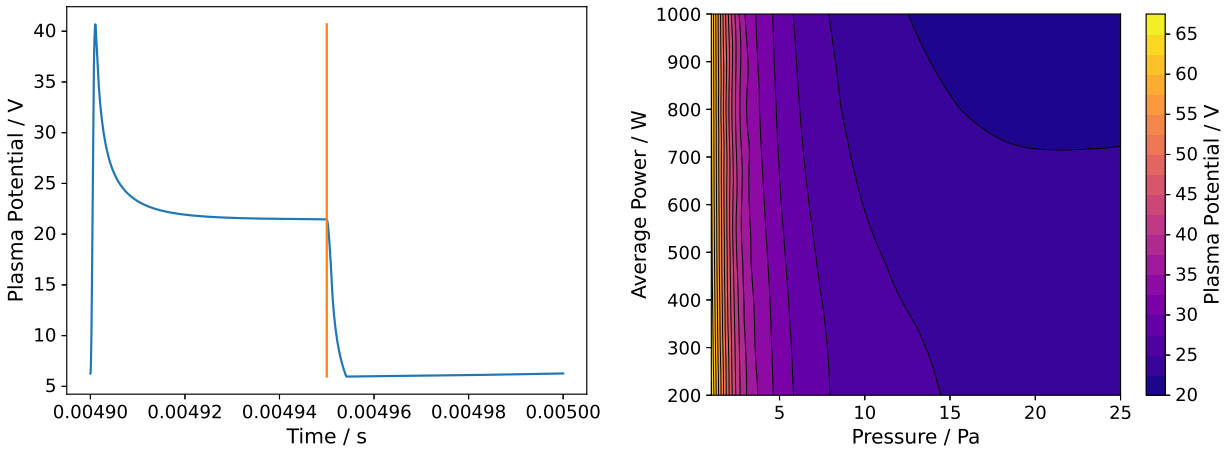

(a) (b)

Figure 4.8: Plasma Potential (a) as a Function of Time over the Last Pulse and the Maximum Value of Plasma Potential in the Last Cycle (b) as a Function Pressure and Average Power

In figure 4.8a the plasma potential spikes when the power is first turned on in the last pulse, afterward the plasma potential decreases to a consistent value. This spike is the only time frame in which the plasma can provide the ions with high enough energy to sputter, therefore, because of the small time frame of the spike, it will cause minimal damage to the surface. In figure 4.8b the value of the maximum of the plasma potential in the last cycle decreases with pressure proportionally to P^{-1}, this is because the plasma potential is directly proportional to the electron temperature, which decreases proportionally to P^{-1} as shown in figure 4.1 and discussed in section 4.1. The highest value of plasma potential at 5 Pa and above is below 30 eV, therefore no ion will possess enough energy to cause sputtering of the surface and therefore no damage to the surface at pressures above this. Therefore, the effect of argon ion flux to ALD using this system is minimal, as there is either minor sputtering at low pressure or none at all in this system.

The number density and diffusion coefficient of Ar^+ and electronegativity are shown in figure 4.9a over the pressure range of 1 - 25 Pa at an average power of 400 W and in figure 4.9b over the average power range of 200 - 1000 W at a pressure of 2.5 Pa. The flux of Ar^+ as a function of pressure and average power is shown in figure 4.9c. Here, the graphs of the number densities and diffusion coefficient of Ar^+ are included again to help illustrate why the trends in the surface flux of Ar^+ appear.

In figure 4.9a the diffusion coefficient decreases proportionally to P^{-1} and the number density of Ar^+ increases until a peak in pressure then drops slightly as discussed in section 4.4.1. The electronegativity increases roughly linearly with pressure; therefore, the number density of negative ions is increasing faster than the number density of electrons. This is because as the pressure increases the electron temperature decreases, this reduces the number of electrons with enough energy to ionise oxygen or argon, as their threshold energies are 13.6 eV and 15.8 eV respectively. Meanwhile, the threshold energy for dissociative electron attachment is 0

eV which means there is a larger production of negative ions compared to electrons at higher pressures, increasing the electronegativity.

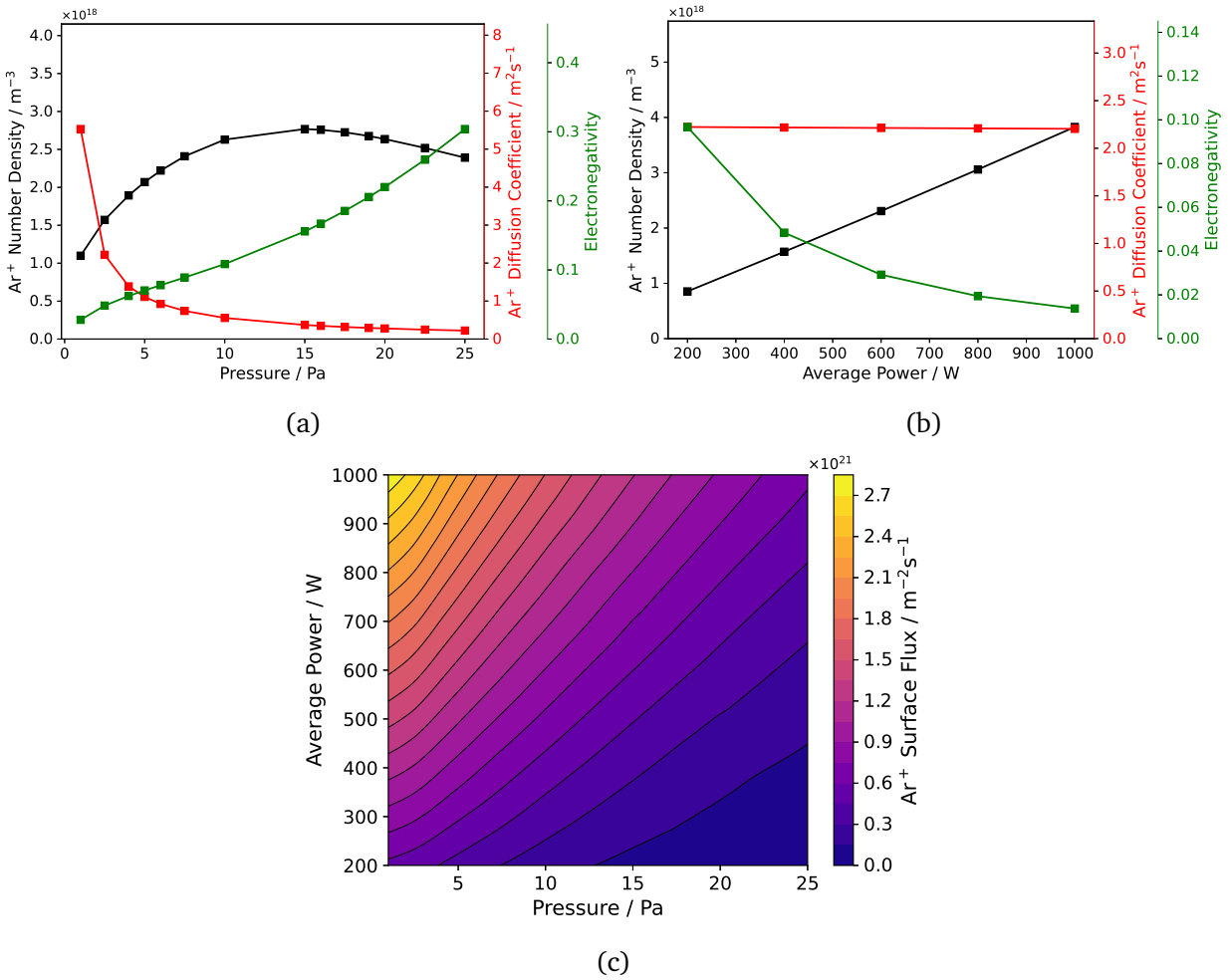

Figure 4.9: Number Density of Ar^+ (m^{-3}), Diffusion Coefficient of Ar^+ (m^2s^{-1}) and Electronegativity (a) as a function of Pressure at an Average Power of 400 W and (b) as a function of Average Power at a Pressure of 2.5 Pa and Flux of Ar^+ (m^2s^{-1}) (c) as a function of Pressure and Average Power

In figure 4.9b the number density of Ar^+ increases linearly with the average power with the diffusion coefficient of Ar^+ remaining constant as discussed in section 4.4.1. The electronegativity decreases with average power, this is because the increase in energy deposited into the plasma increases the number density of electrons through increased ionisation as discussed in section 4.1. However, since the threshold energy for dissociative electron attachment reactions is 0 eV, the increased energy does not increase the rate constant of the production of negative ions. Additionally, the increase in the number density of electrons at higher average powers increases the consumption of negative ions through electron impact detachment, causing the number density of negative ions to decrease, therefore, causing the electronegativity to decrease. In figure 4.9c the flux of Ar^+ decreases with pressure and increases with average power. The de-

crease with pressure is due to the large decrease in the diffusion coefficient Ar^+ by a factor of 0.04 and the increase in electronegativity, both of which hinder the density at the edge of the sheath and thus the surface flux. Although the increase in the number density of Ar^+ causes the density at the edge of the sheath to increase. The decrease in electron temperature, which decreases the Bohm velocity, outweighs the increase in density at the edge of the sheath and, therefore, the flux decreases with pressure. The increase in flux with average power is caused by the increase in the number density of Ar^+ and the decrease in electronegativity that increases the number density at the edge of the sheath. This is combined with the electron temperature and diffusion coefficient of Ar^+ remaining constant with average power, so therefore there is no negative affect on the surface flux from increasing the average power and therefore the flux increases with average power.

4.5.2 The Flux of O^+

The number density and diffusion coefficient of O^+ and the electronegativity are shown in figure 4.10a over the pressure range of 1 - 25 Pa at an average power 400 W and in figure 4.10b over the average power range of 200 - 1000 W at a pressure of 15 Pa. The flux of O^+ as a function of pressure and average power is shown in figure 4.10c. Here, the graphs of the number densities and diffusion coefficient of O^+ are included again to help illustrate why the trends in the surface flux of O^+ appear.

In figure 4.10a the diffusion coefficient decreases proportionally to P^{-1} and the number density of O^+ and electronegativity increases with pressure as discussed in sections 4.4.2 and 4.5.1. In figure 4.10b the diffusion coefficient decreases slightly with the average power, the number density of O^+ increases linearly with the average power and the electronegativity decreases with the average power, as discussed in sections 4.4.2 and 4.5.1. In figure 4.10c the flux of O^+ increases with pressure until a peak is reached in pressure. The initial increase with pressure occurs because the increase in the number density outweighs the loss from the increase in electronegativity and the decreasing diffusion coefficient. This is due to the large diffusion coefficient that enhances the surface flux of O^+, so an increase in the number density of O^+ directly leads to an increase in surface flux. The peak occurs because the decrease in the diffusion coefficient and the increase in the electronegativity hinder the number density of O^+ at the edge of the sheath and the decrease in the electron temperature decreases the Bohm velocity. This counteracts the increase in the number density of O^+, which causes the value of the surface flux to peak as the pressure changes. The surface flux of O^+ also increases with average power; this is due to both the decrease in electronegativity and the increase in the number density of O^+ due to the increase of energy available to ionise. This leads to a higher number density at the edge of the sheath, which creates a higher amount of surface flux. The peak with pressure of O^+ flux changes from 5 Pa at 200 W average power to 15 Pa at 1000 W average power. This is due to the higher number density of O^+ at higher average powers, which means that a higher pressure is required to increase the electronegativity and decrease the diffusion coefficient enough to counteract the effect of the increasing number density of O^+. Therefore, due to competing effects in the flux of O^+, the pressure at which the highest flux is achieved is

affected by the average input power of the reactor.

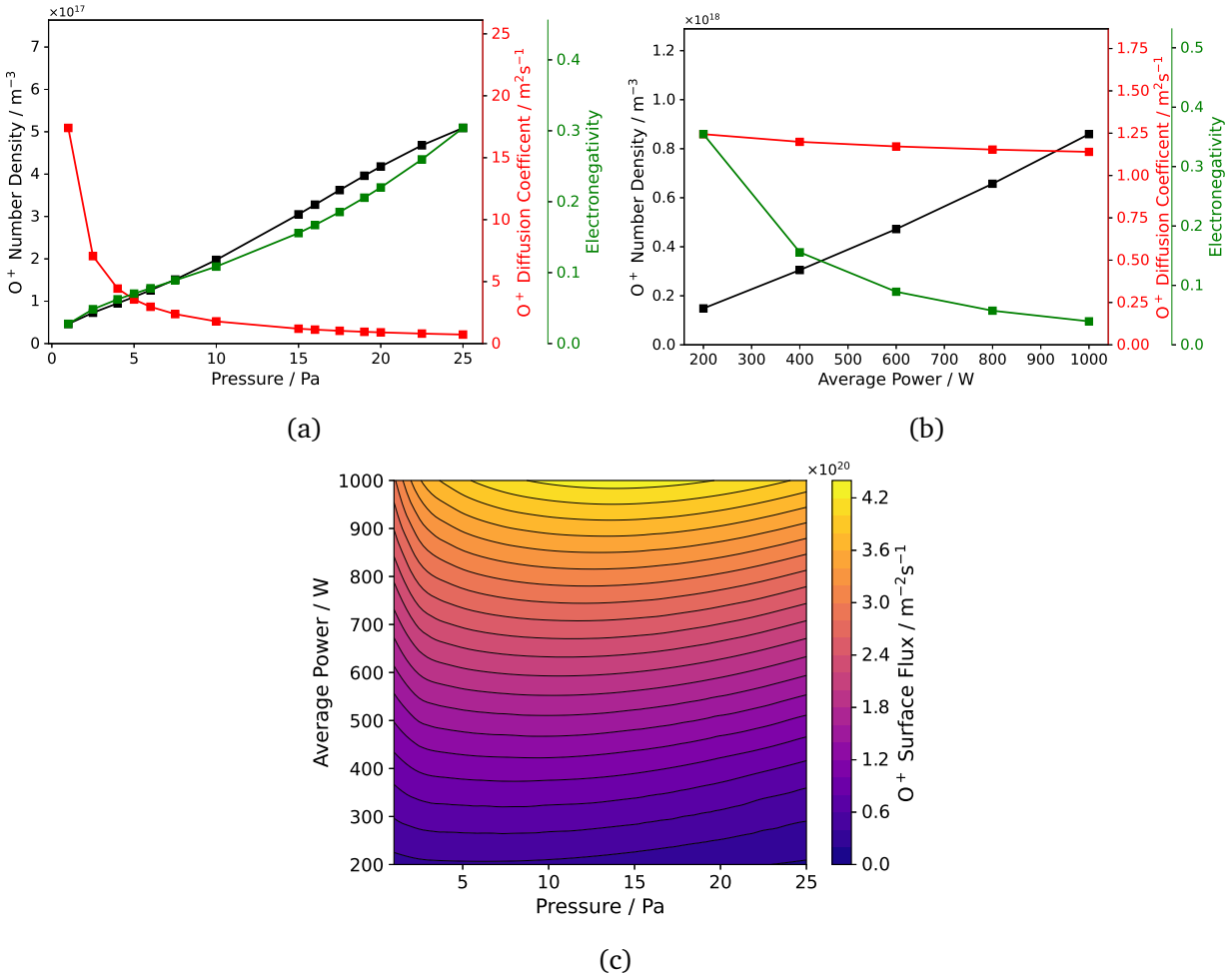

Figure 4.10: Number Density of O^+ (m^{-3}), Diffusion Coefficient of O^+ (m^2s^{-1}) and Electronegativity (a) as a function of Pressure at an Average Power of 400 W and (b) as a function of Average Power at a Pressure of 15 Pa and Flux of O^+ (m^2s^{-1}) (c) as a function of Pressure and Average Power

4.5.3 The Flux of O_2^+

The number density and diffusion coefficient of O_2^+ and the electronegativity are shown in figure 4.11a over the pressure range of 1 - 25 Pa at an average power 400 W and in figure 4.11b over the average power range of 200 - 1000 W at a pressure of 4 Pa. The flux of O_2^+ as a function of pressure and average power is shown in figure 4.11c. Here, the graphs of the number densities and diffusion coefficient of O_2^+ are included again to help illustrate why the trends in the surface flux of O_2^+ appear.

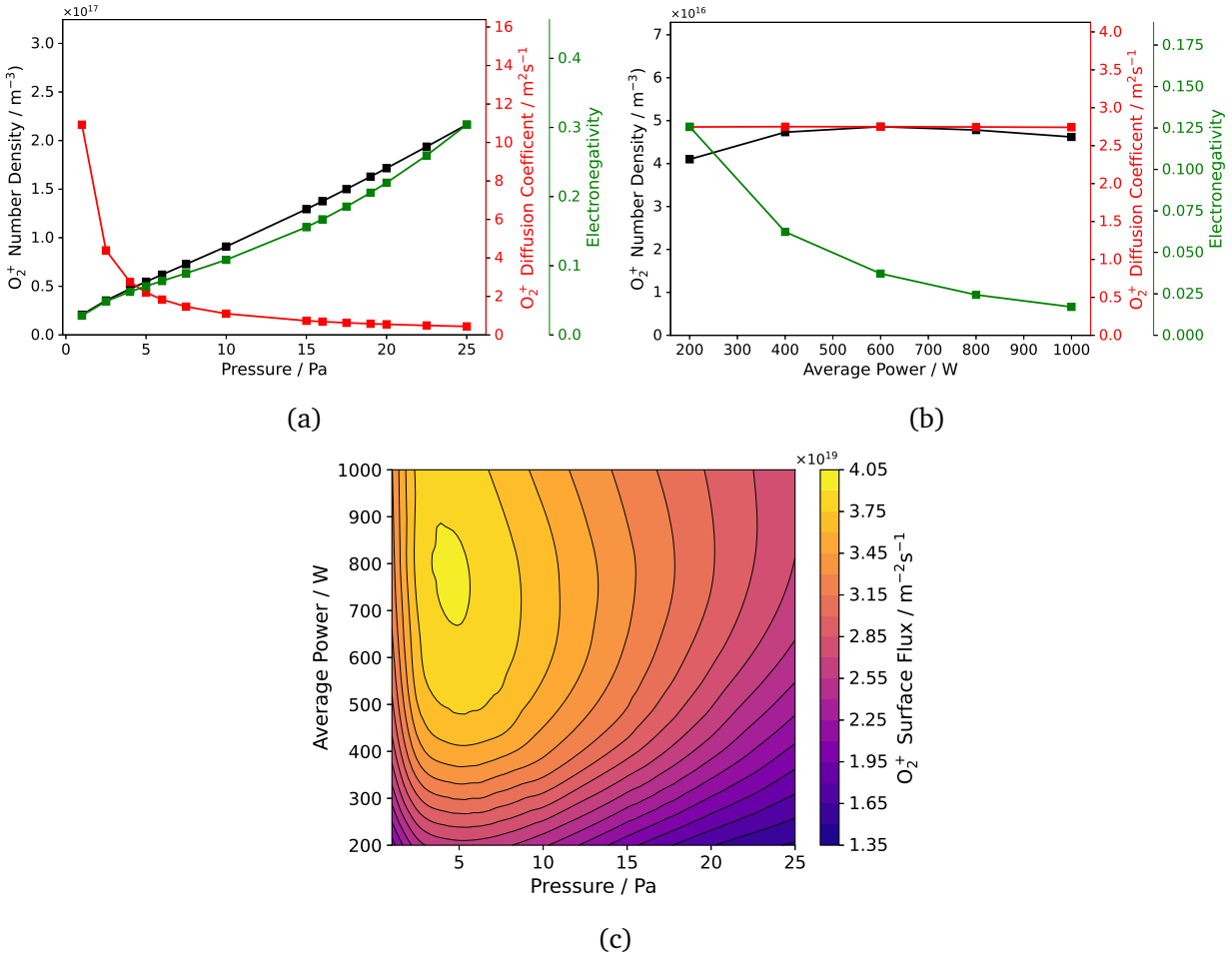

Figure 4.11: Number Density of O_2^+ (m^{-3}), Diffusion Coefficient of O_2^+ (m^2s^{-1}) and Electronegativity (a) as a Function of Pressure at an Average Power of 400 W and (b) as a Function of Average Power at a Pressure of 4 Pa and Flux of O_2^+ (m^2s^{-1}) (c) as a Function of Pressure and Average Power

In figure 4.11a the number density of O_2^+ and electronegativity increase with pressure as discussed in sections 4.4.3 and 4.5.1. The diffusion coefficient of O_2^+ decreases proportionally to P^{-1}; however, the diffusion coefficient is lower at all pressures than the diffusion coefficient of O^+. This is because as pressure increases, more elastic collisions between heavy particles occur due to the increased density of particles in the gas. The lower diffusion coefficient of O_2^+ compared to O^+ is due to the higher atomic mass of O_2^+, which means that the average velocity of the species is lower, and therefore the rate of diffusion is also lower. In figure 4.11b the number density of O_2^+ increases with low average powers but remains constant beyond 400 W with a slight decrease above 600 W, the diffusion coefficient of O_2^+ remains constant with average power, and the electronegativity decreases with average power as discussed in sections 4.4.3 and 4.5.1. In figure 4.11c the surface flux of O_2^+ increases with pressure until a peak is reached at the pressure of 5 Pa after which the surface flux decreases. This is due to the competing effects of the decreasing diffusion coefficient and electron temperature and

the increasing electronegativity and number density of O_2^+. This means that at low pressure as pressure increases the effect of the increasing number density of O_2^+ generates a larger flux. However, at higher pressure, the effects of increasing electronegativity and decreasing electron temperature and diffusion coefficient outweigh the increase in the number density of O_2^+ which reduces the surface flux of O_2^+. The peak remains at the same pressure value for all values of average power because competing effects such as electronegativity electron temperature and O_2^+ diffusion coefficient change either consistently for all pressures or are constant with a change in average power. Due to the number density and electronegativity increasing consistently at all average powers in pressure ranges above 5 Pa whilst the number density does not increase with the average power at 5 Pa. Therefore, changing the average power in this system changes the magnitude of the peak in the O_2^+ surface flux, not the value of the pressure at which it peaks. The flux of O_2^+ increases with average power until a peak is found at 800 W average power and then begins to decrease again. The increase with average power is due to the increase and then remaining constant O_2^+ number density combined with decreasing electronegativity leading to an increase in flux. The peak occurs because the number density of O_2^+ begins to decrease as the average power increases past 800 W.

4.6 Input Energy per Oxygen Ion Fluxed to the Surface

The method used to determine the input energy per oxygen ion fluxed to the surface is shown in chapter 2 section 2.5 where the frequency for all pulses in this chapter is 10 KHz. The input energy per oxygen ion particle fluxed to the surface of O^+ and O_2^+ is shown in figure 4.12a over the pressure range of 1 - 25 Pa at an average power of 400 W and in figure 4.11b over the average power range of 200 - 1000 W at a pressure of 7.5 Pa. The input energy per particle fluxed to the surface of O^+ and O_2^+ as a function of pressure and average power are shown in figures 4.12c and 4.12d, respectively.

In figure 4.12a the input energy per oxygen ion fluxed to the surface of O^+ and O_2^+ decreases to a minima in pressure then increases with pressure. The absolute values of the input energy per O_2^+ particle fluxed to the surface are higher than the values of O^+, which shows that at 400 W average power the plasma uses less input energy per O^+ fluxed to the surface than O_2^+, even though O^+ has to undergo an additional reaction before being produced. This is due to the lack of an increase in the number density of O_2^+ with the average power and the lower diffusion coefficient of O_2^+ hindering the number density at the edge of the sheath. In figure 4.12b the input energy per O^+ particle fluxed to the surface decreases with average power, with a diminishing effect as the average power increases and the input energy per O_2^+ particle fluxed to the surface increases with average power. This shows that the flux of O^+ increases with the average power faster than the input energy used to create that flux; however, the rate of increases in the flux of O^+ diminishes as the average power increases. For O_2^+ this suggests that even though the flux increases with average power to a point, this increase in flux with average power is slower than the increase in the input energy used and therefore the most efficient regime is found at low average power. This occurs because as the average power increases, the higher energies available create more ionisation and dissociation reactions, splitting O_2 into

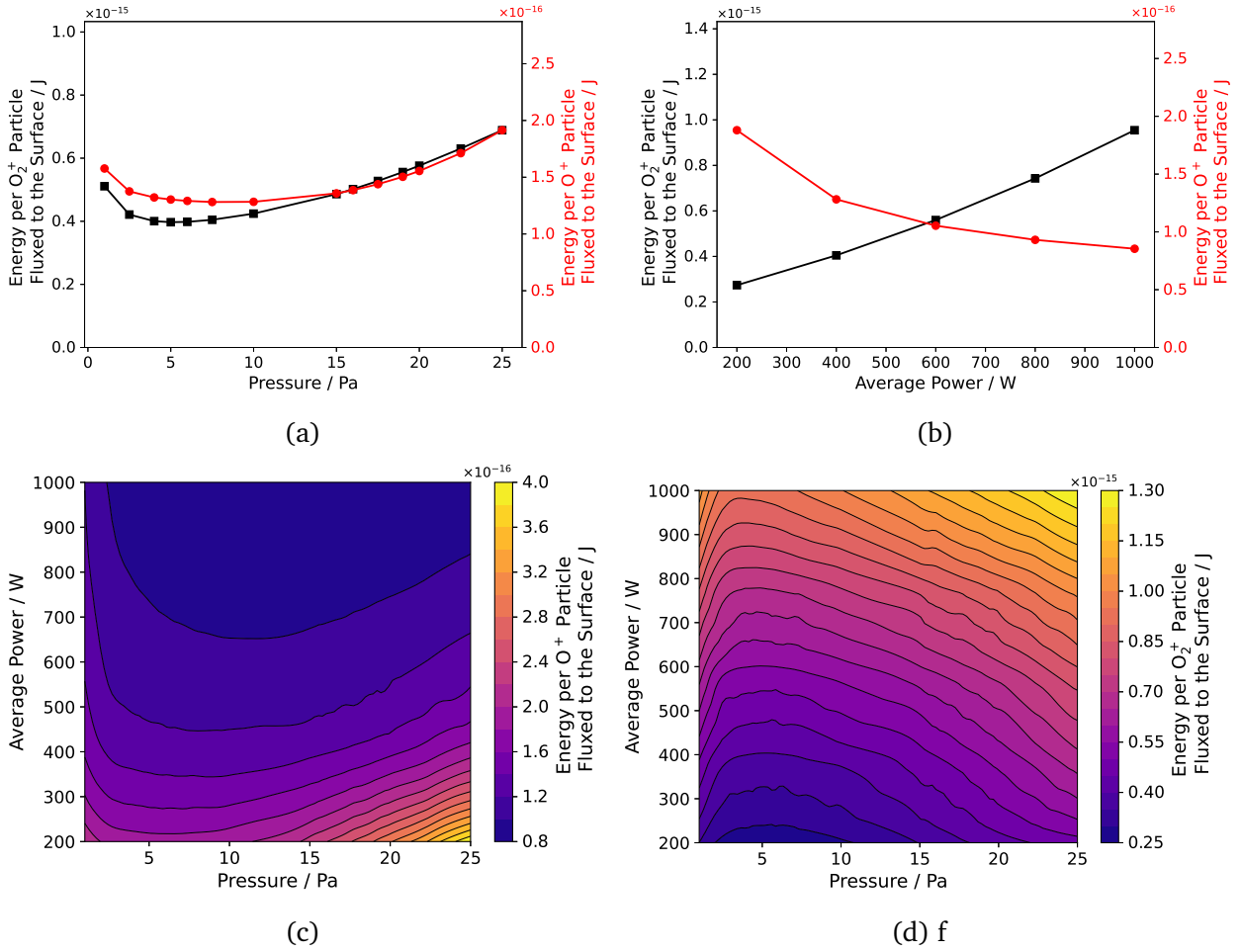

Figure 4.12: Input Energy per Oxygen Ion fluxed to the surface of O^+ and O_2^+ (J) (a) as a function of Pressure at an Average Power of 400 W and (b) as a function of Average Power at a Pressure of 7.5 Pa, Input Energy per O^+ fluxed to the surface (J) (c) as a function of Pressure and Average Power and the Input Energy per O_2^+ fluxed to the surface(J) (d) as a function of Pressure and Average Power

O and ionising it to form O^+, which creates more O^+ relative to O_2^+. Therefore, O^+ decreases in the input energy used per particle fluxed to the surface with average power, whereas O_2^+ does not, as the increase in flux is less than the increase in average power. The decrease in the input energy per O^+ particle fluxed to the surface diminishes because the percentage increase in the surface flux of O^+ decreases relative to the increase in the average power, as the flux increases by 174% from 200 to 400 W but only 150% from 400 to 800 W due to increased charge exchange reactions as the average power increases. In figure 4.12c the input energy per O^+ particle fluxed to the surface decreases with average power with a minima in pressure. The pressure minima moves in pressure as the average power increases because the maxima in flux for each individual average power level moves in pressure as discussed in section 4.5.2. The high values of input energy per O^+ particle fluxed to the surface in high pressure low average power regimes is caused by the low flux of O^+ caused by the decrease in diffusion coefficient and electron temperature and the increase in electronegativity at high pressures. Overall, to reduce

the input energy used per O^+ fluxed to the surfaces, you want to increase the average power and select the pressure for the chosen average power which generates the largest flux; however, the effect of increasing the average power diminishes as it increases; therefore, going above 1000 W in this reactor may have a minimal effect. Furthermore, if the trend of diminishing rate of increase of the flux of O^+ continues with an average power above 1000 W, then it is likely that there is an optimal average power for the reactor; however, this has not been tested. In figure 4.12d the input energy per O_2^+ particle fluxed to the surface increases with average power and reaches a minima in pressure, then increases with the minimum staying at a constant pressure value due to the maximum in flux as discussed in section 4.5.3. Therefore, to decrease the input energy per O_2^+ fluxed to the surfaces, you want low average powers and pressure at 5 Pa for this reactor. However, a low average power comes with a low flux of O_2^+ and therefore it may be necessary to increase the average power of the regime to increase the flux if your process or time restrictions require faster processing.

Chapter 5

Conclusion

In this thesis the ability to effect the input energy per particle fluxed to the surface of a pulsed powered cylindrical inductively coupled Ar/O_2 plasma reactor is tested by changing the plasma input parameters of pressure, frequency and duty cycle. These are performed using a numerical zero dimensional chemical-kinetic plasma global model with an extensive chemical-radiative reaction scheme for Argon and Oxygen species developed and compared to experimental results by Michel Osca Engelbrecht et al. (2024) [32]. The experimental comparison performed by Michel Osca Engelbrecht et al. shows that the simulation results reproduce experimental trends qualitatively over a wide range of pressures, average powers and oxygen mixture fractions. As such, the global model is well suited to investigating the influence of parameter changes on the input energy per particle fluxed to the surface. This is achieved through a broad parameter study that, due to the computational efficiency of the zero dimensional global model, simulations can be performed on relatively short timescales, allowing the rapid identification of optimal operating regimes [91]. However, applications that require quantitatively accurate predictions of flux produced by the system may require higher dimensional simulations or experimental measurements. Nevertheless, global models are still useful to obtain the optimal regime initially. Therefore, reducing the number of computationally expensive higher dimensional simulations or experiment measurements required. Another limitation of using a global model is the lack of spatially resolved information. This is because each data point is a spatially averaged value over the reactor volume. Consequently, where knowledge of spatial behaviour of the plasma is required, higher dimensional simulations are needed to understand if the regime is suitable. An important example is industrial semiconductor manufacturing where spatial uniformity of incident flux across the wafer is vital to ensure uniform depth of etches and depositions across the wafer as well as repeatable results [92].

To test the effect on the input energy per argon ion fluxed to the surface for use in applications in atomic layer etching argon only plasma simulations are used with a range of plasma input parameters. Firstly, the duty cycle is varied between 0.1 and 0.9 at a pressure and frequency of 5 Pa and 10 Khz, respectively. Secondly, the frequency is varied between 5 and 50 Khz at a pressure and duty cycle of 5 Pa and 0.5, respectively. Both frequency and duty cycle are varied at multiple average powers between 200 and 600 W. Finally, the pressure is varied between 0.5

and 25 Pa at multiple average powers between 200 and 1000 W with a duty cycle and frequency of 0.5 and 10 Khz, respectively. The effect of the plasma input parameters on the plasma potential is investigated first to ensure that the ions fluxed to the surface have sufficient energy to enable effective etching, or in other words to be inside the energy window of germanium. Germanium is chosen as the material to be etched as inductively coupled plasmas in the pressure ranges simulated produce plasma potentials inside the energy window of germanium, whereas other materials have energy windows with higher values of energy. It is observed that the plasma potential is only sufficiently high enough to be inside the energy window in the period of the pulse where the power is turned on, and as such only the flux inside the period of the pulse when the power is on is considered in the fluence of the ions to the surface. The average plasma potential within the period where the power is on is found to be sufficient only in the pressure range of 0.5 and 5.0 Pa because increased collisions within the plasma at higher pressures cause the temperature of the electrons to decrease. Additionally, the plasma potential lies inside the energy window in the frequency range of 10 to 50 Khz and for duty cycles between 0.1 and 0.5 here, the range of the duty cycle is cut in half since past 0.5 the lower amplitude of power applied decreases the temperature of the electrons enough to decrease the plasma potential below the energy window. The surface flux of argon ions decreases with duty cycle at a constant average power because the power amplitude decreases, which reduces the intensity of election heating and therefore decreases the production of argon ions. However, as duty cycle increases, the time the power is on during the pulse is longer, which means that the total amount of argon ions fluxed to the surface increases with duty cycle as the difference in the length of time the power is on is larger than the decrease in the per second flux between 0.1 and 0.5. Therefore, since each duty cycle has a constant average power, the input energy of each pulse is the same, so the input energy per argon ion fluxed to the surface is lowest at a duty cycle of 0.5. The surface flux of argon ions decreases with frequency at a constant average power because the number density of argon ions decreases because the frequency increase deposits more energy into the heating of electrons rather than increasing the number of ionisation collisions. Therefore, the lowest input energy per argon ion fluxed to the surface can be found at 10 Khz, although the change in the input energy per particle fluxed to the surface with frequency is minimal. The surface flux of argon ions peaks at a pressure of 1 Pa at a constant average power due to the complex combination of the increasing number density of argon ions and the decreasing number density and temperature of the electrons and the diffusion coefficient of argon ions. The effect of the increasing number density of argon ions is larger than the decrease in diffusion coefficient of argon ions and temperature of the electrons when going from 0.5 to 1 Pa, causing the surface flux of argon ions to increase however, past 1 Pa this is the opposite, causing the surface flux to decrease. Therefore, the lowest input energy per argon ion fluxed to the surface can be found at 1 Pa. The input energy per argon ion fluxed to the surface stays constant at all values of average power regardless of the other plasma input parameters tested. This is because the increase in average power does not increase the heating of electrons but proportionally increases the ionisation of argon, creating a linear increase in the number density of argon ions and, therefore, a linear increase in the surface flux of argon ions. In conclusion, the input energy per argon ion fluxed to the surface can be lowered to reduce the energy usage in atomic layer etching processes by increasing the duty cycle of the pulsed power and optimising the pressure of the reactor for the maximum surface flux in this case to 1 Pa, while changing the frequency has a limited effect, but can decrease the input energy

slightly by decreasing the frequency. In the future, it would be interesting to observe the effect of a combination of a higher duty cycle with a low pressure regime, as the decreased plasma potential from the higher duty cycles is not an issue at lower pressures, due to the pressure increasing the plasma potential, which may allow us to find a lower input energy per argon ion fluxed to the surface. Another point of interest would be to decrease the pressure further to investigate if the plasma potential increases far enough to be in the energy window for other materials like silicon. If this is possible, it would be interesting to investigate the input energy per argon particle fluxed to the surface at low pressure for the etching of other materials.

To test the effect on the input energy per particle fluxed to the surface for use in applications in atomic layer deposition, a plasma made up of 90% Ar and 10% O_2, is used with plasma input parameters of pressure ranging from 1 to 25 Pa at multiple average powers between 200 and 1000 W at a frequency of 10 Khz and a duty cycle of 0.5. This plasma creates multiple different particles that are useful in the atomic layer deposition process, namely the ground and excited $O(^1D)$ and $O(^1S)$ states of atomic oxygen and the O^+ and O_2^+ ions; additionally, it produces Ar^+ ions that can cause damage to the surface in the atomic layer deposition process through physical sputtering and therefore all of these need to be investigated. At all pressures investigated, the value of the plasma potential inside the plasma was found to be below the energy of 30 eV that is required to physically sputter a surface, apart from a spike that occurs when the power is turned on in the pulse. The time frame during which this spike occurs is extremely short on the magnitude of 10 μs, therefore, this will cause minimal damage to the surface. The input energy per ground state atomic oxygen particle fluxed to the surface decreases proportionally to P^{-1} whilst the input energy per excited $O(^1D)$ and $O(^1S)$ states fluxed to the surface also decreases proportionally to P^{-1} until 15 Pa, after 15 Pa the input energy per excited state particle fluxed to the surface begins to increase as pressure increases. This is because as the pressure increases the overall gas density increases, which reduces the diffusion coefficient's of the particles and increases the amount of electrons which in turn leads to a larger number of dissociation collisions inside the plasma. This produces more atomic oxygen, therefore, causing a larger amount of fluxed to the surface. The increase in input energy per particle for the excited $O(^1D)$ and $O(^1S)$ states past 15 Pa is due to the increased collisional quenching at higher pressures. Both the input energy per ground state and the excited $O(^1D)$ and $O(^1S)$ states fluxed to the surface increase with the average power for the ground state, this increase is linear. However, for the excited $O(^1D)$ and $O(^1S)$ there is no change between 200 and 400 W, but at higher average powers there is a linear increase; additionally, over all, the input energy per excited $O(^1D)$ and $O(^1S)$ states fluxed to the surface increases significantly less as the average power increases than the ground state. This is because as the average power increases there is an increase in the ionisation, recombination and collisional quenching reactions. Additionally, despite the number density of the ground state atomic oxygen being 5 times the number density of the combined excited $O(^1D)$ and $O(^1S)$ states the flux and therefore the input energy per particle fluxed to the surfaces is similar. This is due to the sticking coefficient of ground state atomic oxygen being between 0.2 and 0.15 in the investigated pressure range, whereas excited $O(^1D)$ and $O(^1S)$ states have a sticking coefficient of 1. This means that 80% of ground state atomic oxygen is reflected from the surface, and, in addition, this lowers the density gradient, further decreasing the flux. In general, to reduce the input energy per atomic oxygen particle fluxed to the surface, the pressure is required to increase and the average power needs to be decreased

although increasing the pressure beyond 15 Pa results in diminishing returns.

The input energy per O^+ fluxed to the surface decreases with pressure until a minimum is reached. This minimum is caused by the complex relationship between the number density and the diffusion coefficient of O^+, the temperature of the electrons and the electronegativity, where at lower pressures the increase in the number density of O^+ as pressure increases outweighs the increase in electronegativity and decrease in the diffusion coefficient of O^+ and temperature of the electrons to generate a higher flux. However, after a certain pressure the change in the diffusion coefficient of O^+, the temperature of the electrons and the electronegativity begin to outweigh the increase in the number density, creating an optimum pressure where the lowest input energy per O^+ fluxed to the surface is found. This optimal pressure changes according to the average power from 5 Pa at 200 W to 15 Pa at 1000 W, because as the average power increases so does the number density of O^+ because the increase in energy causes more ionisation and dissociation to occur. Therefore, a higher pressure is required to increase the electronegativity and decrease the diffusion coefficient and temperature of the electrons sufficiently to cause the input energy per O^+ fluxed to the surface to reach a minimum. Additionally, as the average power increases, the input energy per O^+ fluxed to the surface decreases with the rate of change decreasing as the average power increases. The reason why this effect decreases as the average power increases is because the percentage increase in the surface flux of O^+ decreases from 174% from 200 to 400 W to 150% from 400 to 800 W due to increased charge exchange reactions as the average power increases. The input energy per O_2^+ fluxed to the surface decreases with pressure until a minimum of 5 Pa is reached. This minimum is caused by the complex relationship between the number density and the diffusion coefficient of O_2^+, the temperature of the electrons and the electronegativity, where at lower pressures the increase in the number density of O_2^+ as the average power increases outweighs the increase in electronegativity and the decrease in the diffusion coefficient of O_2^+ and the temperature of the electrons, to generate a higher flux. However, after a certain pressure this trend reverses with the increase in the number density becoming outweighed creating an optimum pressure where the lowest input energy per O_2^+ fluxed to the surface is found. The input energy per O_2^+ fluxed to the surface increases with average power because as average power increases, more ionisation and dissociation collisions occur. This creates more O^+ relative to the amount of O_2^+ that is produced, causing the number density of O_2^+ to decrease as the average power increases. Additionally, the input energy per O_2^+ fluxed to the surface is higher than that of O^+ for all pressures and average powers because the number of dissociation reactions increases as the pressure and average power increases and because the diffusion coefficient of O_2^+ is lower than that of O^+, which hinders the flux to the surface. In conclusion, to reduce the input energy per O_2^+ fluxed to the surface, a low average power is required at a pressure of 5 Pa; however, this comes with low surface fluxes, which will result in longer processing times. To reduce the input energy per O^+ fluxed to the surface, a high average power is required, and then a pressure needs to be selected so that the input energy per O^+ fluxed to the surface is minimised at the chosen average power. In the future, it would be interesting to investigate the effect of higher average powers and see if there is a minimum of input energy per O^+ fluxed to the surface in average power or if the trend of diminishing returns continues. In addition, it would be interesting to change the duty cycle and frequency of the power waveform as well as to change the oxygen mixture to investigate the effect they have on the plasma and the input

energy per particle fluxed to the surface.

Bibliography

[1] Steve Furber. Microprocessors: The engines of the digital age. *Proceedings of the Royal Society A: Mathematical, Physical and Engineering Sciences*, 473(2199), 3 2017. ISSN 14712946. doi:https://doi.org/10.1098/rspa.2016.0893.

[2] David A. Laws. 13 Sextillion & Counting: The Long & Winding Road to the Most Frequently Manufactured Human Artifact in History, 4 2018. URL https://computerhistory.org/blog/13-sextillion-counting-the-long-winding-road-to-the-most-frequently-manufactured-human-artifact-in-history/?key=13-sextillion-counting-the-long-winding-road-to-the-most-frequently-manufactured-human-artifact-in-history.

[3] G.E. Moore. Cramming More Components Onto Integrated Circuits. *Proceedings of the IEEE*, 86(1):82–85, 1 1998. ISSN 0018-9219. doi:10.1109/JPROC.1998.658762.

[4] The First Intel Microprocessor: The Chip that Changed Everything, 2025. URL https://www.microchipusa.com/manufacturer-articles/the-first-intel-microprocessor-the-chip-that-changed-everything.

[5] Dick James. Apple Joins 3D-Fabric Portfolio with M1 Ultra?, 2025. URL https://www.techinsights.com/blog/apple-joins-3d-fabric-portfolio-m1-ultra?utm_source=direct&utm_medium=website.

[6] S. Borkar. Designing Reliable Systems from Unreliable Components: The Challenges of Transistor Variability and Degradation. *IEEE Micro*, 25(6):10–16, 11 2005. ISSN 0272-1732. doi:10.1109/MM.2005.110.

[7] Max Roser, Hannah Ritchie, and Edouard Mathieu. What is Moore's Law? *Our World in Data*, 2023. URL https://ourworldindata.org/moores-law.

[8] Katharina Buchholz. Advanced Microchip Production Relies On Taiwan [Infographic], 1 2023. URL https://www.forbes.com/sites/katharinabuchholz/2023/01/13/advanced-microchip-production-relies-on-taiwan/.

[9] Gauthier Roussilhe, Thibault Pirson, Mathieu Xhonneux, and David Bol. From silicon shield to carbon lock-in? The environmental footprint of electronic components manufacturing in Taiwan (2015–2020). *Journal of Industrial Ecology*, 28(5):1212–1226,

10 2024. ISSN 1088-1980. doi:10.1111/jiec.13487.

[10] Paris Agreement. In *United Nations*, Paris, 2016. URL https://treaties.un.org/pages/ViewDetails.aspx?src=TREATY&mtdsg_no=XXVII-7-d&chapter=27&clang=_en.

[11] J Reece Roth. *Industrial Plasma Engineering*, volume 1: Priciples. IOP Publishing, 1995. ISBN 0750303174. doi:https://doi.org/10.1201/9780367802615.

[12] Michael A Lieberman and Alan J Lichtenberg. Principles of Plasma Discharges and Materials Processing. In *Principles of Plasma Discharges and Materials Processing*. John Wiley & Sons, Incorporated, United States, 2005. ISBN 0471720011. doi:10.1002/0471724254.

[13] *Plasma etching : an introduction / edited by Dennis M. Manos, Daniel L. Flamm.* Plasma–materials interactions. Academic Press, Boston ; London, 1989. ISBN 9780124693708.

[14] J. Reece Roth. *Industrial Plasma Engineering: Volume 2 - Applications to Nonthermal Plasma Processing*. Institute of Physics Publishing, 2001. ISBN 0750305452. doi:https://doi.org/10.1201/9780203750995.

[15] Keren J. Kanarik, Thorsten Lill, Eric A. Hudson, Saravanapriyan Sriraman, Samantha Tan, Jeffrey Marks, Vahid Vahedi, and Richard A. Gottscho. Overview of atomic layer etching in the semiconductor industry. *Journal of Vacuum Science & Technology A: Vacuum, Surfaces, and Films*, 33(2), 3 2015. ISSN 0734-2101. doi:10.1116/1.4913379.

[16] Mingmei Wang and Mark J. Kushner. Modeling of implantation and mixing damage during etching of SiO_2 over Si in fluorocarbon plasmas. *Journal of Vacuum Science & Technology A: Vacuum, Surfaces, and Films*, 29(5), 9 2011. ISSN 0734-2101. doi:10.1116/1.3626533.

[17] Maria E Barone and David B Graves. Molecular dynamics simulations of plasma - surface chemistry. *Plasma Sources Science and Technology*, 5(2):187–192, 5 1996. ISSN 0963-0252. doi:10.1088/0963-0252/5/2/011.

[18] Yasaman Hamedani, Prathyushakrishna Macha, Timothy J. Bunning, Rajesh R. Naik, and Milana C. Vasudev. Plasma-Enhanced Chemical Vapor Deposition: Where we are and the Outlook for the Future. In *Chemical Vapor Deposition - Recent Advances and Applications in Optical, Solar Cells and Solid State Devices*. InTech, 8 2016. doi:10.5772/64654.

[19] Markku Leskelä and Mikko Ritala. Atomic Layer Deposition Chemistry: Recent Developments and Future Challenges. *Angewandte Chemie - International Edition*, 42 (45):5548–5554, 11 2003. ISSN 14337851. doi:10.1002/anie.200301652.

[20] H. B. Profijt, S. E. Potts, M. C. M. van de Sanden, and W. M. M. Kessels. Plasma-Assisted Atomic Layer Deposition: Basics, Opportunities, and Challenges. *Journal of Vacuum*

Science & Technology A: Vacuum, Surfaces, and Films, 29(5), 9 2011. ISSN 0734-2101. doi:10.1116/1.3609974.

[21] Beth Anthony, Mara Johnson-Groh, and Genna Duberstein. What is Plasma?, 3 2023. URL https://svs.gsfc.nasa.gov/14299.

[22] Francis F. Chen. *Introduction to Plasma Physics and Controlled Fusion*. Springer International Publishing, Cham, 2016. ISBN 978-3-319-22308-7. doi:10.1007/978-3-319-22309-4.

[23] May-Britt Kallenrode. *Space Physics: An Introduction to Plasmas and Particles in the Heliosphere and Magnetospheres*. Springer Berlin Heidelberg, Berlin, Heidelberg, 2004. ISBN 978-3-642-05829-5. doi:10.1007/978-3-662-09959-9.

[24] Jeffrey P. Freidberg. *Plasma Physics and Fusion Energy*. Cambridge University Press, 2 2007. ISBN 9780521851077. doi:10.1017/CBO9780511755705.

[25] Scott James Doyle. Electron, ion and neutral heating in hollow cathode plasma thrusters. Technical report, 2019. URL https://etheses.whiterose.ac.uk/25677/.

[26] Andreas Schütze, James Y Jeong, Steven E Babayan, Jaeyoung Park, Gary S Selwyn, and Robert F Hicks. The Atmospheric-Pressure Plasma Jet: A Review and Comparison to Other Plasma Sources. *IEEE TRANSACTIONS ON PLASMA SCIENCE*, 26(6):1685, 1998. doi:10.1109/27.747887.

[27] Nicholas Braithwaite Chabert Pascal. *Physics of Radio-Frequency Plasmas / Pascal Chabert, Nicholas Braithwaite.* Cambridge University Press, Cambridge, 2011. ISBN 9780511857539. doi:10.1080/00107514.2012.737838.

[28] H. B. Valentini. Bohm criterion for the collisional sheath. *Physics of Plasmas*, 3(4): 1459–1461, 1996. ISSN 1070664X. doi:10.1063/1.871736.

[29] Pascal Braithwaite Chabert Nicholas. *Physics of radio-frequency plasmas*. Cambridge University Press, 12 2010. ISBN 9780511857539. doi:https://doi.org/10.1017/CBO9780511974342.

[30] B. M. (Boris Mikhaĭlovich) Smirnov. *Physics of weakly ionized gases : (problems and solutions)*. Mir Publishers, 1981.

[31] Chenhui Qu, Yukinori Sakiyama, Pulkit Agarwal, and Mark J. Kushner. Plasma-enhanced atomic layer deposition of SiO_2 film using capacitively coupled Ar/O_2 plasmas: A computational investigation. *Journal of Vacuum Science & Technology A: Vacuum, Surfaces, and Films*, 39(5), 9 2021. ISSN 0734-2101. doi:10.1116/6.0001121.

[32] Michel Osca Engelbrecht, Jonathan Jenderny, Henrik Hylla, Dominik Filla, Peter Awakowicz, Ihor Korolov, Christopher P Ridgers, and Andrew R Gibson. Numerical investigation of vacuum ultra-violet emission in Ar/O_2 inductively coupled plasmas.

Plasma Sources Science and Technology, 33(9):095008, 9 2024. ISSN 0963-0252. doi:10.1088/1361-6595/ad7059.

[33] Marcel Fiebrandt, Bastian Hillebrand, Jan-Wilm Lackmann, Marina Raguse, Ralf Moeller, Peter Awakowicz, and Katharina Stapelmann. Inactivation of *B. subtilis* spores by low pressure plasma—influence of optical filters and photon/particle fluxes on the inactivation efficiency. *Journal of Physics D: Applied Physics*, 51(4):045401, 1 2018. ISSN 0022-3727. doi:10.1088/1361-6463/aa9f0a.

[34] Saburo Uchida, Seigo Takashima, Masaru Hori, Masanaga Fukasawa, Keiji Ohshima, Kazunori Nagahata, and Tetsuya Tatsumi. Plasma damage mechanisms for low- k porous SiOCH films due to radiation, radicals, and ions in the plasma etching process. *Journal of Applied Physics*, 103(7), 2008. ISSN 00218979. doi:10.1063/1.2891787.

[35] M. J. Titus, D. B. Graves, Y. Yamaguchi, and E. A. Hudson. Effects of vacuum ultraviolet photons, ion energy and substrate temperature on line width roughness and RMS surface roughness of patterned 193nm photoresist. *Journal of Physics D: Applied Physics*, 44(8), 3 2011. ISSN 00223727. doi:10.1088/0022-3727/44/8/085204.

[36] B deB Darwent. Bond dissociation energies in simple molecules. 1970. doi:10.6028/NBS.NSRDS.31.

[37] James A. R. Samson and J. L. Gardner. On the Ionization Potential of Molecular Oxygen. *Canadian Journal of Physics*, 53(19):1948–1952, 10 1975. ISSN 0008-4204. doi:10.1139/p75-244.

[38] Alexander Fridman. *Plasma Chemistry*. Cambridge University Press, 5 2008. ISBN 9780521847353. doi:10.1017/CBO9780511546075.

[39] Gregory J. Smith, Paola Diomede, Andrew R. Gibson, Scott J. Doyle, Vasco Guerra, Mark J. Kushner, Timo Gans, and James P. Dedrick. Low-pressure inductively coupled plasmas in hydrogen: impact of gas heating on the spatial distribution of atomic hydrogen and vibrationally excited states. *Plasma Sources Science and Technology*, 33(2), 2 2024. ISSN 13616595. doi:10.1088/1361-6595/ad1ece.

[40] Keren J. Kanarik, Samantha Tan, Wenbing Yang, Taeseung Kim, Thorsten Lill, Alexander Kabansky, Eric A. Hudson, Tomihito Ohba, Kazuo Nojiri, Jengyi Yu, Rich Wise, Ivan L. Berry, Yang Pan, Jeffrey Marks, and Richard A. Gottscho. Predicting synergy in atomic layer etching. *Journal of Vacuum Science & Technology A: Vacuum, Surfaces, and Films*, 35 (5), 9 2017. ISSN 0734-2101. doi:10.1116/1.4979019.

[41] Ankur Agarwal, Phillip J. Stout, Samer Banna, Shahid Rauf, and Ken Collins. Recouping etch rates in pulsed inductively coupled plasmas. *Journal of Vacuum Science & Technology A: Vacuum, Surfaces, and Films*, 29(1), 1 2011. ISSN 0734-2101. doi:10.1116/1.3521315.

[42] Marcel Fiebrandt, Jan Wilm Lackmann, and Katharina Stapelmann. From patent to

product? 50 years of low-pressure plasma sterilization. *Plasma Processes and Polymers*, 15(12), 12 2018. ISSN 16128869. doi:10.1002/ppap.201800139.

[43] Samer Banna, Ankur Agarwal, Ken Tokashiki, Hong Cho, Shahid Rauf, Valentin Todorow, Kartik Ramaswamy, Ken Collins, Phillip Stout, Jeong Yun Lee, Junho Yoon, Kyoungsub Shin, Sang Jun Choi, Han Soo Cho, Hyun Joong Kim, Changhun Lee, and Dimitris Lymberopoulos. Inductively coupled pulsed plasmas in the presence of synchronous pulsed substrate bias for robust, reliable, and fine conductor etching. *IEEE Transactions on Plasma Science*, 37(9 SPEC. ISS. PART 1):1730–1746, 2009. ISSN 00933813. doi:10.1109/TPS.2009.2028071.

[44] J. G. Cook, L. Lebrun, Li Zhongming, and E. A. Ogryzlo. Characterization of a radio-frequency discharge used for downstream plasma oxidation of Si. *Journal of Applied Physics*, 77(4):1690–1695, 1995. ISSN 00218979. doi:10.1063/1.358859.

[45] Felix Mitschker, Jan Dietrich, Berkem Ozkaya, Teresa De los Arcos, Ignacio Giner, Peter Awakowicz, and Guido Grundmeier. Spectroscopic and Microscopic Investigations of Degradation Processes in Polymer Surface-Near Regions during the Deposition of SiO_x Films. *Plasma Processes and Polymers*, 12(9):1002–1009, 9 2015. ISSN 16128869. doi:10.1002/ppap.201500085.

[46] Michel Moisan, Karim Boudam, Denis Carignan, Danielle Kéroack, Pierre Levif, Jean Barbeau, Jacynthe Séguin, Kinga Kutasi, Benaïssa Elmoualij, Olivier Thellin, and Willy Zorzi. Sterilization/disinfection of medical devices using plasma: The flowing afterglow of the reduced-pressure N_2-O_2 discharge as the inactivating medium. *EPJ Applied Physics*, 63(1):1–10001, 7 2013. ISSN 12860050. doi:10.1051/epjap/2013120510.

[47] Ville Miikkulainen, Markku Leskelä, Mikko Ritala, and Riikka L. Puurunen. Crystallinity of inorganic films grown by atomic layer deposition: Overview and general trends. *Journal of Applied Physics*, 113(2), 1 2013. ISSN 00218979. doi:10.1063/1.4757907.

[48] Andrew Robert and Gibson Msci. Harnessing the non-linear coupling of odd harmonics for control of charged particle dynamics in radio-frequency plasmas. 2015.

[49] D. Vender and R.W. Boswell. Numerical modeling of low-pressure RF plasmas. *IEEE Transactions on Plasma Science*, 18(4):725–732, 8 1990. ISSN 0093-3813. doi:10.1109/27.57527.

[50] K. Nishida, S. Mattei, J. Lettry, and A. Hatayama. Numerical analysis of effects of ion-neutral collision processes on RF ICP discharge. *Journal of Applied Physics*, 123(4), 1 2018. ISSN 10897550. doi:10.1063/1.5002169.

[51] Justine Johannes, Timothy Bartel, Gregory A. Hebner, Joseph Woodworth, and Demetre J. Economou. Direct Simulation Monte Carlo of Inductively Coupled Plasma and Comparison with Experiments. *Journal of The Electrochemical Society*, 144(7): 2448–2455, 7 1997. ISSN 0013-4651. doi:10.1149/1.1837835.

[52] C.K. Birdsall and A.B Langdon. *Plasma physics via computer simulation*. Adam Hilger series on plasma physics. Hilger, Bristol, 1991. ISBN 0750301171. doi:10.1201/9781315275048.

[53] J. Van Dijk, G. M.W. Kroesen, and A. Bogaerts. Plasma modelling and numerical simulation. *Journal of Physics D: Applied Physics*, 42(19), 2009. doi:10.1088/0022-3727/42/19/190301.

[54] H. C. Kim, F. Iza, S. S. Yang, M. Radmilović-Radjenović, and J. K. Lee. Particle and fluid simulations of low-temperature plasma discharges: Benchmarks and kinetic effects. *Journal of Physics D: Applied Physics*, 38(19), 10 2005. ISSN 00223727. doi:10.1088/0022-3727/38/19/R01.

[55] G. J.M. Hagelaar and L. C. Pitchford. Solving the Boltzmann equation to obtain electron transport coefficients and rate coefficients for fluid models. *Plasma Sources Science and Technology*, 14(4):722–733, 11 2005. ISSN 09630252. doi:10.1088/0963-0252/14/4/011.

[56] Mark J. Kushner. Hybrid modelling of low temperature plasmas for fundamental investigations and equipment design. *Journal of Physics D: Applied Physics*, 42(19), 2009. doi:10.1088/0022-3727/42/19/194013.

[57] Pedro Viegas, Tiago Cunha Dias, Chloé Fromentin, Alexander Chukalovsky, Yuri Mankelevich, Olga Proshina, Tatyana Rakhimova, Vasco Guerra, and Dmitry Voloshin. Comparison between 1D radial and 0D global models for low-pressure oxygen DC glow discharges. *Plasma Sources Science and Technology*, 32(2), 2 2023. ISSN 13616595. doi:10.1088/1361-6595/acbb9c.

[58] Andrew Hurlbatt, Andrew Robert Gibson, Sandra Schröter, Jérôme Bredin, Alexander Paul Stuart Foote, Pascaline Grondein, Deborah O'Connell, and Timo Gans. Concepts, Capabilities, and Limitations of Global Models: A Review. *Plasma Processes and Polymers*, 14(1-2), 1 2017. ISSN 16128869. doi:10.1002/ppap.201600138.

[59] L. L. Alves, A. Bogaerts, V. Guerra, and M. M. Turner. Foundations of modelling of nonequilibrium low-temperature plasmas. *Plasma Sources Science and Technology*, 27(2), 2 2018. ISSN 13616595. doi:10.1088/1361-6595/aaa86d.

[60] Marcel Fiebrandt, Nikita Bibinov, and Peter Awakowicz. Determination of atomic oxygen state densities in a double inductively coupled plasma using optical emission and absorption spectroscopy and probe measurements. *Plasma Sources Science and Technology*, 29(4), 4 2020. ISSN 13616595. doi:10.1088/1361-6595/ab7cbe.

[61] J. T. Gudmundsson and E. G. Thorsteinsson. Oxygen discharges diluted with argon: Dissociation processes. *Plasma Sources Science and Technology*, 16(2):399–412, 5 2007. ISSN 09630252. doi:10.1088/0963-0252/16/2/025.

[62] Jeff Bezanson, Alan Edelman, Stefan Karpinski, and Viral B. Shah. Julia: A Fresh

Approach to Numerical Computing. *SIAM Review*, 59(1):65–98, 1 2017. ISSN 0036-1445. doi:10.1137/141000671.

[63] Demetre J Economou. Pulsed plasma etching for semiconductor manufacturing. *Journal of Physics D: Applied Physics*, 47(30):303001, 7 2014. ISSN 0022-3727. doi:10.1088/0022-3727/47/30/303001.

[64] Christopher Rackauckas and Qing Nie. DifferentialEquations.jl – A Performant and Feature-Rich Ecosystem for Solving Differential Equations in Julia. *Journal of Open Research Software*, 5(1):15, 5 2017. doi:10.5334/jors.151.

[65] Miles M. Turner. Uncertainty and error in complex plasma chemistry models. *Plasma Sources Science and Technology*, 24(3), 5 2015. ISSN 13616595. doi:10.1088/0963-0252/24/3/035027.

[66] Marcel Fiebrandt. Influence of photon energy and photon / particle fluxes on the inactivation efficiency of B. subtilis spores in low-pressure plasmas. 2018.

[67] Russ R. Laher and Forrest R. Gilmore. Updated Excitation and Ionization Cross Sections for Electron Impact on Atomic Oxygen. *Journal of Physical and Chemical Reference Data*, 19(1):277–305, 1 1990. ISSN 0047-2689. doi:10.1063/1.555872.

[68] H. C. Straub, P. Renault, B. G. Lindsay, K. A. Smith, and R. F. Stebbings. Absolute partial cross sections for electron-impact ionization of H_2, N_2, and O_2 from threshold to 1000 eV. *Physical Review A*, 54(3):2146–2153, 9 1996. ISSN 1050-2947. doi:10.1103/PhysRevA.54.2146.

[69] J. W. McConkey, C. P. Malone, P. V. Johnson, C. Winstead, V. McKoy, and I. Kanik. Electron impact dissociation of oxygen-containing molecules-A critical review. *Physics Reports*, 466(1-3):1–103, 9 2008. ISSN 03701573. doi:10.1016/j.physrep.2008.05.001.

[70] S. A. Lawton and A. V. Phelps. Excitation of the b $^1\Sigma_g^+$ state of O_2 by low energy electrons. *The Journal of Chemical Physics*, 69(3):1007–1009, 1978. ISSN 00219606. doi:10.1063/1.436700.

[71] E Alge, N G Adams, and D Smith. Measurements of the dissociative recombination coefficients of O_2^+, NO^+ and NH_4^+ in the temperature range 200-600K. *Journal of Physics B: Atomic and Molecular Physics*, 16(8):1433–1444, 4 1983. ISSN 0022-3700. doi:10.1088/0022-3700/16/8/017.

[72] A. I. Florescu-Mitchell and J. B.A. Mitchell. Dissociative recombination. *Physics Reports*, 430(5-6):277–374, 2006. ISSN 03701573. doi:10.1016/j.physrep.2006.04.002.

[73] J. L. Queffelec, B. R. Rowe, F. Vallée, J. C. Gomet, and M. Morlais. The yield of metastable atoms through dissociative recombination of O_2^+ ions with electrons. *The Journal of Chemical Physics*, 91(9):5335–5342, 1989. ISSN 00219606. doi:10.1063/1.457582.

[74] H. C. Straub, P. Renault, B. G. Lindsay, K. A. Smith, and R. F. Stebbings. Absolute partial and total cross sections for electron-impact ionization of argon from threshold to 1000 eV. *Physical Review A*, 52(2):1115–1124, 8 1995. ISSN 1050-2947. doi:10.1103/PhysRevA.52.1115.

[75] Anthony J. Midey and A. A. Viggiano. Rate constants for the reaction of Ar^+ with O_2 and CO as a function of temperature from 300 to 1400 K: Derivation of rotational and vibrational energy effects. *Journal of Chemical Physics*, 109(13):5257–5263, 1998. ISSN 00219606. doi:10.1063/1.477142.

[76] Philippe Gaucherel and Bertrand Rowe. Measurement of rates of charge exchange and dissociative recombination reactions in Ar N_2, Ar H_2 and Ar O_2 mixtures. *International Journal of Mass Spectrometry and Ion Physics*, 25(2):211–227, 10 1977. ISSN 00207381. doi:10.1016/0020-7381(77)80050-8.

[77] Thomas M. Miller, Nicholas S. Shuman, and A. A. Viggiano. Behavior of rate coefficients for ion-ion mutual neutralization, 300-550 K. *Journal of Chemical Physics*, 136(20), 5 2012. ISSN 00219606. doi:10.1063/1.4720499.

[78] J T Gudmundsson, Takashi Kimura, and M A Lieberman. Experimental studies of O_2 /Ar plasma in a planar inductive discharge. *Plasma Sources Science and Technology*, 8(1): 22–30, 2 1999. ISSN 0963-0252. doi:10.1088/0963-0252/8/1/003.

[79] E. G. Thorsteinsson and J. T. Gudmundsson. The low pressure Cl_2/O_2 discharge and the role of ClO. *Plasma Sources Science and Technology*, 19(5), 10 2010. ISSN 09630252. doi:10.1088/0963-0252/19/5/055008.

[80] C. Lee and M. A. Lieberman. Global model of Ar, O_2, Cl_2, and Ar/O_2 high-density plasma discharges. *Journal of Vacuum Science & Technology A: Vacuum, Surfaces, and Films*, 13 (2):368–380, 3 1995. ISSN 0734-2101. doi:10.1116/1.579366.

[81] B. M. Smirnov. *Introduction To Plasma Physics*. Mir Publishers, 1977.

[82] J T Gudmundsson, A M Marakhtanov, K K Patel, V P Gopinath, and M A Lieberman. On the plasma parameters of a planar inductive oxygen discharge. *Journal of Physics D: Applied Physics*, 33(11):1323–1331, 6 2000. ISSN 0022-3727. doi:10.1088/0022-3727/33/11/311.

[83] P. J. Chantry. A simple formula for diffusion calculations involving wall reflection and low density. *Journal of Applied Physics*, 62(4):1141–1148, 1987. ISSN 00218979. doi:10.1063/1.339662.

[84] J. P. Booth and N. Sadeghi. Oxygen and fluorine atom kinetics in electron cyclotron resonance plasmas by time-resolved actinometry. *Journal of Applied Physics*, 70(2): 611–620, 1991. ISSN 00218979. doi:10.1063/1.349662.

[85] A. Kramida, Yu. Ralchenko, J. Reader, and NIST ASD Team. NIST Atomic Spectra

Database (version 5.12), 2024. URL https://physics.nist.gov/asd.

[86] R Mewe. Relative intensity of helium spectral lines as a function of electron temperature and density. *British Journal of Applied Physics*, 18(1):107–118, 1 1967. ISSN 0508-3443. doi:10.1088/0508-3443/18/1/315.

[87] T. Holstein. Imprisonment of Resonance Radiation in Gases. *Physical Review*, 72(12): 1212–1233, 12 1947. ISSN 0031-899X. doi:10.1103/PhysRev.72.1212.

[88] P.A. Miller, G.A. Hebner, K.E. Greenberg, P.D. Pochan, and B.P. Aragon. An Inductively-Coupled Plasma Source for the Gaseous Electronics Conference Rf Reference Cell. *Journal of Research of the National Institute of Standards and Technology*, 100(4): 427, 7 1995. ISSN 1044677X. doi:10.6028/jres.100.032.

[89] Arthur Greb. *Dynamics Of The Plasma-Surface Interface In Capacitively Couped Radio-Frequency Oxygen Plasmas: Coupling Numerical Simulations With Optical Diagnostics*. Random House Audio, 2013. URL https://etheses.whiterose.ac.uk/id/eprint/4980/.

[90] Charles R. Harris, K. Jarrod Millman, Stéfan J. van der Walt, Ralf Gommers, Pauli Virtanen, David Cournapeau, Eric Wieser, Julian Taylor, Sebastian Berg, Nathaniel J. Smith, Robert Kern, Matti Picus, Stephan Hoyer, Marten H. van Kerkwijk, Matthew Brett, Allan Haldane, Jaime Fernández del Río, Mark Wiebe, Pearu Peterson, Pierre Gérard-Marchant, Kevin Sheppard, Tyler Reddy, Warren Weckesser, Hameer Abbasi, Christoph Gohlke, and Travis E. Oliphant. Array programming with NumPy. *Nature*, 585 (7825):357–362, 9 2020. ISSN 0028-0836. doi:10.1038/s41586-020-2649-2.

[91] A. Hurlbatt, D. O'Connell, and T. Gans. Bridging the gap between global models and full fluid models: A fast 1D semi-analytical fluid model for electronegative plasmas. *Plasma Sources Science and Technology*, 25(4), 6 2016. ISSN 13616595. doi:10.1088/0963-0252/25/4/045011.

[92] Stephen Hwang and Keren Kanarik. Evolution of across-wafer uniformity control in plasma etch. 8 2016. URL https://sst.semiconductor-digest.com/2016/08/evolution-of-across-wafer-uniformity-control-in-plasma-etch/.